UNIVERSITÀ DEGLI STUDI DI PADOVA

DIPARTIMENTO DI INGEGNERIA INDUSTRIALE

CORSO DI LAUREA MAGISTRALE IN INGEGNERIA CHIMICA E DEI PROCESSI INDUSTRIALI

Tesi di laurea magistrale in

Ingegneria Chimica e dei Processi Industriali

EXPERIMENTS AND MODELING OF SUPERCRITICAL CO_2 EXTRACTION OF LIPIDS FROM MICROALGAE
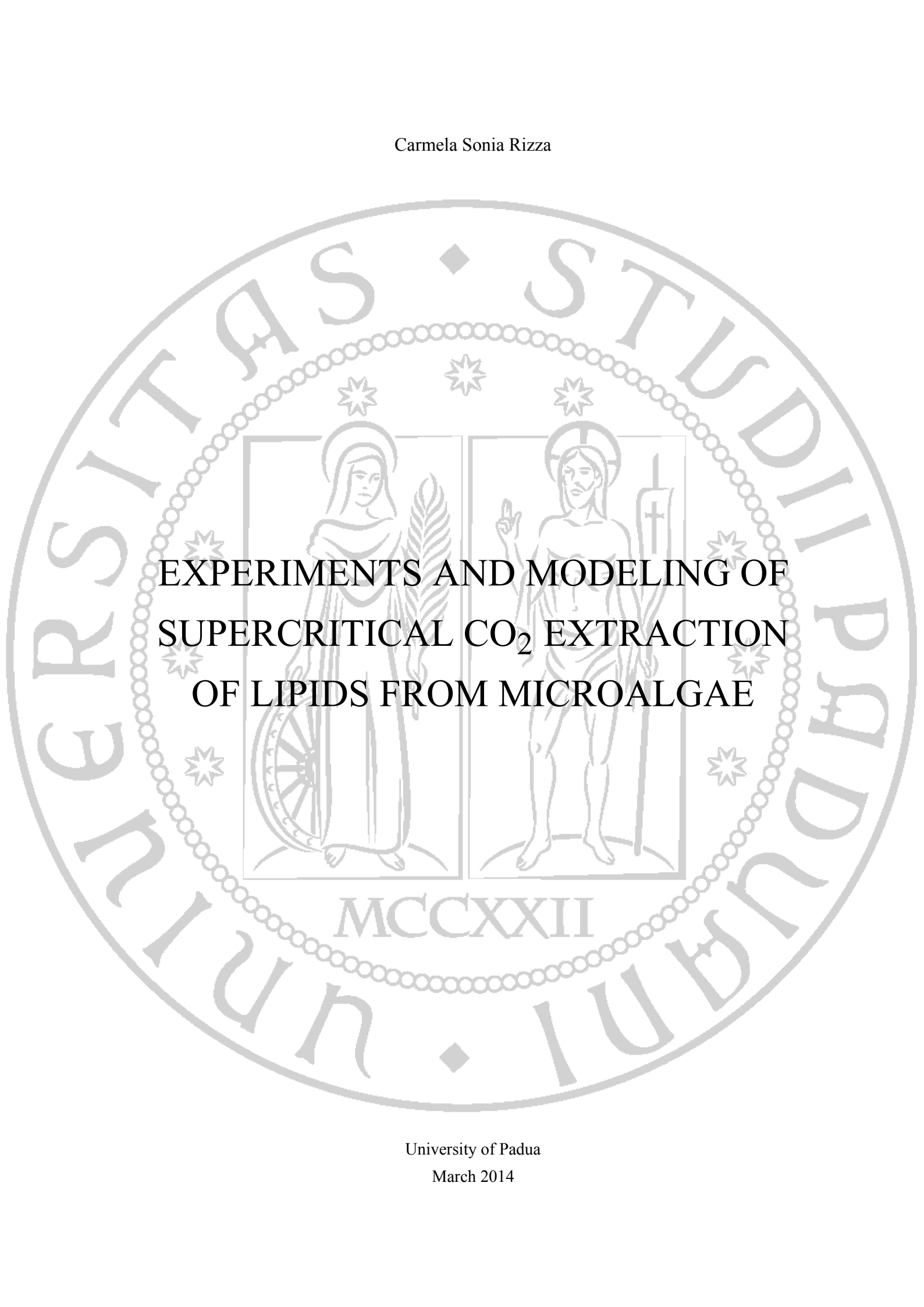
Relatore: Prof. Alberto Bertucco

Correlatrice: Miriam Solana Ciprés

Laureanda: CARMELA SONIA RIZZA

ANNO ACCADEMICO 2013 - 2014

Carmela Sonia Rizza

EXPERIMENTS AND MODELING OF SUPERCRITICAL CO$_2$ EXTRACTION OF LIPIDS FROM MICROALGAE

University of Padua

March 2014

UNIVERSITÀ DEGLI STUDI DI PADOVA

DIPARTIMENTO DI INGEGNERIA INDUSTRIALE

CORSO DI LAUREA MAGISTRALE IN INGEGNERIA CHIMICA E DEI PROCESSI INDUSTRIALI

Tesi di laurea magistrale in

Ingegneria Chimica e dei Processi Industriali

EXPERIMENTS AND MODELING OF SUPERCRITICAL CO_2 EXTRACTION OF LIPIDS FROM MICROALGAE

Relatore: Prof. Alberto Bertucco

Correlatrice: Miriam Solana Ciprés

Laureanda: **CARMELA SONIA RIZZA**

ANNO ACCADEMICO 2013 - 2014

To my father

Riassunto

Al giorno d'oggi, la ricerca in ingegneria chimica è sempre più mirata allo studio di nuove tecniche che siano efficienti e al tempo stesso sicure, nel rispetto della salute umana e dell'ambiente in cui viviamo. Alcuni fra i principi chiavi dello sviluppo di tecniche alternative sono sostenibilità, efficienza, minimizzazione dell'impatto ambientale e del consumo energetico.

Il presente lavoro di tesi ha avuto l'obiettivo di studiare la solubilità e la cinetica del processo di estrazione di lipidi dalle microalghe, mediante l'utilizzo di anidride carbonica in condizioni supercritiche. Si tratta di una nuova tecnica che si è sviluppata negli ultimi anni per sostituire la tradizionale estrazione con solvente, la quale ha un maggiore impatto ambientale in quanto richiede l'impiego di sostanze tossiche.

Un fluido diventa supercritico quando supera pressione e temperatura critiche. In questo stato le fasi liquida e gassosa non sono più distinguibili e il fluido possiede alcune proprietà simili a quelle della fase liquida, come la densità, e alcune proprietà simili a quelle del gas, come la viscosità. In particolare, la solubilità, che è strettamente correlata con la densità, aumenta in tali condizioni e può essere agevolmente variata cambiando pressione e temperatura. L'anidride carbonica risulta in questo caso molto conveniente perché raggiunge lo stato supercritico a bassa temperatura (31.35 °C), riuscendo così ad estrarre composti termosensibili senza degradarli. Inoltre, è facilmente reperibile a un prezzo contenuto, non è tossica né infiammabile e ha un alta selettività con composti non polari. È anche possibile estrarre componenti polari con l'aggiunta di un co-solvente, come etanolo, metanolo o acqua.

Le microalghe sono oggetto di molti studi perché contengono prodotti utili alle industrie alimentari, farmaceutiche e cosmetiche. Si tratta principalmente di acidi grassi polinsaturi, capaci di prevenire e curare diverse malattie causate da disturbi alimentari e cattiva alimentazione, e di pigmenti naturali (come i carotenoidi), che possono sostituire quelli artificiali. Le microalghe inoltre sono considerate una fonte di biodiesel di terza generazione, che potrebbe sostituire le prime due generazioni, le quali comportano una serie di svantaggi come l'utilizzo di terre destinate alla coltivazione di cibo e la competizione con il mercato alimentare.

Trovare un modello cinetico quantitativamente adatto a descrivere l'estrazione di lipidi dalle microalghe con CO_2 supercritica è quindi fondamentale per poter ottimizzare il processo, aumentarne l'efficienza e promuoverne la fattibilità su scala industriale. In questa

ricerca sono stati calcolati i valori di resa e solubilità dell'estrazione con CO_2 supercritica di lipidi contenuti nelle microalghe, al variare di condizioni operative quali temperatura, pressione e tempo di estrazione. Infine, è stato utilizzato un modello inizialmente creato per l'estrazione di oli vegetali dalle piante. Si tratta del modello delle cellule rotte e intatte, che descrive la struttura della particella dopo l'effetto del pre-trattamento meccanico. La macinatura riesce infatti a rompere le pareti delle cellule vicino la superficie, lasciando intatte quelle più interne. In questo modo si crea una zona in cui il soluto è facilmente accessibile e viene estratto più velocemente, mentre quello contenuto dentro le cellule intatte avrà più difficoltà a passare dalla matrice solida al bulk del solvente. La prima parte dell'estrazione è quindi governata dal trasporto di materia esterno, mentre la seconda parte da quello interno. I coefficienti di trasporto di materia e la percentuale di cellule rotte sono i parametri da determinare con l'ausilio di dati sperimentali. In tal modo è possibile ottenere la curva di estrazione che rappresenta la resa in funzione del tempo o del solvente passato.

La parte iniziale del lavoro di ricerca prevedeva la raccolta di dati sperimentali da utilizzare per il fitting del modello. Gli esperimenti di estrazione con CO_2 supercritica sono stati svolti in un impianto in scala di laboratorio. Diverse condizioni operative sono state valutate, cambiando di volta in volta pressione e temperatura. Le pressioni sono state variate da 15 MPa a 30 MPa, mentre la temperatura da 45 °C a 65 °C. L'etanolo è stato impiegato come co-solvente, per aumentare l'efficienza di estrazione di composti polari. Un apparato Soxhlet è stato utilizzato per l'estrazione con solvente e un evaporatore rotante per recuperare l'estratto. Sono state studiate tre specie di microalghe: *Scenedesmus obliquus*, *Chlorella protothecoides* e *Nannochloropsis salina*.

Il fitting dei modelli sulla base dei dati sperimentali è stato eseguito con l'ausilio di MATLAB®. Sono stati approfonditi: un modello semplificato che dà una prima stima dei parametri, utilizzata come valore iniziale nel modello completo; un modello completo costituito da equazioni più elaborate; un ulteriore modello semplificato che stima i tempi caratteristici del processo di estrazione. I risultati mostrano che i modelli, sebbene siano stati sviluppati per le piante, ben si adattano all'estrazione di lipidi dalle microalghe, dando risultati soddisfacenti in tutti gli esperimenti eseguiti con diverse condizioni operative. Inoltre anche i modelli semplificati danno buoni risultati, nonostante abbiano un numero inferiore di parametri.

Data l'importanza della solubilità dell'olio nella CO_2 supercritica, ai fini dell'efficienza del processo, è stata investigata la sua relazione con la densità utilizzando dei modelli che hanno un approccio semi-empirico. Il modello di Chrastil è stato confrontato con altri due modelli successivi, quello di Del Valle-Aguilera e quello di Adachi-Lu. L'equazione di Del Valle-Aguilera è risultata la più precisa, mentre quella di Adachi-Lu ha riportato valori molto bassi dei parametri aggiuntivi, così da essere ricondotta all'equazione di Chrastil.

Infine, la composizione dell'olio ottenuto dalle varie estrazioni è stata analizzata per confrontare diverse tecniche, diverse specie di microalghe e diverse condizioni operative nell'estrazione supercritica. In tal modo, si è dimostrato che l'estrazione con CO_2 supercritica è capace di estrarre circa una quantità di olio simile a quella ottenuta con l'estrazione con solvente, senza però degradare i composti termo-sensibili e senza le impurezze che inevitabilmente restano con il processo tradizionale. Nelle diverse specie si è riscontrata, come previsto, una diversa composizione di lipidi: *S. obliquus* e *C. protothecoides* sono più ricche di acidi grassi polinsaturi, mentre *N. salina* contiene più acidi grassi saturi. La resa più alta è stata ottenuta a 30 MPa e 65 °C, con un'estrazione di 90 minuti, mentre la concentrazione più alta di acido α-linolenico, essenziale per la salute del corpo umano, è stata ottenuta a 15 MPa e 45 °C, con un'estrazione di 30 minuti. Temperatura, pressione e soprattutto tempo di estrazione, influiscono dunque negativamente sulla quantità degli acidi grassi omega-3, noti come "oli essenziali", in quanto il corpo umano non è in grado di sintetizzarli. Inoltre, riportando la resa e la solubilità in funzione della pressione, è stato osservato un cross-over tra 25 e 30 MPa. Sotto tale punto resa e solubilità hanno un andamento decrescente all'aumentare della temperatura, mentre sopra il cross-over si verifica il contrario. Tale fenomeno è comune in questo tipo di estrazioni ed è causato da cambiamenti rapidi della densità vicino il punto critico, che influiscono negativamente sulla solubilità, e quindi sulla resa. La sua conoscenza è di fondamentale importanza ai fini della progettazione e dell'ottimizzazione del processo.

Abstract

The aim of this work is to optimize the experimental conditions and to model the kinetics and the solubility of supercritical CO_2 extraction of lipids from microalgae, a new promising technique that has been studied in recent years as alternative to older ones that involve the use of toxic solvents and have a greater environmental impact. Experiments were performed at different conditions to optimize pressure and temperature and to study their influence on extraction yield and solubility. The model of broken and intact cells, initially developed for plant materials, was used to fit the experimental data, and it was proved to be able to describe the microalgae structure as well. The solubility of oil in supercritical CO_2 was correlated to density using the Chrastil model. This model was also compared with those developed by Del Valle-Aguilera and Adachi-Lu. Finally, lipids composition was analyzed and the results with different techniques (supercritical CO_2 extraction and solvent extraction), different microalgae strains (*Scenedesmus obliquus*, *Chlorella protothecoides*, and *Nannochloropsis salina*), and different operative conditions (pressure, temperature, and extraction time) were compared.

Acknowledgments

Contents

List of Figures

List of Tables

Nomenclature

a_0 Specific surface area per unit volume of extraction bed (1/m)

a_s Specific area between intact and broken cells (1/m)

c_u Solute content in the untreated solid ($\text{kg}_{\text{solute}}/\text{kg}_{\text{solid}}$)

c_v Isochoric specific heat ($\text{kJ kg}^{-1}\text{ K}^{-1}$)

d Particle diameter (m)

E Extract (kg)

e Extraction yield ($\text{kg}_{\text{extract}}/\text{kg}_{\text{insoluble solid}}$)

e' Extraction yield ($\text{kg}_{\text{extract}}/\text{kg}_{\text{solid}}$)

$e'(t_1)$ Extraction yield at the end of the first extraction period ($\text{kg}_{\text{extract}}/\text{kg}_{\text{solid}}$)

f_i^F Fugacity of component i in the supercritical phase

f_i^S Fugacity of component i in the solid phase

G Initial fraction of extract in open cells

H Enthalpy (J)

h Specific enthalpy (kJ/kg)

I Intercept in the Chrastil model

j_f Flux from broken cells to solvent ($\text{kg m}^{-3}\text{ s}^{-1}$)

j_s Flux from intact cells to broken cells ($\text{kg m}^{-3}\text{ s}^{-1}$)

K Partition coefficient

k	Association number
K_eq	Equilibrium constant
k_f	Fluid phase mass transfer coefficient (1/s)
k_s	Solid phase mass transfer coefficient (1/s)
M	Mass of passed solvent (kg)
MW	Molecular weight (g/mol)
N	Solid load in the extractor (kg)
N_m	Load of insoluble solid (kg)
P	Pressure (MPa)
$\dot{Q}$	Solvent flow rate (kg/s)
q	Relative amount of passed solvent ($kg_{solvent}/kg_{insoluble\ solid}$)
q'	Specific solvent flow rate ($kg_{solvent}\ kg_{solid}^{-1}\ s^{-1}$)
R	Ideal gas constant ($kJ\ kg^{-1}\ K^{-1}$)
r	Grinding efficiency (fraction of broken cells)
S	Solubility in the Chrastil model (g/L)
T	Absolute temperature (K)
T	Temperature (°C)
t	Extraction time (s)
t_1	Extraction time at the end of the first extraction period (s)
t_i	Characteristic time of the solid phase mass transfer (s)
U	Interstitial fluid velocity (m/s)
V	Volume of passed solvent (m^3)
v	Molar volume (m^3/mol)
x_1	Concentration in broken cells ($kg_{solute}/kg_{insoluble\ solid}$)

x_2 Concentration in intact cells ($kg_{solute}/kg_{insoluble\ solid}$)

x_t Transition concentration ($kg_{solute}/kg_{insoluble\ solid}$)

x_u Concentration in the untreated solid ($kg_{solute}/kg_{insoluble\ solid}$)

$x_{1,0}$ Initial concentration in broken cells ($kg_{solute}/kg_{insoluble\ solid}$)

$x_{2,0}$ Initial concentration in intact cells ($kg_{solute}/kg_{insoluble\ solid}$)

y Fluid phase concentration ($kg_{solute}/kg_{solvent}$)

$y^*(x_1)$ Equilibrium fluid phase concentration ($kg_{solute}/kg_{solvent}$)

y_0 Initial fluid phase concentration ($kg_{solute}/kg_{solvent}$)

y_s Solubility ($kg_{solute}/kg_{solvent}$)

Z Extraction bed length (m)

z Axial coordinate (m)

Greek Letters

Δ Difference operator

γ Solvent to matrix ratio in the bed ($kg_{solvent}/kg_{insoluble\ solid}$)

ρ Density (kg/m^3)

ρ_a Solid apparent density (kg/m^3)

ρ_f Solvent density (kg/m^3)

ρ_s Solid real density ($kg_{insoluble\ solid}/m^3_{solid\ phase}$)

ρ_{CO_2} CO_2 density (kg/m^3)

ρ_{EtOH} Ethanol density (kg/m^3)

θ_e Dimensionless external mass transfer resistance

θ_i Dimensionless internal mass transfer resistance

$\tilde{\rho}$ Molar density (mol/dm^3)

ε Bed void fraction

φ_i^G Fugacity coefficient of component i in the supercritical phase

φ_i^S Fugacity coefficient of component i at sublimation pressure

Introduction

Nowadays, research in chemical engineering is mostly focused on new techniques that combine efficiency and safety, in regard to human health and environmental protection. Key principles in the development of alternative techniques are eco-sustainability, efficiency, minimization of environmental impact, low energy and water consumption, and of course economic feasibility.

This work is about the supercritical fluid extraction of lipids from microalgae, a new technique developed in recent years whose purpose is to replace conventional solvent extraction, that has a greater environmental impact mainly due to the use of toxic substances.

A supercritical fluid is a substance over its critical temperature and pressure. In this state liquid and gas phases are not distinguishable and the fluid has some properties similar to those of the liquid, like density, and other properties similar to those of the gas, like viscosity. The solvent power of this fluid depends on density, and since density increases with pressure, solubility is enhanced when pressure is higher. Therefore, operating pressure and temperature can be varied to optimize thermo-physical properties like diffusivity, viscosity, and, especially, solubility [Sovová, 2005]. Carbon dioxide is particularly convenient as a supercritical fluid since its critical conditions are at quite lower pressure (7.38 MPa) and temperature (31.35 °C), so that thermo-sensible compounds are not degraded. Furthermore, it is cheap, easy available, and non-toxic nor flammable, being Generally Recognized As Safe (GRAS). With respect to solvent extraction, supercritical CO_2 extraction has higher selectivity, lower extraction time and no healthy nor safety concerns. Moreover, no separation step is required, since carbon dioxide is gaseous at ambient conditions [Mercer and Amenta, 2011].

Full scale plants that operates with supercritical CO_2 extraction are spread all over the world, mostly in the food industry, for coffee decaffeination and hop extraction. However, many extraction processes concern the recovery of useful biological substances from plants or other materials [Sovová and Stateva, 2011]. In particular, the interest in "functional food" has increased in recent years, since it brings several benefits to human health. Functional foods are for example anti-oxidants, anti-flammatory, anti-hypertensive substances, that can treat cardiovascular diseases, improve physiological functions, and decrease the risk of several other diseases [Herrero *et al.*, 2006]. Furthermore, natural pigments are also extracted

from several sources to replace synthetic colorants, widely used in food industry [Gouveia *et al.*, 2007]. Microalgae are in this case of particular interest since they contain carotenoids (antioxidants) and other pigments used in food, pharmaceutical and cosmetic industries. Many strains are also rich in polyunsaturated fatty acids, including the "essential oils", so called since they are essential for human health but the body is not able to synthesize them. In particular, omega-3 fatty acids can prevent and cure several diseases caused by poor diets or eating disorders [Rubio-Rodríguez *et al.*, 2010].

Moreover, microalgae have often a high content of non polar lipids, so that they can be a valuable source of bio-oils suitable to produce biodiesel, and are currently considered as the third generation biofuels source. First generation biofuels come from food crops but have many disadvantages such as the use of big extension lands and the competition with food markets. Second generation biofuels are extracted from vegetable plants or animal fats, but they have poor properties, like poor performances in cold temperatures. Microalgae are very promising since they do not require cultivation lands, they have higher growth rates, higher productivity, higher lipids content and higher yields with respect to conventional crops [Ahmad *et al.*, 2011; Rawat *et al.*, 2013; Santana *et al.*, 2012].

Supercritical CO_2 extraction of lipids from microalgae exploits the high solubility of lipids in supercritical CO_2 and its high selectivity towards non polar and low polar compounds. Furthermore, a co-solvent (such as methanol, ethanol, water), can improve the solubility of polar compounds as well [Sovová and Stateva, 2011].

Finding a model that describes adequately the extraction process is essential to optimize the parameters that govern it and to improve therefore its efficiency. During the extraction, the solute (in this case the oil) migrates from the microalgae cells to the solvent bulk, so that the models are focused on the description of mass transfer from a solid matrix to a supercritical fluid. Key parameters are the solubility and the mass transfer coefficients. The model of broken and intact cells, developed by Sovová [Sovová, 2005], describes the structure of a microalgae particle that results after the mechanical pretreatment, which breaks the cell walls creating a fraction of broken cells near the surface, while the internal ones remain intact. Mass balances and phase equilibrium relations are solved to express the extraction yield as a function of time or passed solvent. These equations contain the parameters that govern the process, the fraction of broken cells and the mass transfer coefficients, which can be evaluated with a fitting to experimental data. In this work, three models based on the concept of broken and intact cells are discussed: a complete model, a simplified model that allows to calculate a first parameters estimation and a simplified model that allows to determine the characteristic times of the process.

Another important step in supercritical fluid extraction is to understand the relation be-

tween solubility and density. In this process, pressure and temperature are varied to optimize the process, since density depends on them and solubility depends on density. Different empirical or semi-empirical correlations link solubility with density, like the Chrastil model, the Del Valle-Aguilera model and the Adachi-Lu model. In the present work, these model were fitted to experimental data and compared. The limit of these model is that they cannot predict phase equilibria, since they are empirical correlations. Other models have different approaches that allow to calculate the solubility from phase equilibrium relations, which are built starting from the concept of thermodynamic equilibrium.

The work performed during this thesis provides both original extraction data for three microalgae strains (*Scenedesmus obliquus*, *Chlorella protothecoides*, and *Nannochloropsis salina*) and a simple approach to simulate the supercritical CO_2 extraction of lipids by a physically-sound model.

Chapter 1

Supercritical fluid extraction of oil from microalgae

Microalgae are recognized as an important renewable source of lipids that can be used as biofuels [Brennan and Owende, 2010] or as nutritional supplements able to prevent and treat several diseases [Andrich *et al.*, 2006]. The lipids content and composition vary from species to species, so that some strains are a better biofuels source while other strains are richer in bioactive lipids useful in functional food for pharmaceutical or nutritional purposes.

The extraction of lipids from microalgae can be performed using an organic solvent such as n-hexane, methanol or chloroform. Nevertheless, these solvents are toxic, flammable and usually have a low selectivity [Crampon *et al.*, 2013]. Furthermore, high costs, healthy and safety problems are usually associate with these issues [Santana *et al.*, 2012]. A valid alternative is the supercritical carbon dioxide, since the CO_2 is not toxic or flammable and it is a Generally Recognized As Safe (GRAS) solvent [Crampon *et al.*, 2013]. In addition, supercritical CO_2 extraction is faster than solvent extraction and has a higher selectivity [Santana *et al.*, 2012]. These and other aspects will be discussed below.

1.1 Microalgae

The structure of microalgae is very simple since they are primitive organisms without roots, stems or leaves and they have chlorophyll a as photosynthetic pigment. Their cellular organization can be prokaryotic (with the DNA that lies free in the cytoplasm and without membrane-bounded organelles) or eukaryotic (with a membrane-bounded nucleus and the cytoplasm divided into compartments) [Tomaselli, 2004]. Microalgae can be also divided in autotrophic or heterotrophic: the former need only CO_2, salts (of nitrogen and phosphorous) and light energy to grow, while the latter are not photosynthetic organisms and then require

organic compounds, nutrients and an energy source [Brennan and Owende, 2010].

Owing to the need of light energy, microalgae cultivation usually takes place in open ponds that use sunlight as a free natural resource, or in photobioreactors in which the light is artificially distributed. The first system is cheaper and requires low energy inputs, but it has poor biomass productivity, requires large extension of lands and contamination is easy to happen. On the other hand, photobioreactors are more compact, have a large illumination surface area and a good mixing respect to the open ponds. There are different types of photobioreactors (tubular, flat plate and column), each of them with different advantages and disadvantages. Common disadvantages are that they are more expensive than open ponds, consume more energy and it is more difficult to scale them up for industrial applications. However, the aim is to replace the open ponds with photobioreactors since they have many disadvantages, including mostly the contamination risks that preclude their use for high-value products [Brennan and Owende, 2010].

1.2   Microalgae as a source of biofuels

Current research is devoted to the study of new sustainable and renewable sources that minimize the environmental impact. Climate changes, water, lands and energy consumption are some of the major global problems caused mainly by fossil fuels [Demirbas, 2011]. They are considered to be responsible of 80% of greenhouse gas emissions [Quadrelli and Peterson, 2007], hence the need to replace them with renewable and clean energy resources. Furthermore, the cost is intended to rise in the next dedaces due to the constant increase of the number of light motor vehicles and the depletion of fossil fuels [Rawat *et al.*, 2013]. Biofuels are gaining then importance and interest being a renewable energy source that lowers the environmental impact and greenhouse gas emissions.

The studies on microalgae have increased in these last years, so that they are considered the third generation biofuels source [Rawat *et al.*, 2013]. The first generation source are food crops, such as rapeseed, palm, sunflower, soybean, but biofuels production from this source has a great impact on food security and could increase the costs of food crops making the biodiesel production too expensive [Rawat *et al.*, 2013]. Furthermore, first generation biofuels consume food that should be fit for human consumption, therefore it has a great impact on global food markets [Ahmad *et al.*, 2011]. The biodiesel obtained from this source has also been strongly criticized because the cultivation of food crops requires big agricultural lands: this would increase the competition with other crops intended to feed the human population and could increase the deforestation issue [Santana *et al.*, 2012]. The second generation biofuels come from non-food feedstocks and comprehend vegetable oils (for example jatropha

oil, waste cooking oils, etc.) and animal fats. They have some advantages with respect to the first generation because they do not intact the food security, nor the food market and less lands are required since they can be cultivated in wastelands not suitable for food crops. However, these oils have poor performance in cold temperatures, and their great amount of saturated fatty acids makes the transesterification process (necessary to obtain biodiesel) difficult. First and second generation have moreover high raw materials and production costs that make the process unsustainable and inefficient [Ahmad *et al.*, 2011]. These are the main reasons that brought the attention to third generation biofuels, i. e. biofuels which are derived from microalgae.

Microalgae production has many advantages with respect to the other biofuels sources since, in regard to terrestrial plants, they have higher growth rates, higher productivity, are easier to cultivate and can reach higher yields of oil for biodiesel production [Santana *et al.*, 2012]. In particular, the high yields and growth rates could possibly satisfy the massive demand of biofuels. Other differences are that microalgae do not require farmlands since they can grow on wastelands, or even above the sea surface, and require less water than conventional crops [Demirbas, 2011]. Despite microaglae require more fertilizer (they need 55–111 times more fertilizer than rapeseed [Demirbas, 2011]), they do not need herbicides and pesticides, minimizing therefore the environmental impact [Rawat *et al.*, 2013]. Another big advantage is that microalgae can remove phosphates and nitrates from wastewater, so that their cultivation could be combined with a tertiary wastewater treatment [Rawat *et al.*, 2013]. Furthermore, biomass productivity and lipid content can be varied by changing cultivation conditions (e. g., lower nitrogen administration, lower CO_2 concentration, etc.), thus increasing the efficiency of the process [Lv *et al.*, 2010; Mairet *et al.*, 2011]. However, these advantages are followed by problems like the high capital costs due to low biomass concentration and the difficulties associated with their cultivation, since they are vulnerable to many bacteria that could lower substantially their concentration; these are the main obstacles that complicate the scale-up of the process [Demirbas, 2011]. Current research is focused on solving these problems since microalgae are the most promising source for biodiesel.

1.3 Microalgae as a source of essential fatty acids

Microalgae are well known not only as a valuable biofuels source, but also for several other compounds since the biomass is able to synthesize proteins, carbohydrates and lipids [Rawat *et al.*, 2013]. Several chemicals and biochemicals can be extracted from various microalgae strains. For example, some microalgae species contain natural pigments (carotenes and chlorophylls, like beta-carotene from *Dunaliella spp.* or phycocyanin from *Spirulina*) that
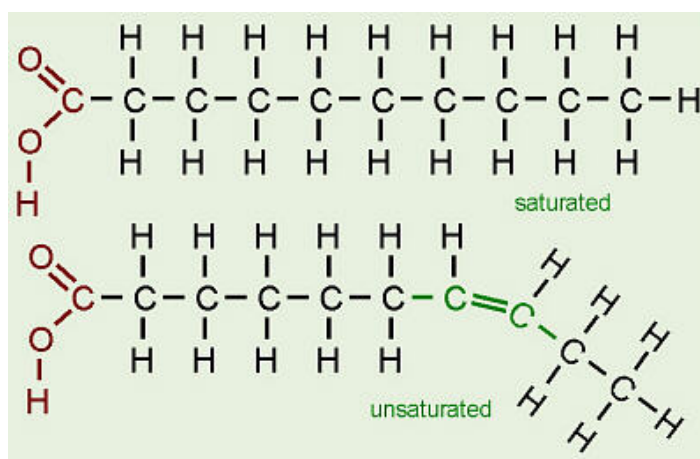
Figure 1.1: *Comparison between saturated fatty acids (SFA) and unsaturated fatty acids (UFA).*

could replace the synthetic pigments in food, drug and cosmetic industries. Polymers can also be extracted from microalgae as well, for example heteropolysaccharides such as agar and alginic acid from red microalgae. There are indeed thousands of different species of microalgae and only a few of them have been studied in detail [Vonshak, 1997].

Above all, microalgae are known for bioactive lipids synthesis that are rare in plant or animal sources, such as polyunsaturated fatty acids [Vonshak, 1997]. Fatty acids are lipid molecules characterized by a head with a carboxylic acid and a tail that is a long aliphatic chain. They can be saturated, with no double bounds, and unsaturated, with one or more double bonds, as can be seen in Figure 1.1. The carboxylic head can be bonded to an uncharged group (i.e., glycerol), to form neutral lipids, or to a charged group, to form polar lipids. Neutral lipids are for example acylglycerols and free fatty acids (FFA), while polar lipids can be divided in phospholipids (PL) and glycolipids (GL) [Halim *et al.*, 2012].

The most desirable lipid composition for biodiesel production is the one that has mainly acylglycerols, as they have a lower degree of unsaturation and produce a biodiesel with an higher oxidation stability. Polyunsaturated fatty acids (PUFA) are not suitable for biodiesel production since they have poor volatility, low oxidation stability and the tendency for gum formation [Halim *et al.*, 2012].

Polyunsaturated fatty acids are important for many other reasons. Among them, there are the $\omega 3$ fatty acids that can prevent and suppress many diseases caused by poor diets rich in $\omega 6$ fatty acids. It is indeed reported that a high $\omega 6/\omega 3$ ratio promotes illnesses such as cardiovascular problems, cancer and inflammatory diseases [Simopoulos, 2002]. Many studies have reported the importance of omega-3 enriched diets that are able to prevent deseases like myocardial infarction or bronchial asthma [Rubio-Rodríguez *et al.*, 2010].

Omega-3 fatty acids are mainly present in fish, but global fish stocks are in danger and, moreover, some fishes could have heavy metals as impurities, especially marine ones (salmone,

tuna, sardine, etc.) that can contain traces of copper, mercury or persistent organic pollutants like PCB (polychlorinated biphenyls), which are dangerous for human health [Domingo *et al.*, 2007]. Hence the importance of finding another PFA source that does not have these risks.

Microalgae lipids content and composition vary from species to species. However, many strains are rich in linoleic acid (LA) and α-linolenic acids (ALA). The first one is an $\omega6$ fatty acid and is generally indicated with the formula C18:2ω6, where the first part, "C18", indicates the number of carbon atoms, the second number, "2", indicates the number of double bonds, and the last part, "ω6", specifies the position of the first double bond. The second fatty acid is an ω3 fatty acid and its formula is C18:3ω3. Figure 1.2a shows the differences between the structures of these two fatty acids. The human body is able to synthesize other acids from them, like arachidonic acid (C20:4ω6, AA) from linoleic acid and eicosapentaenoic acid (C20:5ω3, EPA), docosapentaenoic acid (C22:5ω3, DPA), and docosahexaenoic acid (C22:6ω3, DHA), from α-linolenic acid [Rubio-Rodríguez *et al.*, 2010].

Omega-3 and omega-6 fatty acids are known as "essential fatty acids" because they are essential for the good health of the human body but cannot be synthesized by the latter (even if EPA, DPA and DHA can be synthesized, the conversion is low so they are considered essential too) [Rubio-Rodríguez *et al.*, 2010]. Generally, they are extracted using different techniques like steam distillation, hydrodistillation or solvent extraction. However, these compounds are very sensitive to high temperatures that can cause their degradation, and can be subjected to hydrosolubilization and hydrolysis, which affect their quality [Bruno *et al.*, 1993]. Other common techniques are supercritical fluid extraction, mechanical cell disruption, ultra-sonic assisted extraction, metabolic engineering (genetic methods), or even the use of pulse electric field technology, but the most diffused is the solvent extraction, often coupled with mechanical cell disruption [Mercer and Amenta, 2011]. Since this method has many disadvantages, like the use of toxic solvents, the aim of current research is to find other non-solvent techniques that are efficient and cost-effective not only in bench-scale, but also in large-scale. Solvent extraction and supercritical fluid extraction will be analyzed with their pros and cons in the following sections.

1.4   Solvent extraction

Solvent extraction is a simple process in which the solute is dissolved in a solvent and then is recovered with a separation step. Usually the solvent has a low boiling point, therefore it can be easily separated from the solute increasing the temperature. A further condensation step permits the solvent recovery and eventually a recycle. A schematic block diagram is represented in Figure 1.3.
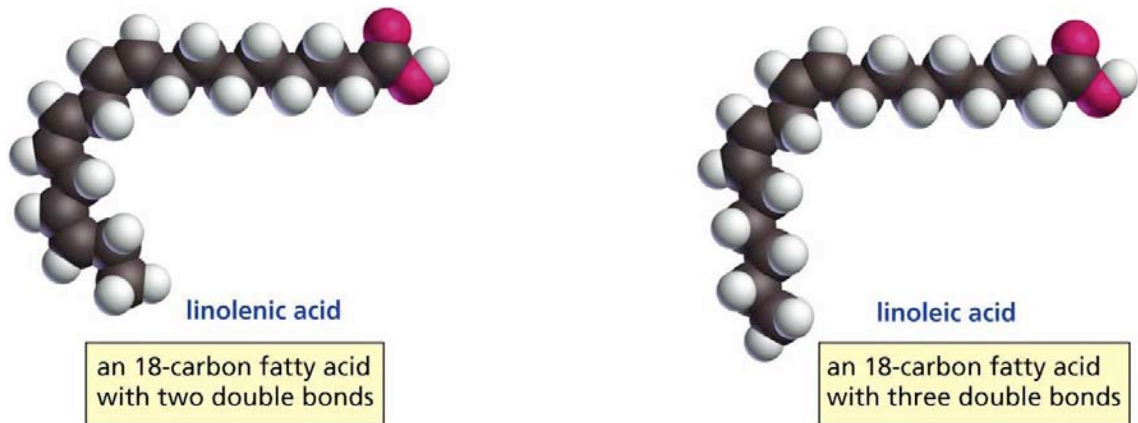
(a) *3D images of linoleic and α-linolenic acid.*
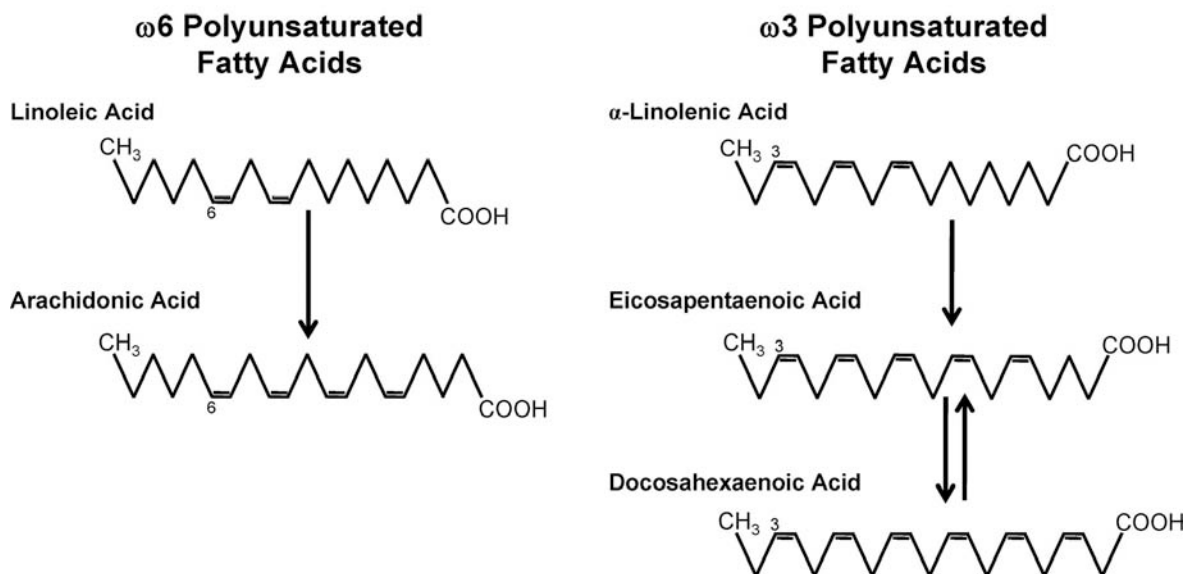
(b) *PUFA derived from linoleic acid and α linolenic acid.*

Figure 1.2: *Comparison between linoleic acid and α-linolenic acid and their derivatives.*

Microalgae lipids are soluble in organic solvents, like benzene, hexane, cyclohexane, methanol, chloroform, etc. Usually the solvent degrades microalgae cell walls and extracts the oil. The solvent extraction is often coupled with a mechanical cell disruption that breaks the cell walls and facilitates the extraction. The solvent must have high solute solubility, low boiling point, in order to facilitate the extraction, and it should be cheap, easily sourced and reusable. For these reasons, hexane is the commonly used solvent for large-scale processes [Mercer and Amenta, 2011]. Another possibility is the use of mixtures of solvents, like in the Bligh and Dyer method [Bligh and Dyer, 1959], where the solvent is a mixture of methanol, chloroform and water. This method is however not suitable for large-scale productions, since large amounts of solvents are wasted, being the recycling expensive [Mercer and Amenta, 2011]. There are also healthy concerns due to the presence of large amounts of organic toxic solvents. Since removing all traces of solvent is impossible, there are safety
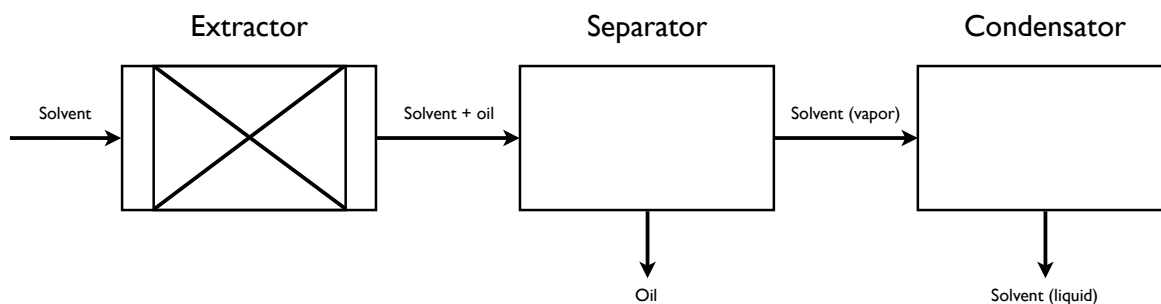
Figure 1.3: *Block diagram of solvent extraction.*

problems when the lipids are needed for pharmaceutical or dietary purposes. The European Economic Community and the Food and Drugs administration had, indeed, imposed great restrictions in the use of organic solvents [Palavra *et al.*, 2011].

This process requires also long extraction times and low selectivity that causes the extraction of non-target compounds. Other safety problems are possible when flammable solvents are used and the solute could contain traces of heavy metals depending on the solvent used. The extraction temperature is usually high and could degrade thermo-sensible compounds. Moreover, the solvent recovery is costly and is not always possible to recycle [Mercer and Amenta, 2011]. These reasons increased the interest in other much tempting alternatives like supercritical fluid extraction.

1.5 Supercritical CO_2 extraction

Supercritical CO_2 extraction is a new and promising technique for the extraction of lipids from plants or other sources. The supercritical state is reached when temperature and pressure exceed the critical point of the solvent. In a typical pressure versus temperature diagram, the liquid-vapor equilibrium is represented by a curve that starts at the triple point and ends at the critical point, like the diagram that Figure 1.4 shows. Over this point the supercritical region starts, in which liquid and vapor phase coexist and are not distinguishable. A supercritical fluid has some properties more similar to those of a liquid, like density, and some properties like those of a gas, like viscosity.

The CO_2 reaches his critical state at 31.35 °C and 7.38 MPa (Figure 1.5). A particular characteristic of supercritical CO_2 is the enhancement of the solubility in this state with the density, at constant temperature. When the temperature is fixed, the solubility increases with density and density increases with pressure, so the solubility is enhanced by pressure. At constant pressure, instead, varying the temperature could lead to different phenomena, since near the critical point density decreases so rapidly with the temperature that the solvent power
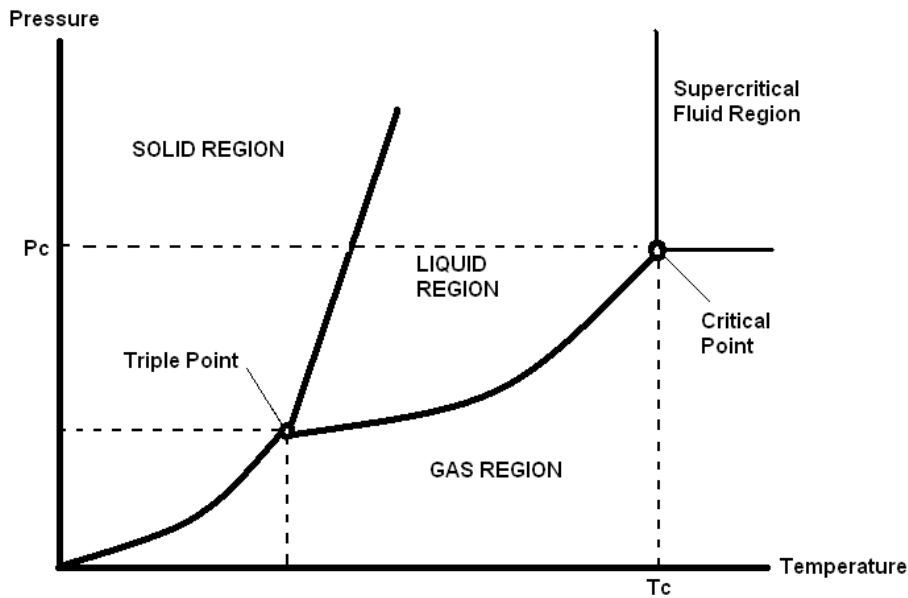
Figure 1.4: *Generic pressure-temperature phase diagram.*

is reduced.

The process of supercritical CO_2 extraction is illustrated in the block diagram of Figure 1.6. First, CO_2 has to reach the supercritical conditions, therefore a pump or compressor is needed to rise the pressure over the critical pressure and a heat exchanger to increase the temperature over the critical temperature. The pump needs a cooler before it to lower the CO_2 temperature to have the latter in its liquid state, so that cavitation phenomenon is prevented. Supercritical CO_2 goes then into the extractor, where a fixed bed of microalgae is loaded before the beginning of the process, and goes out from it with the dissolved solute. The oil is then separated from CO_2 lowering pressure or raising temperature, to bring back the CO_2 in the gaseous state. A more detailed diagram of the process will be presented in Chapter 2.

The big advantage of using the supercritical CO_2 is that the critical state is reached at lower temperature: the extraction temperatures are then moderate and thermo-sensible compounds are not compromised. Moreover, the process is solvent-free since CO_2 is a substance Generally Recognized As Safe (GRAS), not toxic nor flammable [Crampon *et al.*, 2013] and there are no metal nor solvent traces in the final product. Furthermore, CO_2 is gas at room temperature and the extracted lipids have low volatility, therefore the separation occurs easily by lowering pressure and increasing temperature. Another difference with solvent extraction is that CO_2 is cheaper, since it can be recovered from industrial waste emissions [Mercer and Amenta, 2011].

Supercritical CO_2 has low viscosity, high diffusivity and low surface tension, that allows it to penetrate into small pores [Sovová and Stateva, 2011]. It has also a great affinity with non
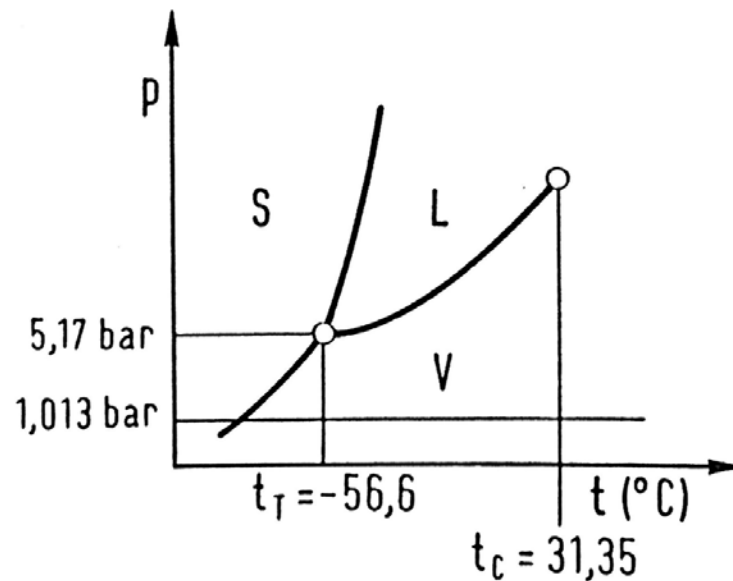
Figure 1.5: *CO_2 pressure-temperature phase diagram [Cavallini and Mattarolo, 1990].*
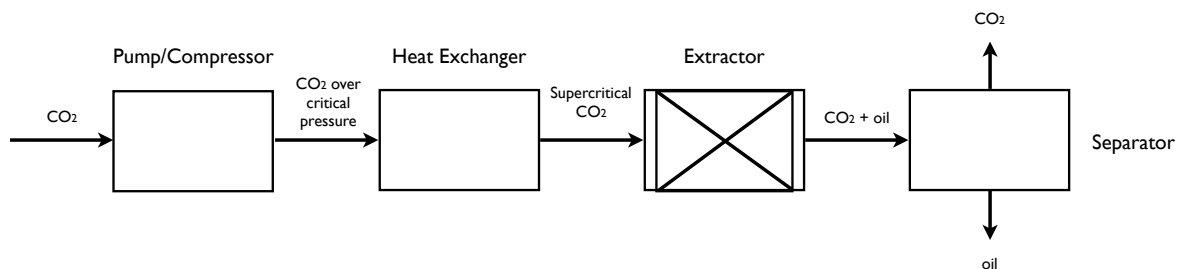
Figure 1.6: *Block diagram of supercritical CO_2 extraction.*

polar and low polar compounds, therefore the selectivity is higher and there are no polar substances that could form polymers [Mercer and Amenta, 2011]. This is very favorable when the lipids are extracted for biodiesel production because non-polar compounds like triglycerides are extracted without polar compounds like phospholipids, which are not desirable [Crampon *et al.*, 2013]. However, some polar compounds could be of interest, so to increase their solubility a co-solvent is used in small percentages. Ethanol is the most common co-solvent used in supercritical CO_2 extraction, usually with percentages from 5% to 10% of the CO_2 flow rate. It enhances the extraction of carotenoids and chlorophill [Macías-Sánchez *et al.*, 2008, 2009], but also the extraction of polyunsaturated fatty acids and polar lipids in general [Lam and Lee, 2013; Mendes *et al.*, 2006].

Pretreatment is usually needed to increase the efficiency of supercritical extraction. Usually, microalgae are dried and milled before loading them into the extraction vessel. The drying process, that can be done under air flow or with freeze-drying, is essential since humidity

negatively affects the process if in great amount, because it reduces the contact between solvent and sample [Mercer and Amenta, 2011]. However, it is reported in literature that in the case of microalgae, a moisture content up to 20% does not influence the system [Crampon *et al.*, 2013]. Another common pretreatment is the grinding of microalgae to reduce the particle size and increase the contact surface, favoring the extraction process [Crampon *et al.*, 2013].

The main factors that influence the supercritical CO_2 extraction are pressure, temperature, CO_2 flow rate and extraction time. These factors can be adjusted to optimize the process, in conjunction with the pretreatments and the co-solvent addition [Mercer and Amenta, 2011].

1.5.1 The Bender equation

Since the solubility in supercritical CO_2 is strongly influenced by density, which in turn depends on pressure and temperature, it is essential to use an equation of state that adequately describes the CO_2 in its supercritical state.

In this present work the density and enthalpy of CO_2 are calculated using the Bender equation, which expresses the pressure as a function of temperature and density using a 20 parameters expression, fitted on property data. The Bender equation of state is considered a good compromise between simple and more elaborate equations. It is used to calculate all fluid properties like density, enthalpy, entropy, specific heats, etc., and it has a high reliability in homogeneous fluids regions as well as the vapor-liquid equilibrium curve [Ghazouani *et al.*, 2005]. The equation of state model is [Sievers, 1984]:

$$
\begin{aligned}
P = {} & RT\rho + B\rho^2 + C\rho^3 + D\rho^4 + E\rho^5 + F\rho^6 + \\
& + (G + H\rho^2)\rho^3 \exp(-a_{20}\rho^2) \,,
\end{aligned}
\tag{1.1}
$$

where P is the pressure, R is the ideal gas constant, T is the temperature, ρ is the density and B, C, D, E, F, G, and H are defined as:

$$
\begin{aligned}
B &= a_1 T - a_2 - \frac{a_3}{T} - \frac{a_4}{T^2} - \frac{a_5}{T^3} \,, \\
C &= a_6 T + a_7 + \frac{a_8}{T} \,, \\
D &= a_9 T + a_{10} \,, \\
E &= a_{11} T + a_{12} \,, \\
F &= a_{13} \,, \\
G &= \frac{a_{14}}{T^2} + \frac{a_{15}}{T^3} + \frac{a_{16}}{T^4} \,, \\
H &= \frac{a_{17}}{T^2} + \frac{a_{18}}{T^3} + \frac{a_{19}}{T} \,,
\end{aligned}
\tag{1.2}
$$

where a_i, for $i = 1, ..., 20$, are the equation parameters, listed in Appendix A.

The enthalpy, useful for the evaluation of energy consumption for CO_2 circulation in supercritical extraction, is calculated as [Sievers, 1984]:

$$h(T, \rho) = h^0(T_0) + \int_{T_0}^{T} c_v^0(T)\, \mathrm{d}T - RT_0 + \\ + \int_{0}^{\rho} \left[p(T, \rho) - T \left(\frac{\partial p(T, \rho)}{\partial T} \right)_\rho \right] \frac{\mathrm{d}\rho}{\rho^2} \ . \tag{1.3}$$

where h is the specific enthalpy, T_0 is the standard temperature, equal to 298.15 K, and h_0 is the ideal gas enthalpy at T_0 fixed at 0 kJ/kg.

The integration of Eq. 1.3 leads to an expression containing the 20 parameters already cited and 7 additional parameters [Sievers, 1984]:

$$h(T, \rho) = h^0(T_0) + RT_B \left\{ -\frac{e_1}{3} \left[\left(\frac{T}{T_B} \right)^{-3} - \left(\frac{T_0}{T_B} \right)^{-3} \right] - \frac{e_2}{2} \left[\left(\frac{T}{T_B} \right)^{-2} - \left(\frac{T_0}{T_B} \right)^{-2} \right] + \right.$$
$$- e_3 \left[\left(\frac{T}{T_B} \right)^{-1} - \left(\frac{T_0}{T_B} \right)^{-1} \right] + e_4 \ln \frac{T}{T_0} + e_5 \left[\left(\frac{T}{T_B} \right) - \left(\frac{T_0}{T_B} \right) \right] +$$
$$\left. + \frac{e_6}{2} \left[\left(\frac{T}{T_B} \right)^2 - \left(\frac{T_0}{T_B} \right)^2 \right] + \frac{e_7}{3} \left[\left(\frac{T}{T_B} \right)^3 - \left(\frac{T_0}{T_B} \right)^3 \right] \right\} +$$
$$+ \left(2B - T \frac{dB}{dT} \right) \rho + \frac{1}{2} \left(3C - T \frac{dC}{dT} \right) \rho^2 +$$
$$+ \frac{1}{3} \left(4D - T \frac{dD}{dT} \right) \rho^3 + \frac{1}{4} \left(5E - T \frac{dE}{dT} \right) \rho^4 +$$
$$+ \frac{1}{5} \left(6F - T \frac{dF}{dT} \right) \rho^5 + (G + H\rho^2)\rho^2 \exp(-a_{20}\rho^2) +$$
$$+ \left(G - T \frac{dG}{dT} \right) \frac{1}{2a_{20}} [1 - \exp(a_{20}\rho^2)] +$$
$$+ \left(H - T \frac{dH}{dT} \right) \frac{1}{2a_{20}^2} [1 - (a_{20}\rho^2 + 1)\exp(-a_{20}\rho^2)] +$$
$$+ R(T - T_0) \ . \tag{1.4}$$

The new parameters are indicated with e_j for $j = 1, ..., 7$, and are reported in Appendix A, together with the derivatives B, C, D, F, G, and H. Appendix A shows also a MATLAB® program implemented to solve the Bender equations of density and enthalpy as a function of pressure and temperature.

1.5.2 Energy consumption for the circulation of CO_2 in supercritical extraction

The major problem in supercritical CO_2 extraction is the high installation costs required for the high pressure equipment and the high energy consumption since fluid compression and heating are needed to reach the supercritical state and to circulate the solvent after solute recovery [Halim *et al.*, 2012].

In fact, costs are reduced by recycling the CO_2. There are two possible schemes: one with a high pressure pump and another one with a compressor. They both have advantages and disadvantages, therefore an economic evaluation is needed to evaluate the two options. To compare the processes a CO_2 $p - h$ diagram will be used, that represents pressure as a function of enthalpy with parametric curves at constant temperature, entropy and volume.

The CO_2 pumping and circulation process is illustrated in Figure 1.7, where Figure 1.7a shows the process flow diagram and Figure 1.7b the CO_2 cycle in the $p - h$ diagram [Urieli, 2013]. CO_2 is collected in a vessel at 5 MPa and 10 °C. Before it is pumped, a cooling system is necessary to prevent cavitation (line $1 - 2$). Line $2 - 3$ represents the pressurization at constant entropy from 5 MPa to 20 MPa, with an increase in temperature up to 20 °C. CO_2 is then heated to reach the supercritical state before going into the extractor (line $3 - 4$, from 20 °C to 45 °C). The extraction is carried out at constant temperature and pressure, so when the mixture CO_2+solute leaves the extractor it is still at 20 MPa and 45 °C. Line $4 - 5$ is the lamination where the pressure goes down to 5 MPa at constant enthalpy. Point 5 is inside the bell, where vapor and liquid coexist, so the binodal line is traced leading to points 6 and 7. The mixture is then heated to separate the CO_2 from the solute up to point 8 and to recycle it. Before doing this, the gaseous CO_2 is brought back to the liquid state with a condensation from 8 to 1.

The values of enthalpy at each step of the process can be read in the $p - h$ diagram. The Bender equation allows to calculate enthalpy with Eq. 1.4, but the values differ from those of the diagram because of the reference state, that for the Bender equation is $h_0(T_0) = 0$ kJ/kg for $T_0 = 298.15$ K. However, the ΔH required to calculate the energy consumption will be equal in both cases, either using the Bender equation or the $p - h$ diagram. The enthalpy values at each step are reported in Table 1.1.

The energy cost is calculated assuming that the pump efficiency is 60%, cold water $(2.0 \cdot 10^{-5}$ \$/kJ) is used for cooling and steam $(3.18 \cdot 10^{-6}$ \$/kJ) for heating [Rosa and Meireles, 2005]. The cost of electricity is assumed equal to $7.4 \cdot 10^{-5}$ \$/kJ. The changes in enthalpy are calculated using the values reported in Table 1.1:

- pump (line $2 - 3$): -273 kJ/kg + 288 kJ/kg = 15 kJ/kg;
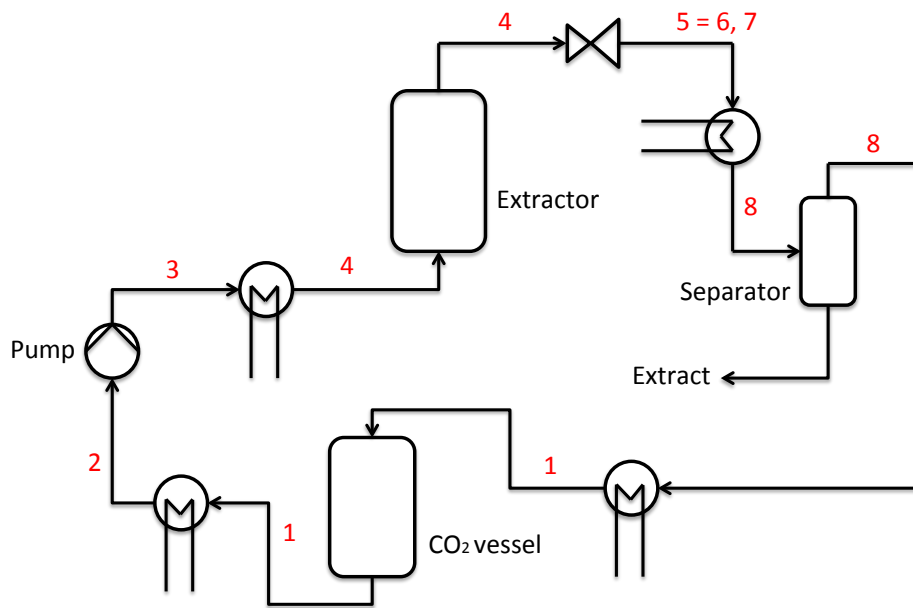
(a) *Process flow diagram.*
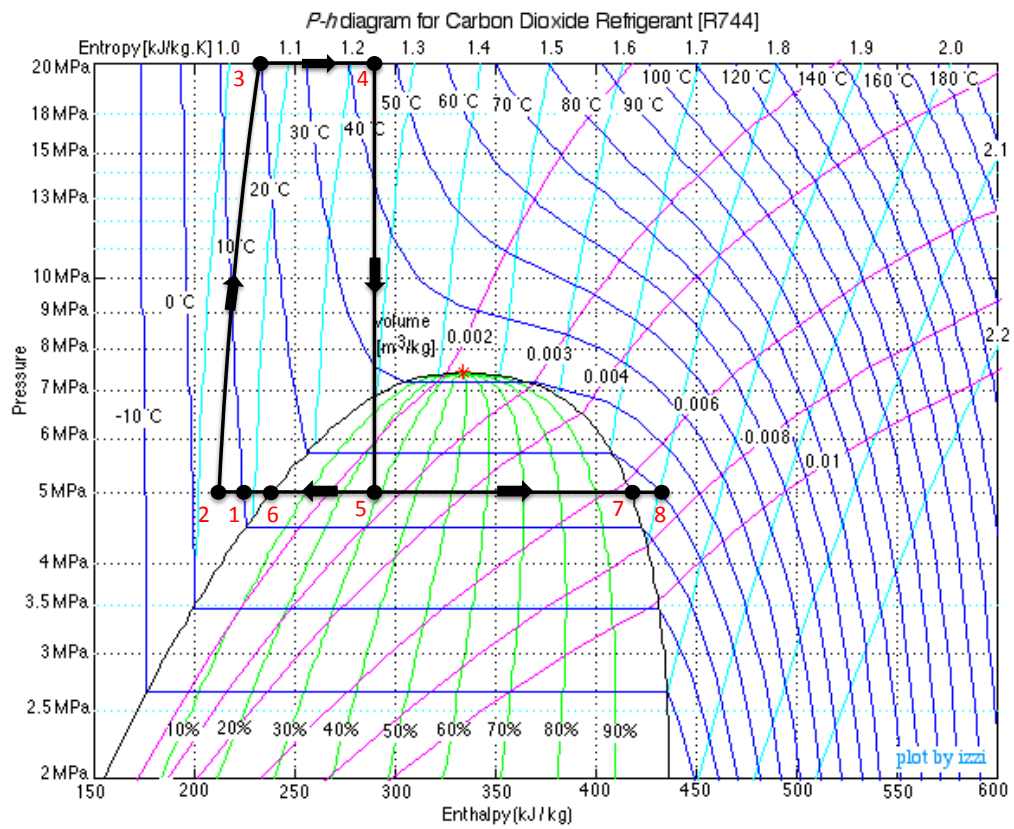
(b) *P-h diagram [Urieli, 2013].*

Figure 1.7: *Supercritical CO_2 extraction with high pressure pump.*

Table 1.1: *Enthalpy values in the pump process calculated with the Bender equation of state.*

Step	Pressure MPa	Temperature °C	Enthalpy kJ/kg
1	5	10	−282
2	5	8	−288
3	20	20	−273
4	20	45	−219
8	5	20	−74

These steps are referred to Figure 1.7

Table 1.2: *Enthalpy values in the compressor process calculated with the Bender equation of state.*

Step	Pressure MPa	Temperature °C	Enthalpy kJ/kg
1	5	20	−74
2	20	135	−10
3	20	45	−219

These steps are referred to Figure 1.8

- heater (line $3 − 4$): $−219 \, \text{kJ/kg} + 273 \, \text{kJ/kg} = 54 \, \text{kJ/kg}$;

- separator (line $4 − 8$): $−74 \, \text{kJ/kg} + 219 \, \text{kJ/kg} = 145 \, \text{kJ/kg}$;

- condenser+cooler (line $8 − 2$): $−288 \, \text{kJ/kg} + 74 \, \text{kJ/kg} = −214 \, \text{kJ/kg}$.

The cost of the energy consumed to circulate 1 kg of CO_2 is then:

$$C_{pump} = (145 + 54) \times 3.18 \cdot 10^{-6} + 214 \times 2.0 \cdot 10^{-5} + 15 \times 7.4 \cdot 10^{-5}/0.6 =$$
$$= 0.00676 \, \text{\$/kg}. \tag{1.5}$$

When the high pressure is achieved by a compressor, CO_2 does not need to be condensed before being compressed but it has to be cooled after it, since compression rises its temperature. Therefore, the circuit is now counterclockwise, as shown in Figure 1.8b. The process is illustrated in Figure 1.8a: CO_2 goes from its storage vessel, at 5 MPa and 20 °C, to the compressor, after which it reaches 20 MPa and 135 °C (line $1 − 2$). A cooler lowers the temperature down to 45 °C (line $2 − 3$), so that CO_2 is fed to the extractor at the same conditions as before (200 MPa and 45 °C). The pressure is then lowered from 20 MPa to 5 MPa (line $3 − 4$) and then heated up to 20 °C (line $4 − 1$), to separate the CO_2 from the product and recycle it.
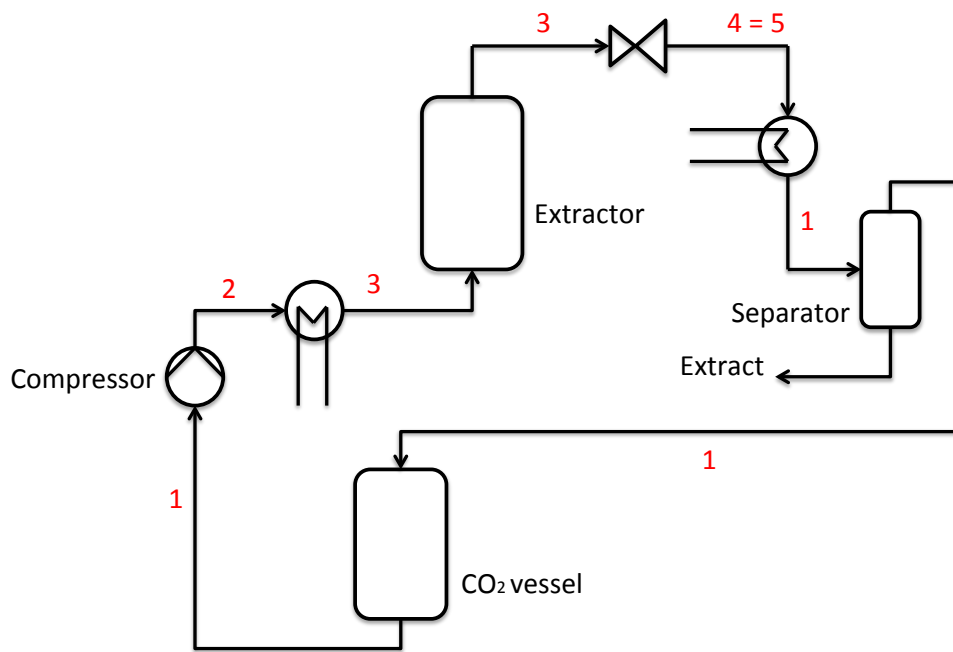
(a) *Process flow diagram.*
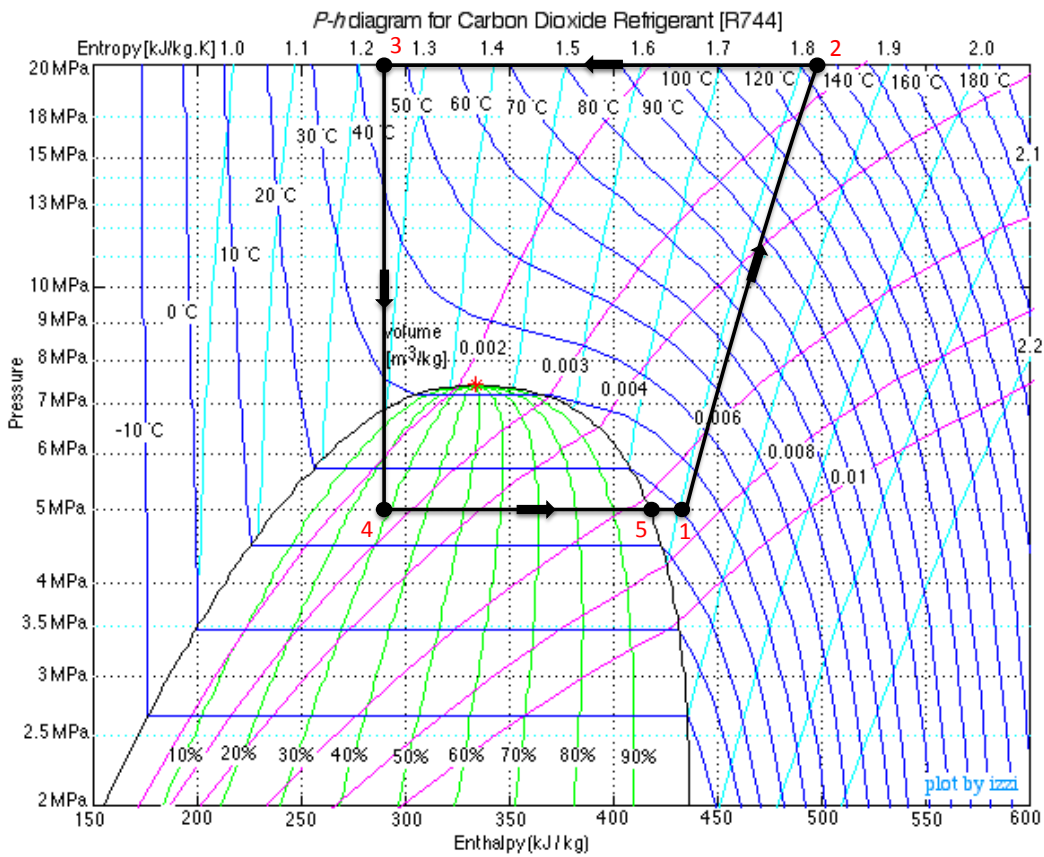
(b) *P-h diagram [Urieli, 2013].*

Figure 1.8: *Supercritical CO_2 extraction with compressor.*
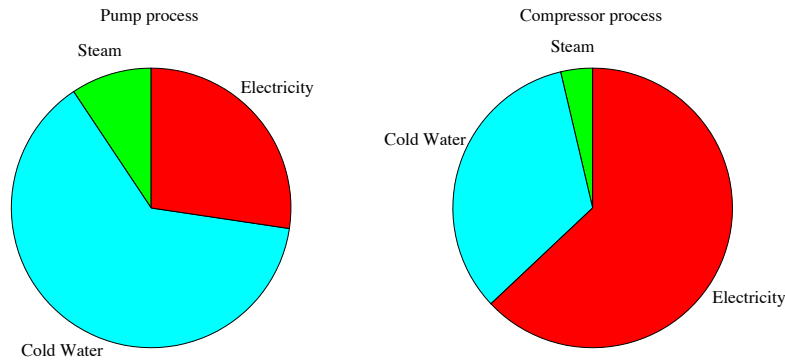
Figure 1.9: *Cost impact on pump and compressor processes.*

Table 1.3: *Costs comparison between pump and compressor processes.*

Pressure (MPa)	Energy Cost ($)	
	Pump	Compressor
10	0.005 80	0.006 54
20	0.006 76	0.0125
30	0.008 32	0.0154

The enthalpy at each step is calculated again with the Bender equation and it is reported in Table 1.2. The ΔH are:

- compressor (line $1 - 2$): $-10\,\text{kJ/kg} + 74\,\text{kJ/kg} = 64\,\text{kJ/kg}$;

- cooler (line $2 - 3$): $-219\,\text{kJ/kg} + 10\,\text{kJ/kg} = -209\,\text{kJ/kg}$;

- separator (line $3 - 1$): $-74\,\text{kJ/kg} + 219\,\text{kJ/kg} = 145\,\text{kJ/kg}$.

The energy costs necessary to circulate $1\,\text{kg}$ of CO_2 with the compressor are:

$$
\begin{aligned}
C_{compr} &= 145 \times 3.18 \cdot 10^{-6} + 209 \times 2.0 \cdot 10^{-5} + 64 \times 7.4 \cdot 10^{-5}/0.6 = \\
&= 0.0125\,\text{\$/kg}.
\end{aligned}
\tag{1.6}
$$

Figure 1.9 shows which costs have a greater impact on each process: in the pump process the condenser has more influence, while in the compressor process the more expensive one is the electricity required for the compressor. In the comparison at 20 MPa the compressor process resulted more expensive. Generally, this process should be more convenient when the pressure is not high so that the compression and cooling costs are reduced. Furthermore, unlike the pump process, it does not require a condenser, which has high equipment costs. Table 1.3 shows the energy cost at different pressures for the pump process and the compressor process: in this case the pump is always cheaper than the compressor. However, one

can see that there is a big difference from 10 to 20 MPa in the compressor costs, while the difference between 20 and 30 MPa is smaller. This shows that the compressor cost increases with pressure.

1.6   The aim of the work

The work of this thesis is divided in two parts: the experimental part and the modeling part.

The experimental part has been focused on obtaining the optimal conditions in supercritical CO_2 extraction of lipids from microalgae, with a laboratory plant built for the purpose. At first, particle size, humidity content, co-solvent flow rate and extraction time were optimized, then extraction pressure and temperature were varied to investigate their role in the process, since they influence considerably density, and therefore solubility. Pressure was varied between 15 and 30 MPa, while temperature from 45 to 65 °C. Furthermore, a Soxhlet apparatus was used to extract the oil with the conventional technique of solvent extraction and compared with supercritical extraction. Chapter 2 will present materials and methods employed during the experiments.

The experimental data collected during these tests were used to model the kinetics of the supercritical extraction process and the solubility of oil in supercritical CO_2. The kinetics was modeled using the principle of broken and intact cells, developed by Sovová [Sovová, 2005], whose objective was to describe the structure of the plant material and the extraction of vegetable oil from them. Nevertheless, it will be proved that this model is suitable for microalgae as well, and allows to calculate the parameters that govern the process. Three models based on the principle of broken and intact cells will be discussed and applied: the simplified model, the complete model and the model based on the evaluation of the characteristic times of the process [Sovová, 2012]. Chapter 3 will illustrate these model and the physical theories that support them, while results and discussions are presented in Chapter 4. Furthermore, a lipids profile analysis was performed after the experiments to investigate the influence of pressure, temperature and extraction time in lipids composition, to compare supercritical CO_2 extraction with solvent extraction, and to compare three different strains of microalgae: *Scenedesmus obliquus*, *Chlorella protothecoides*, and *Nannochloropsis salina*. These results are showed in Chapter 4, section 4.4.

The modeling part contain also a solubility modeling with an empirical approach, using three expressions: Chrastil equation [Chrastil, 1982], Del Valle-Aguilera equation [Del Valle and Aguilera, 1988] and Adachi-Lu equation [Adachi and Lu, 1983]. These expressions correlate the solubility of oil in supercritical CO_2 with its density, differing from each other in the number of adjustable parameters, since the second and third equations are modifications

of the first one. Chapter 5 will extensively discuss the role of solubility in supercritical CO_2 extraction and its dependence from pressure, temperature and density.

Chapter 2

Materials and methods

Supercritical extraction experiments were performed at the laboratory scale, in a plant assembled for the purpose. For solvent extractions a Soxhlet apparatus was used.

This chapter will describe procedures and materials used to carry out the experimental runs.

2.1   Chemicals and microalgae

Carbon dioxide and ethanol were used for supercritical extraction, while the mixture for the solvent extraction was methanol and chloroform 2:1. Hexane was used to store the samples until the analysis. Carbon dioxide, 4.0 type, with purity greater than 99.99% was provided by Rivoira. The solvents were purchased from Sigma Aldrich, with a purity of 99.8% for hexane, methanol and chloroform, and a purity greater than 99.8% for ethanol.

Microalgae were obtained from SAG-Goettingen. The strains used in the experiments were: *Scenedesmus obliquus* 276-7, *Chlorella protothecoides* 33.80, and *Nannochloropsis salina* 40.85. The first two strains are freshwater species while *N. salina* is a marine species. The growth temperature was 24 ± 1 °C, with artificial lighting (fluorescent tubes) under a continuous photon flux density of 150 ± 10 Eμm^{-2}s^{-1}, measured by a photoradiometer (LI-COR, Model LI-189). *C. protothecoides* and *S. obliquus* were grown in BG11 medium, following SAG indications. *N. salina* was cultured in sterilized sea salts with 22 g/L solution enriched with $f/2$ Guillard solution modified by adding an excess of 1.5 g/L of NaNO$_3$. Medium was buffered with 40 mM Tris–HCl pH 8, to avoid alterations due to excess CO$_2$ supply. Maintenance and propagation of cultures were performed using the same medium added with 10 g/L of Plant Agar (Duchefa Biochemie). These conditions had been previously optimized in our laboratory [Sforza *et al.*, 2012, 2013].

Before extraction, microalgae needs to be dried and milled. Indeed, it is favorable to

have a low moisture content, since water could compromise the extraction diminishing the contact between solvent and solute [Mercer and Amenta, 2011]. For that purpose, after harvest, microalgae were then centrifuged at 24 °C and 4425 rpm for 10 minutes, and left inside an oven for 2 days at 37 °C, to reduce the water content. The moisture was calculated leaving a microalgae sample inside the oven for one day at 80 °C and measuring the mass loss. The moisture content left in the three microalgae strains was: 8% in *Scenedesmus obliquus*, 16% in *Chlorella prototheicoides*, and 20% in *Nannochloropsis salina*. The dried samples were then ground and sieved with a filter in order to obtain a particle diameter less than 0.5 mm.

2.2   Soxhlet extractor

Solvent extraction was performed in a laboratory apparatus, called Soxhlet. A typical Soxhlet extractor is shown in Figure 2.1. This extractor is characterized by three parts: a lower chamber with the solvent, an upper chamber with the solid material and a condenser with cold water. The lower chamber is heated to evaporate the solvent that passes, through an extern tube called "distillation arm", to the upper chamber. The condenser is composed by two concentric tubes, where cold water is passed externally to condense the solvent that drips down to the upper chamber. Inside this chamber there is a "thimble" with the solid material in it. The thimble is made from thick filter paper, so that the solute can pass through it but not the solid. The upper chamber is then filled with solvent that impregnates the material and extracts the solute. From the bottom, a little tube, the "siphon side arm", connects the upper chamber with the lower one. Therefore the solvent fills the upper chamber until the pressure inside the siphon arm goes down and swallows up the solvent (plus the extract) back again to the lower chamber. The process goes on until all the solute is extracted.

To extract lipids from microalgae a mixture of methanol and chloroform (2:1) was used as the solvent [Mercer and Amenta, 2011]. The extraction was conducted at 105 °C for 18 hours. Then, a rotary evaporator was used to remove the solvent from the extract. This apparatus, represented in Figure 2.2, is characterized by two chambers (the evaporation flask and the collecting flask), a condenser and a water bath. The evaporating flask, with the mixture that has to be separated, is placed in a water bath and rotates with a velocity set manually by the speed controller. The water bath is heated so that the solvent can evaporate leaving the solute in the flask. The gas goes then inside the condenser, where cold water passes inside a serpentine, and returns to the liquid state, dropping inside the collecting flask. A vacuum pump is used to decrease the pressure inside the evaporator system.

The water bath temperature was kept at 40 °C. The process took place until all the solvent was evaporated, so that only the solute remained in the evaporation flask. At this point, the
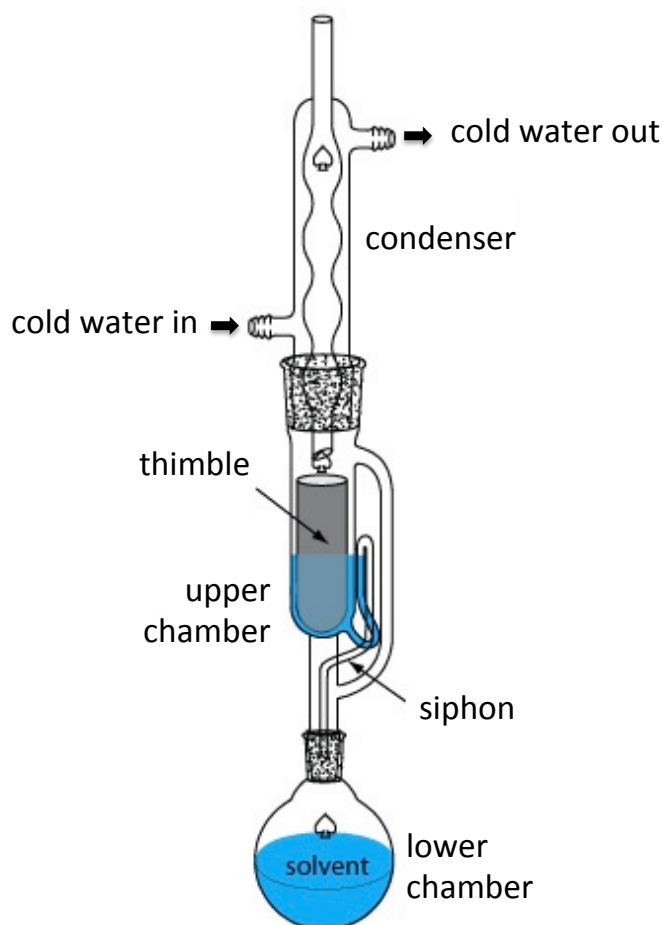
Figure 2.1: *Soxhlet extractor.*

oil was weighed to calculate the extraction yield as the ratio of the amount of oil over the initial mass of microalgae (weighed before the experiment).

2.3 Supercritical CO_2 extraction plant

The supercritical extraction plant has been constructed with high pressure equipment supplied by Swagelok. The process flow diagram of the experimental setup is illustrated in Figure 2.3. The CO_2 is stored in a tank, and then it passes in a container located before the pump to ensure a continuous flow rate. This container is equipped with a manometer and a vent valve. The pressure indicated in the manometer aims to let us know if the CO_2 is sufficient to be pumped, while the vent valve is activated when the pressure exceeds 9 MPa. Before the pump, a heat exchanger lowers the CO_2 temperature to makes it liquid, in order to prevent the pump cavitation. The heat exchanger is a serpentine with concentric tubes where the CO_2 is the inner stream and ethylene glycol solution, cooled by a chiller, is the outer stream. A
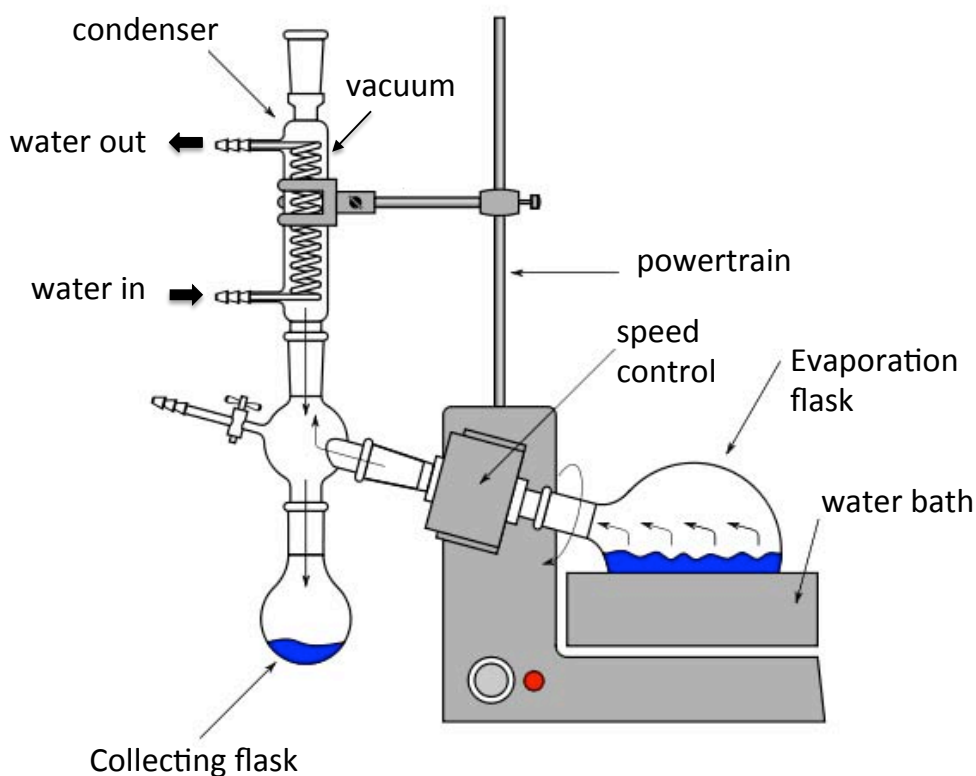
Figure 2.2: *Rotary Evaporator.*

temperature controller keep the temperature before the pump at 5 °C. The desired pressure is fixed with a regulator in the pump, and a manometer verifies that the pressure is reached. The supercritical temperature is achieved by an insulated electrical resistance that is placed around the tube before the extractor. A temperature regulator ensures a constant temperature. After that, a manometer indicates the pressure right before the extractor. The co-solvent is pumped with a HPLC (High Pressure Liquid Chromatography) pump, that is connected to a little ethanol vessel. The CO_2 and the co-solvent line are joined by a tee. The CO_2-ethanol mixture flows through the extractor where the microalgae are placed. The extractor is characterized by two pieces made of stainless steel that are screwed one with the other. The microalgae extractor chamber is a cylindric chamber with a diameter of 15 mm and a length of 15 mm. Other geometric specifications are reported in Appendix B. A resistance, placed around the extractor, keeps constant the temperature. On the bottom of the extractor, a filter is placed to avoid the passage of solid particles. The expansion valve (a Medium-Flow High-Pressure Metering Valve) follows the extractor and regulates the CO_2 flow rate. A water bath (kept at 40 °C) heats the valve in order to prevent freezing of the solvent. The collecting vessel is placed after the valve, where CO_2 in its gaseous state, is automatically separated from the oil, that is collected in the separation chamber. A flow meter and a volumetric
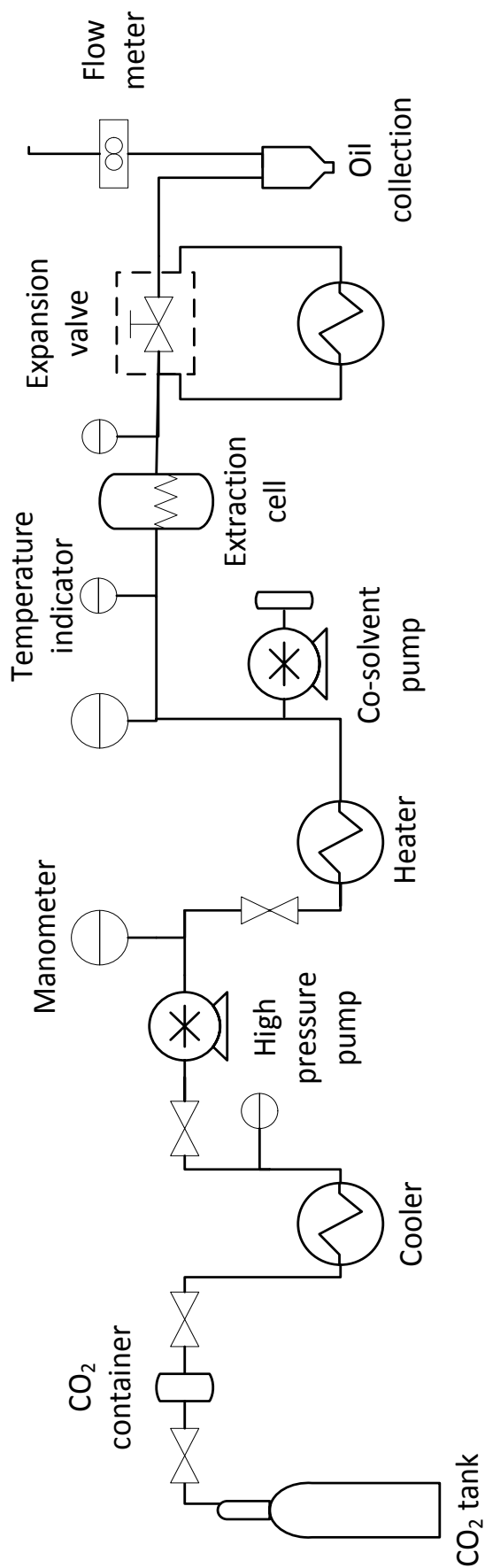
Figure 2.3: *Supercritical CO₂ extraction flow diagram.*
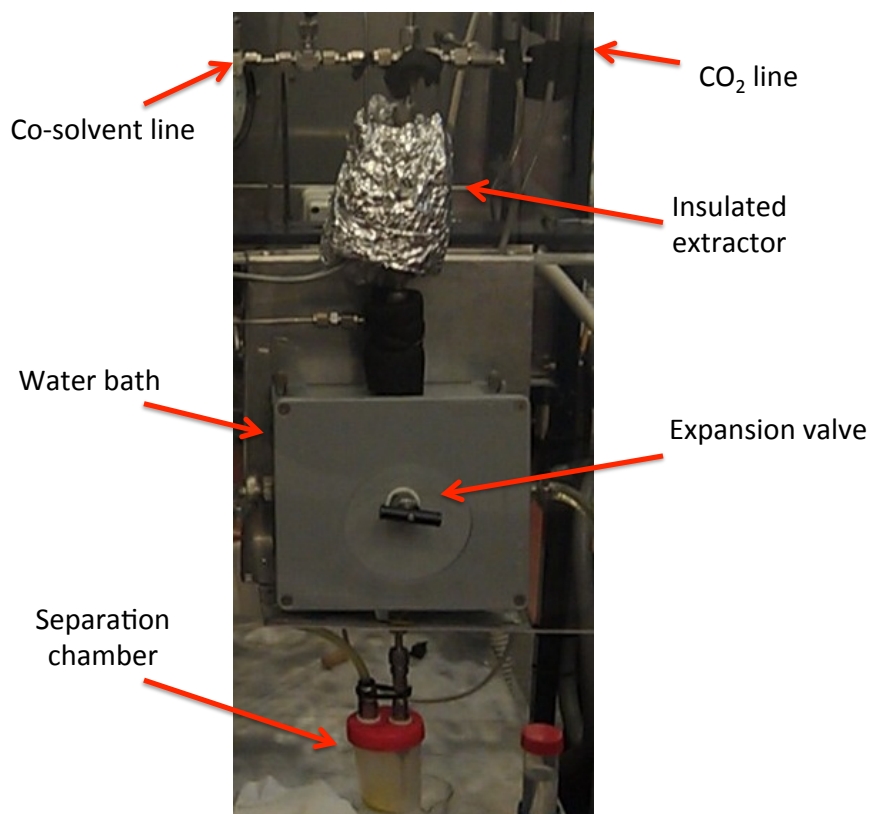
Figure 2.4: *Extractor and separation chamber.*

counter measure the CO_2 flow rate and the passed volume. Figure 2.4 shows the section of
the plant with extractor and separation chamber.

At the end of each extraction, the oil was stored in 12 mL of ethanol. A rotary evaporator
(Figure 2.2) was used to separate oil and ethanol, and then the oil remained was weighed.

The experiments can be divided in two blocks. The first test runs were focused on find-
ing the optimal particle size, ethanol flow rate and quantity of microalgae loaded into the
extractor. Afterwards, these values were kept fixed, and the experiments were performed
at different operative conditions to understand the influence of pressure and temperature on
supercritical extraction. Indeed, density depends upon them, and therefore solubility, which
in turn depends on density. The operating extraction pressures were 15, 20, 25, and 30 MPa,
while the extraction temperatures were 45, 55, and 65 °C. All the experiments were performed
with a constant CO_2 flow rate of 0.4 kg/h. Extraction time was also varied, between 30 and
90 minutes, to investigate its influence on microalgae lipids composition. The oil samples
were collected in each experiments every 15 minutes: for example, with an extraction of
90 minutes, 6 samples were collected, showed in Figure 2.5. The green color is due to the
microalgae chlorophyll, and it becomes lighter from the first samples to the last ones. As
expected, the first samples contain more oil than the last samples, since in the first part of the

Figure 2.5: *Microalgae lipids samples collected with ethanol during the experiment.*

extraction the microalgae lipids content is higher and decreases along the extraction.

The experimental data were used to model supercritical CO_2 extraction of lipids from microalgae, with a model based on broken and intact cells, developed by Sovová [Sovová, 2005]. This model is discussed in the next chapter, while the results are reported in Chapter 4.

2.4   Analysis of free fatty acids

The extract is a complex mixture of lipids, pigments, waxes and other compounds. After each experiment, the fatty acids composition of the extract was measured by gas chromatography. The method was performed according to reported procedures [Jenkins, 2010; Sukhija and Palmquist, 1988]. A GC Agilent Technologies (Model 7890) with a FID detector was used. The columns were Supelco (75 m $\times$ 180 μm $\times$ 0.14 μm film thickness) Model 23348-U, and J&W (3.8 m $\times$ 250 μm $\times$ 0.25 μm film thickness) Model 190915-431.The carrier gas was H_2.

These analyses allowed to compare the free fatty acids composition of the oil extracted from different microalgae strains (*S. obliquus*, *C. protothecoides* and *N. salina*), using different techniques (supercritical CO_2 extraction and solvent extraction) and different operative conditions in the case of supercritical extraction.

Chapter 3

Modeling of supercritical fluid extraction

There are many models that describe the supercritical extraction process, all of them based on different assumptions and equations. In this case, the model based on broken and intact cells, developed by Sovová [Sovová, 2005], was chosen because it illustrates particularly well the microalgae structure after the pre-treatment. Although it was built at first to describe the supercritical fluid extraction of vegetable oil from plants, it will be shown that it works as well with the extraction of oil from microalgae.

The model allows to calculate the values of the parameters that govern the process. Several steps are followed to calculate these parameters, starting from the evaluation of the experimental extraction curve, through a simplified model based on two parameters, to apply finally the mathematical model based on three parameters. Moreover, another simplified model is described, also developed by Sovová, with slightly different equations that allow to calculate the characteristic times of the process steps [Sovová, 2012].

3.1 Supercritical fluid extraction models

The models used to describe the process have different complexity that depends on the equations used to characterize the extraction process and on the number of parameters.

During the process, the oil inside the cells migrates from the particle to the solvent bulk, so the model should describe both the mass transfer inside the particle (solid phase) and the mass transfer from particle to the solvent bulk (fluid phase). Therefore the extraction process is represented with mass balance equations for the solute, both in the solid phase and in the fluid phase. The differences are in the characterization of phase equilibrium, solvent flow pattern and solute diffusion in the solid phase.

Phase equilibrium depends on pressure and temperature of the system and on the compositions of the solvent, the solute and the solid matrix [Sovová, 2005]. Two cases should be

distinguished: one with high solute concentration and another one with low solute concentration. In the first case, the solubility of the solute in the solvent achieves the phase equilibrium value. This happens in the first period of the extraction, when the oil is still in the particles at high concentration. Going on with the extraction, the concentration decreases and then the phase equilibrium is no longer equal to solubility but lower. In this case the process is governed by mass transfer and solute-matrix interaction.

The solvent flow pattern is particularly important in the first period of the extraction. The plug flow is the ideal flow pattern, since the solvent velocity is radially homogeneous and it ensures a good distribution and high extraction performance. However, in a real extractor axial dispersion, the risk of channeling and natural convection should be taken into account. Axial dispersion occurs mostly when the ratio between length and diameter of the bed is low; the risk of channeling is high when the bed is tightly packed; natural convection is a consequence of density gradients caused by differences in concentration or in temperature (supercritical CO_2 has, indeed, a low kinematic viscosity that makes it vulnerable to natural convection). Usually, two ideal flow patterns are used in supercritical fluid extraction models: plug flow and ideal mixer, the former for longer extraction beds and the latter for shorter ones.

Finally, the solute diffusion in the solid phase is important in the second period of the extraction, when the concentration is low and the internal mass transfer resistance governs the process. So, the particles shape, size, surface area, and, above all, the structure of the material should be considered. Also, the solute-matrix interaction should be taken into account.

The models can be divided in two groups: the one-stage models and the model based on complex structure of the solid material [Sovová and Stateva, 2011]. The first category considers the process characterized by one single stage, while the second type of models is more focused on the description of the structure of the material and divides the extraction in several periods, each one governed by different parameters.

The one-stage models are the diffusion model, the desorption model and the shrinking core model. The first one considers the material as an homogeneous and non-porous solid and characterizes the process with: internal diffusion in the particle, phase equilibrium at the surface and external mass transfer from the surface to the bulk fluid. The desorption model differs from the first one because it considers porous material and solute desorption from the pore walls, followed again by internal diffusion, phase equilibrium at the surface and external mass transfer. The shrinking core model consider the particle characterized by a core, full of solute, that initially fills the particle. During the extraction, the core dimensions decrease because the solute moves through its boundary, dissolves in the solvent and then diffuses through the external shell of the particle.

The models based on complex structure of the particle comprehend the models based on
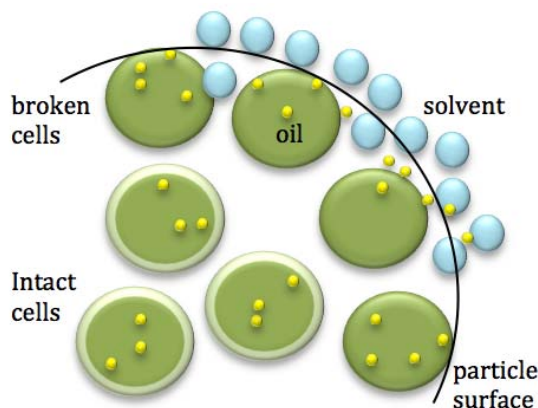
Figure 3.1: *Simplified representation of the particle structure according to the model of broken and intact cells.*

plant microstructure, the models for supercritical fluid extraction of mixture and the model of broken and intact cells. The first one describes the structure, shape and location of secretory structures, investigating their behavior during the extraction. The second one is specific for the extraction of many components, with different solubility, from the same material. Finally, the model of broken and intact cells is extensively discussed in the next section, being the one applied in the present work.

3.2   The model of broken and intact cells

The structure of the microalgae particles is very simple, being the microalgae a primitive unicellular organism. Furthermore, microalgae withstand a mechanical pre-treatment before they are loaded into the extractor. The model of broken and intact cells describes exactly the structure of the particle with broken cells as a result of the pre-treatment. During the milling, the particles suffer a big stress and the cells near the surface break their walls making the solute more accessible [Sovová and Stateva, 2011].

Therefore, as shown in Figure 3.1, two regions can be distinguished in the particle: the region of broken cells near the surface with easy accessible solute and another region, in the core, with intact cells that were not affected by the mechanical pre-treatment.

These considerations lead to divide the extraction process in two periods. In the first extraction period the free solute inside the broken cells goes easily from the particle to the solvent (Figure 3.2a). The process is governed by the external mass transfer resistance and the solubility is usually equal to the phase equilibrium since the solute concentration is high. The extraction during this period is fast as the external mass transfer resistance is low (the external mass transfer coefficient, inversely related to the resistance, is indeed high). At the end of this extraction period the easy accessible solute is depleted and the oil inside the intact
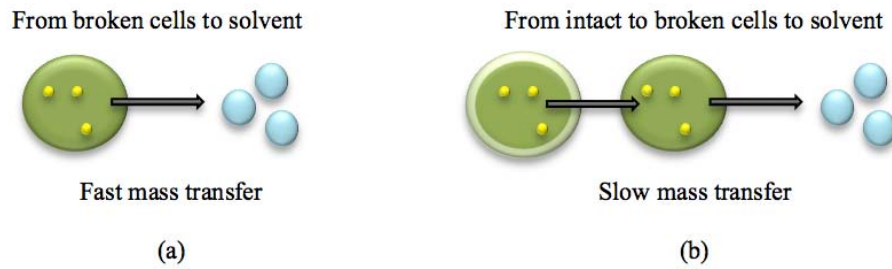
Figure 3.2: *Simplified representation of solute transfer from the matrix to the solvent, according to the model of broken and intact cells, in the first extraction period (a) and in the second extraction period (b).*

cells starts going from the intact cells to the broken cells and then from the broken cells to the solvent (Figure 3.2b). This time the process is governed by the internal mass transfer resistance, the extraction process is slower, and the external mass transfer resistance can be neglected, being several orders of magnitude lower than the first one.

The most important parameters that govern the entire extraction process are:

- *the external mass transfer coefficient, k_f.* This parameter is inversely proportional to the external mass transfer resistance, θ_e, and governs the first extraction period in which the oil goes from the broken cells to the solvent;

- *the grinding efficiency, r,* namely the fraction of broken cells. It indicates how effective was the pre-treatment;

- *the internal mass transfer resistance, k_s.* This one, similarly to the other mass transfer coefficient, is inversely proportional to the internal mass transfer resistance, θ_i, and governs the second extraction period. In the model equations the product between k_s and a_s is often considered, where a_s is the specific area between the regions of intact and broken cells.

3.3   Model equations

The Sovová model is characterized by equations for the mass balances, the phase equilibrium and the mass transfer that allow to calculate the extraction curve [Sovová, 2005]. The equations for the extraction curve are fitted to experimental data to calculate and optimize the parameters r, k_f and $k_s a_s$.

To solve the mass balance equations, dimensionless parameters are introduced and different equations are formulated for the two extraction periods, both in the cases of plug flow or ideal mixer. Furthermore, a transition period is considered between the first and the second extraction period, which represents the passage from the period governed by solubility to

the one governed by internal mass transfer. These equations, published by Sovová in 2005, represent a new general model that extends the group of models based on broken and intact cells [Sovová, 2005]. From this model, an approximated version is derived (always made by Sovová) to evaluate the extraction curve and to estimate the model parameters. Previously, other authors applied this mathematical method to fit supercritical fluid extraction curves [Mouahid *et al.*, 2013].

3.3.1 Mass balance equations

It is assumed that the solute is homogeneously distributed in the microalgae particles, that solvent density is not affected by the solute dissolved in the solvent, and that the characteristics of the bed (porosity, surface area, etc.) are not affected by the reduction of the oil content in the solid during the extraction. The mass balances are written for plug flow, per unit volume of extraction bed.

The mass balance equations are written for the solute in three phases [Sovová, 2005]: the fluid phase (Eq. 3.1), the solid phase with broken cells (Eq. 3.2) and the solid phase with intact cells (Eq. 3.3). For the mass balance in the fluid phase the accumulation part and the convective part have to be considered:

$$\rho_f \varepsilon \left(\frac{\partial y}{\partial t} + U \frac{\partial y}{\partial z} \right) = j_f \, , \tag{3.1}$$

where: ρ_f is the solvent density, ε is the porosity, y is the solute concentration in the fluid phase, t is the extraction time, U is the interstitial velocity, z is the axial coordinate, j_f is the flux from broken cells to solvent.

In the solid phase with broken cells there is no convective term and the flux from intact cells to broken cells is included, that in the previous equation was supposed to be equal to zero:

$$r \rho_s \left(1 - \varepsilon \right) \frac{\partial x_1}{\partial t} = j_s - j_f \, , \tag{3.2}$$

where: r is the grinding efficiency, ρ_s is the solid density, x_1 is the solute concentration in broken cells, j_s is the flux from intact cells to broken cells, and the others were already defined previously.

Finally, in the solid phase from intact to broken cells only the flux in the solid phase affects the accumulation of solute over time:

$$(1 - r) \rho_s \left(1 - \varepsilon \right) \frac{\partial x_2}{\partial t} = -j_s \, , \tag{3.3}$$

where x_2 is the solute concentration in intact cells and all the other variables are already

defined.

To solve the differential equations 3.1, 3.2, and 3.3, the initial concentrations are used as boundary conditions:

$$y|_{t=0} = y_0; \qquad \frac{y}{y_0}\Big|_{z=0} = 0; \qquad x_1|_{t=0} = x_{1,0}; \qquad x_2|_{t=0} = x_{2,0}; \qquad (3.4)$$

where y_0 is the initial solute concentration in the fluid phase while $x_{1,0}$ and $x_{2,0}$ are the initial solute concentrations in broken and intact cells, respectively.

3.3.2 Phase equilibrium equations

To write the phase equilibrium equations the solute-matrix interaction should be taken into account. A solute concentration x_t is then defined, that indicates the capacity of the matrix for interaction with the solute. Above this concentration, solubility is equal to phase equilibrium, while below x_t it depends on a partition coefficient:

$$\begin{aligned} y^*\left(x_1\right) &= y_s \,, & for\ x_1 > x_t \,, \\ y^*\left(x_1\right) &= Kx_1 \,, & for\ x_1 \leq x_t \,, \end{aligned} \qquad (3.5)$$

where: $y^*\left(x_1\right)$ is the equilibrium fluid phase concentration, y_s is the thermodynamic solubility of the solute in the solvent and K is the partition coefficient.

3.3.3 Mass transfer equations

To solve the mass balance equations, fluxes j_f and j_s have to be defined, being aware that for j_f the discontinuity of the phase equilibrium has to be considered. Therefore, the flux from broken cells to the solvent is defined as:

$$\begin{aligned} j_f &= k_f a_0 \rho_f \left(y^* - y\right) \,, & for\ y < Kx_t \,, \\ j_f &= 0 \,, & for\ y \geq Kx_t \,, \end{aligned} \qquad (3.6)$$

where all the variable have already been defined except a_0, that is the specific surface area per unit volume of extraction bed.

The flux from intact cells to broken cells is:

$$j_s = k_s a_s \rho_s \left(x_2 - x_1\right) \,. \qquad (3.7)$$

3.3.4 Extraction curve equation

The amount of oil extracted, E, collected during the extraction is calculated as:

$$E = \dot{Q} \int_0^t y|_{z=Z} \, \mathrm{d}t \,, \tag{3.8}$$

where $\dot{Q}$ is the solvent flow rate and Z is the length of the extraction bed.

The extraction curve represents the extraction yield as a function of the amount of solvent passed during the extraction. This curve allows to find and optimize the variables that govern the process. In order to calculate them, the model of the extraction curve is fitted with experimental data and the model parameters are adjusted to. The experimental data and the model equations necessary for the fitting are explained in the following paragraphs.

3.4 Input data

The initial data are:

- The extraction pressure, $\boldsymbol{P}$;
- The extraction temperature, $\boldsymbol{T}$;
- The extraction time, $\boldsymbol{t}$;
- The extractor dimensions, $\boldsymbol{D}$ and $\boldsymbol{L}$;
- The mass of microalgae loaded into the extractor, $\boldsymbol{N}$;
- The microalgae humidity, $\boldsymbol{u}$;
- The microalgae density and the ethanol density, $\boldsymbol{\rho_s}$ and $\boldsymbol{\rho_{EtOH}}$;
- The mass of extract, $\boldsymbol{E}$;
- The volume of CO_2 passed during the extraction, $\boldsymbol{V}$.

Pressure, temperature and mass of microalgae loaded into the extractor are set for each experiment, while the microalgae humidity and density are measured before the experiments for each type of microalgae. The mass of extract and the volume of CO_2 passed during the extraction are collected during the experiment. Therefore, all the variables required by the model can be calculated from them. They are:

- The experimental extraction yield, $\boldsymbol{e_{exp}}$;
- The relative amount of passed solvent, $\boldsymbol{q}$;
- The solvent density, $\boldsymbol{\rho_f}$;
- The solubility of the solute into the solvent, $\boldsymbol{y_s}$;
- The bed porosity, $\boldsymbol{\varepsilon}$;

- The specific surface area per unit volume of extraction bed, a_0;
- The solvent to matrix ratio in the bed, γ.

3.4.1 Experimental extraction yield and amount of passed solvent

The experimental extraction yield, e_{exp}, is expressed as the ratio between the mass of extract and the insoluble mass of microalgae loaded in the extractor, N_m:

$$e_{exp} = \frac{E}{N_m} \ . \tag{3.9}$$

The relative amount of passed solvent, q, is the ratio between the mass of passed solvent, M, and N_m:

$$q = \frac{M}{N_m} \ . \tag{3.10}$$

Since the volume of passed solvent V is measured from experiments, M can be calculated as ρV, being ρ the CO_2 density at atmospheric pressure and temperature, equal to $1.81 \ \text{kg/m}^3$.

The mass of insoluble solid, N_m, is calculated as:

$$N_m = (1 - c_u) \, N \ , \tag{3.11}$$

where c_u is the solute content in the untreated solid, expressed in weight fraction, and N is the solid loaded in the extractor. The value of c_u is equal to the asymptotic extraction yield at infinite time and it is calculated by a preliminary fitting of the model equations on experimental data. It is possible then to calculate the weight fraction in the untreated solid, x_u, with the relation:

$$x_u = \frac{c_u}{1 - c_u} \ . \tag{3.12}$$

3.4.2 Density and solubility

Density plays an essential role in the supercritical extraction because the solubility of the oil into the solvent is correlated to it, as will be discussed in Chapter 5.

Recalling that the solvent used for the extraction is a system with supercritical CO_2 and 6% of ethanol, the solvent density is calculated as:

$$\frac{1}{\rho_f} = \frac{0.94}{\rho_{CO_2}} + \frac{0.06}{\rho_{EtOH}} \ , \tag{3.13}$$

where ρ_{CO_2} is the supercritical CO_2 density and ρ_{EtOH} is the ethanol density. The CO_2 density is a function of the extraction pressure and temperature and it is calculated using the Bender equation of state (Eq. 1.1, in Chapter 1), while the ethanol is considered an incompressible fluid and its density is calculated from the correlation:

$$\tilde{\rho} = \frac{C_1}{C_2^{1+(1-T/C_3)^{C_4}}} \ .$$

(3.14)

where $\tilde{\rho}$ is the molar density, expressed in mol/dm^3, T is the temperature expressed in K and C_1, C_2, C_3 and C_4 are constant that depends on the component. For ethanol, they are: $C_1 = 1.6288, C_2 = 0.27469, C_3 = 514$ and $C_4 = 0.23178$ [Poling *et al.*, 2008]. The mass density is then calculated using the molecular weight of the ethanol (46.068 g/mol).

The solubility is calculated from experimental data, being the slope of the first part of the extraction curve. There is a relation between solubility and density, since the first one can be expressed as a function of the second one, using the Chrastil model or others (this relation will be discussed more extensively in Chapter 5).

3.4.3 Bed characteristics

The characteristics of the bed, determined from experimental data, are the porosity and the specific surface area per unit volume of extraction bed.

The porosity is the void fraction of the solid bed and it is calculated knowing the apparent density and the real density of the microalgae. The apparent density is the ratio between the mass of the microalgae loaded in the extractor and its volume, while the real density is calculated measuring the displaced volume of ethanol in a test tube with a known volume of ethanol after immersing a known amount of microalgae. The porosity is then:

$$\varepsilon = 1 - \frac{\rho_a}{\rho_s} \ ,$$

(3.15)

where ρ_a is the apparent density and ρ_s is the real density. The specific surface area per unit volume of extraction bed, a_0 is calculated assuming spherical particles:

$$a_0 = 6\frac{1-\varepsilon}{d} \ ,$$

(3.16)

where d is the particle diameter.

Once the solvent density, the solid density and the bed porosity are known, it is possible

to calculate the solvent to matrix ratio in the bed, γ, expressed as:

$$\gamma = \frac{\rho_f \varepsilon}{\rho_s (1 - \varepsilon)} \ .$$

(3.17)

The extraction curve is then obtained fitting the equations of the Sovová model to the experimental data. The adjustable parameters are the grinding efficiency, r, the external mass transfer coefficient, k_f, and the product between the internal mass transfer coefficient and the specific area between broken and intact cells, $k_s a_s$. Before applying these equations, a simplified model is used to have a first estimation of r and $k_s a_s$. These results are then used as initial values of the complete model characterized by three equations: one for the first extraction period, one for the transition period and another one for the second extraction period.

All the equations, for both the simplified model and the complete model, are written considering the hypothesis of plug flow without solute-matrix interaction.

3.5 Simplified model

A simplified version of the model of broken and intact cells is characterized by two equations that describe the extraction yield, e, in the two extraction periods:

$$e = q y_s \ , \qquad\qquad for \ 0 \leq q \leq q_c \ , \qquad (3.18)$$

$$e = x_u \left[1 - C_1 \exp(-C_2 q) \right] \ , \qquad for \ q > q_c \ , \qquad (3.19)$$

where x_u is the solute weight fraction in the untreated solid, q_c is the relative amount of passed solvent at the end of the first extraction period and C_1 and C_2 are the adjustable parameters. It can be seen from Eq. 3.18 that in the simplified model the yield of the first extraction period does not depend on the external mass transfer resistance, but only on the solubility y_s. In this hypothesis the solubility is that of phase equilibrium but this period should be also influenced by the external mass transfer resistance, as will be seen in the complete model. Accordingly, the extraction yield is then described by a straight line, and it proceeds very fast compared to the second period. Furthermore, it is underlined that the extraction is fast from the very beginning of the experiment, since it is preceded by a period of static extraction in which the solute is dissolved in the solvent but does not come out of the extractor.

The second extraction period is instead described by Eq. 3.19, and the parameters C_1 and C_2 are calculated fitting the expression with the experimental data, using the programming language MATLAB®. The passed solvent at the end of the first period, q_c, is also calculated
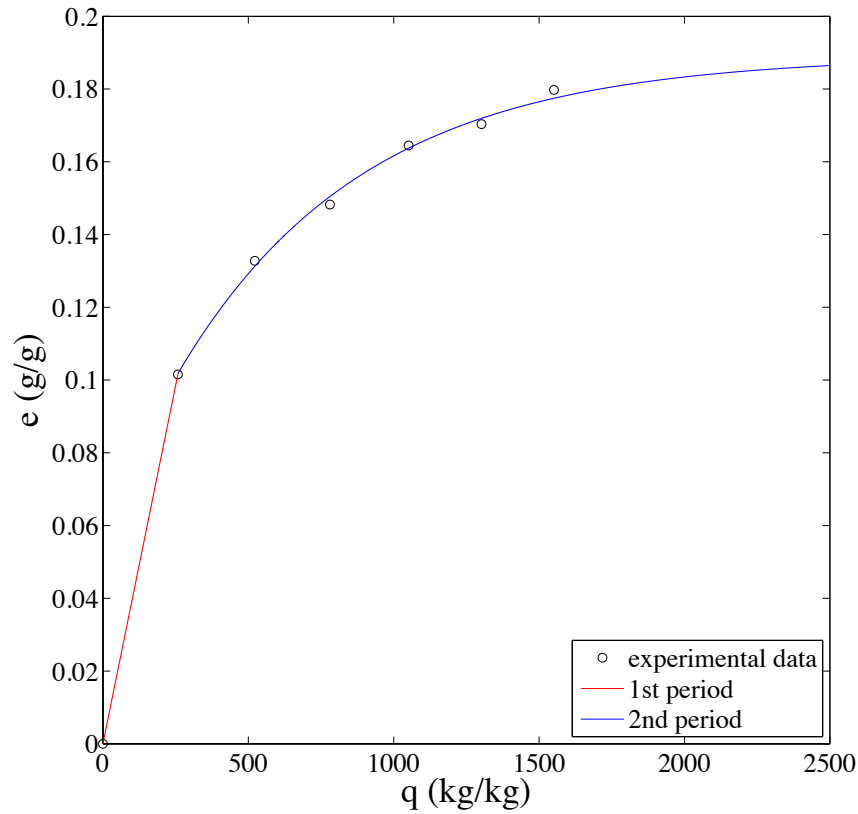
Figure 3.3: *Simplified model applied to the $SCCO_2$ extraction of oil from microalgae at 30 MPa and 45 °C; fitted values: $r = 0.44$, $k_s a_s = 2.71 \cdot 10^{-5}$ m^{-1}s^{-1}*

imposing the second equation equal to the first one, with q_c as unknown value. When C_1, C_2, and q_c are calculated, the grinding efficiency and the internal mass transfer coefficient are calculated with the following equations:

$$r = 1 - C_1 \exp\left(-\frac{C_2 q_c}{2}\right) , \qquad (3.20)$$

$$k_s a_s = (1 - r)(1 - \varepsilon)\dot{Q}\frac{C_2}{N_m} . \qquad (3.21)$$

The parameters defined in the equations above, are used as the initial values of r and $k_s a_s$ in the complete model. Finally, Eq. 3.18 and Eq. 3.19 can be compared with experimental data, as shown in Figure 3.3. It is interesting to note from this figure that the simplified model already gives good results.

3.6   Complete model

The complete model is characterized by more complex equations,involving more variables. One important difference is that the extraction process is now described by three equations, since the second equation characterizes a transition period from the first period to the third one. Another dissimilarity is the appearance of the external mass transfer coefficient, k_f, that is an additional adjustable parameter besides the already mentioned r and $k_s a_s$. In this model the internal and external mass transfer resistances, θ_i and θ_e respectively, are also present, defined as:

$$\theta_i = \frac{(1-\varepsilon)\,\dot{Q}}{\gamma k_s a_s N_m} \;, \tag{3.22}$$

$$\theta_e = \frac{\varepsilon \dot{Q}}{\gamma k_f a_0 N_m} \;. \tag{3.23}$$

Clearly, the internal mass transfer resistance is inversely related to the coefficient k_s (Eq. 3.22), while the external mass transfer resistance is inversely related to the coefficient k_f (Eq. 3.23). It is also anticipated that in the model equations the resistances will appear, but, for the fitting with experimental data, the coefficients are considered.

The crossing points between the first and the second period, and between the second and the third period are calculated using the equations:

$$q_m = \frac{r x_u \theta_e}{y_s} \;, \tag{3.24}$$

$$q_n = q_m + \gamma \theta_i \ln \left[1 - r + r \exp \left(\frac{1}{\beta} \right) \right] \;, \tag{3.25}$$

where q_m and q_n are the relative amount of passed solvent at the end of the first and second extraction period, respectively, and β is a variable introduced to simplify the form of the equation, and it is defined as:

$$\beta = \frac{\gamma \theta_i y_s}{x_u} \;. \tag{3.26}$$

The equations are written for plug flow without solute-matrix interaction. Other assumptions are that the solute is homogeneously distributed in the solid matrix and that the solvent density and the bed characteristics (void fraction and specific surface area) are not affected by the displacement of the solute from particles to solvent. The complete model equations

are [Sovová, 2005]:

$$e = qy_s \left[1 - \exp\left(-\frac{1}{\theta_e} \right) \right] , \qquad\qquad for \ 0 \le q < q_m ,$$

(3.27)

$$e = qy_s - rx_i\theta_e \exp\left(\frac{\beta}{\theta_e} \ln\left\{ 1 + \frac{1}{r} \left[\exp\left(\frac{q - q_m}{\gamma\theta_i} \right) - 1 \right] \right\} - \frac{1}{\theta_e} \right) , \quad for \ q_m \le q < q_n ,$$

(3.28)

$$e = x_u \left[1 - \beta \ln\left\{ 1 + (1 - r) \left[\exp\left(\frac{1}{\beta} \right) - 1 \right] \exp\left(\frac{q - q_m}{\gamma\theta_i} \right) \right\} \right] , \quad for \ q \ge q_n .$$

(3.29)

The first extraction period (Eq. 3.27) is governed by phase equilibrium, with solubility as key parameter, and by the external mass resistance, θ_e. Again, this curve is a straight line since the extraction is very fast.

The second extraction period (Eq. 3.28) is a transition period from the one governed by phase equilibrium to that one governed by internal diffusion. The solubility affects also this part of the extraction, but it can be seen in the second part of the equation that both the internal and external mass transfer resistances are important. The extraction is slacked by mass transfer, whether in the particles or from particles to solvent, and this slowdown is proportional to the fraction of broken cells (that is the grinding efficiency) and to the solute concentration in the untreated solid. The increase of the value of this second part of the equation changes the shape of the curve, so the straight line of the first period becomes more curved.

In the third extraction period (Eq. 3.29), the solubility does not have a key role because the internal diffusion governs the process and the internal mass transfer resistance is the most important parameter (that appears also in the β coefficient), together with the fraction of intact cells, $(1 - r)$. Furthermore, the initial fraction of solute in open cells, G, can be calculated dividing the extraction yield at the beginning of the third extraction period by the concentration in the untreated solid:

$$G = \frac{e(q_n)}{x_u} .$$

(3.30)

This parameter gives an idea of how much oil the open cells contain.

The experimental data are used to correlate the optimal values of the grinding efficiency, the internal mass transfer resistance and the external mass transfer resistance are the unknown values. Like in the simplified model, MATLAB$^{\circledR}$ is used to fit the equations to experimental
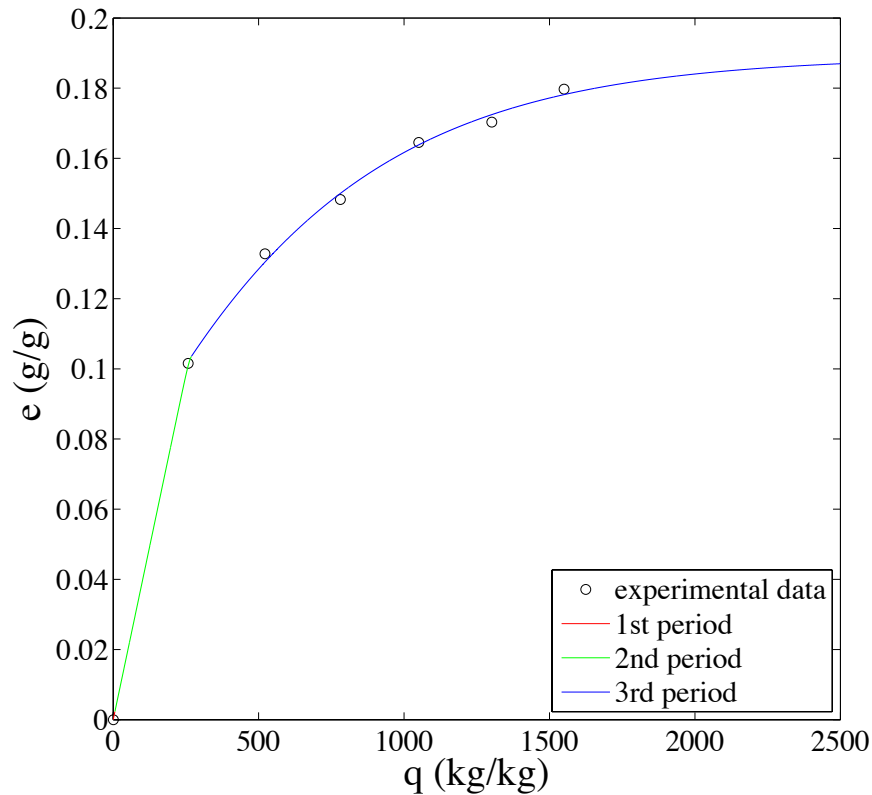
Figure 3.4: *Complete model applied to the $SCCO_2$ extraction of oil from microalgae at 30 MPa and 45 °C; fitted values: $r = 0.44$, $k_f a_0 = 1.96$ m^{-1}s^{-1}, $k_s a_s = 0.54 \cdot 10^{-4}$ m^{-1}s^{-1}*

data to obtain the parameters and to create the extraction curve that can be compared to the experimental data, as shown in Figure 3.4. Although the equations contain the mass transfer resistances, the fitted parameters are the grinding efficiency and the mass transfer coefficients, inversely related to the resistance according to Eqs. 3.22 and 3.23. Figure 3.5 shows the algorithm followed to estimate the complete model parameters. At first, the input data are specified and the physical properties are calculated. Then the fitting of the simplified model is applied to obtain the first estimation of r and $k_s a_s$. To these values is added another one for k_f to supply the initial values for the complete model. After the fitting of the complete model the parameter values are estimated and it is possible to calculate the extraction curve. The Matlab functions and scripts are reported in Appendix C, section C.1.

Figure 3.4 shows the three extraction periods in different colors, showing that the first extraction period is almost negligible. However, the second extraction period is a straight line too, so the effect of the second part of the equation is not visible for most of the period and becomes important only in the final part, near the beginning of the third period.

Figure 3.6 shows an enlargement of the beginning of the extraction (a) and another one representing the end of the second extraction period and the beginning of the third one (b). It
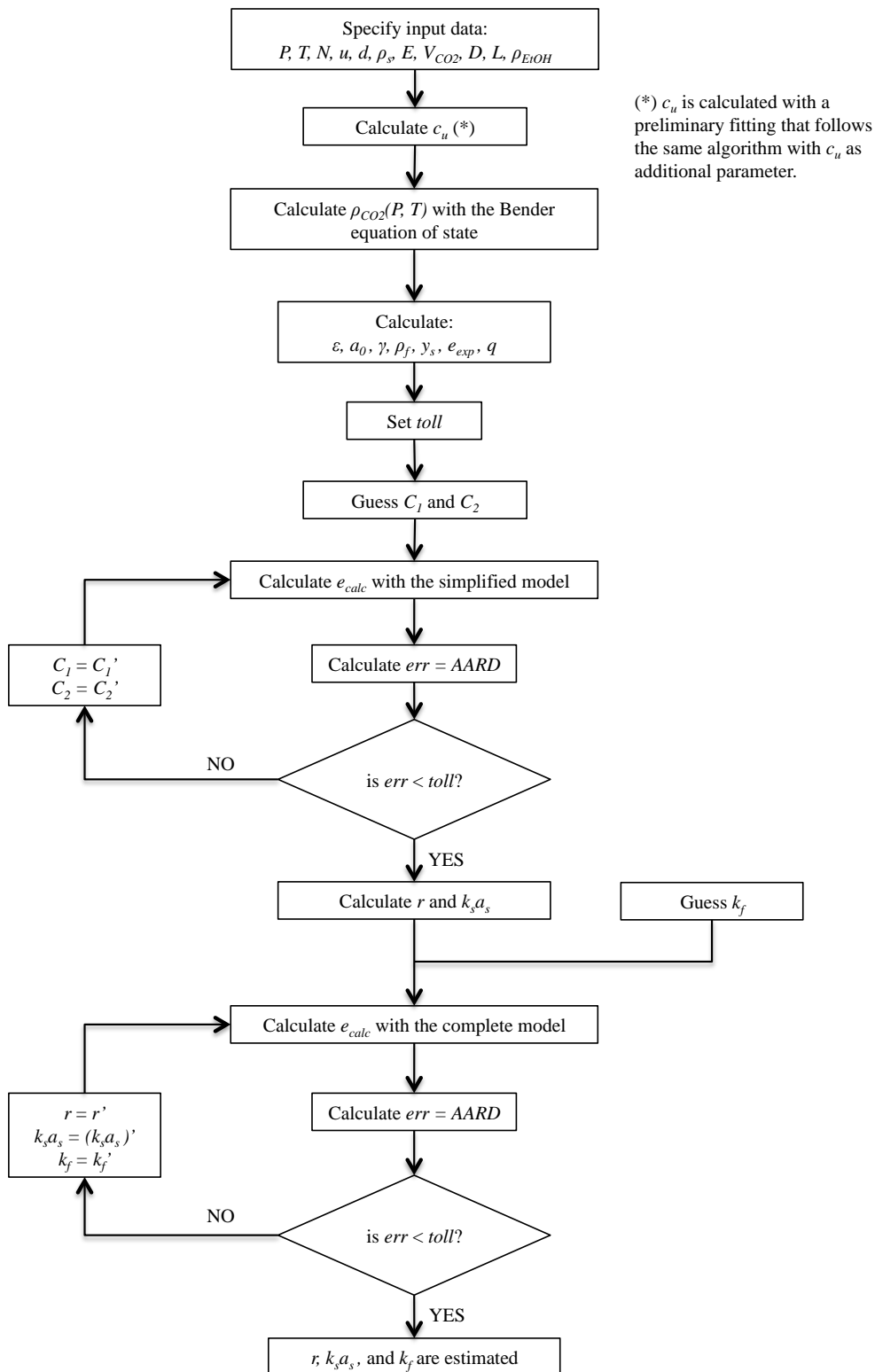
Figure 3.5: *Flow chart for complete model parameters evaluation.*
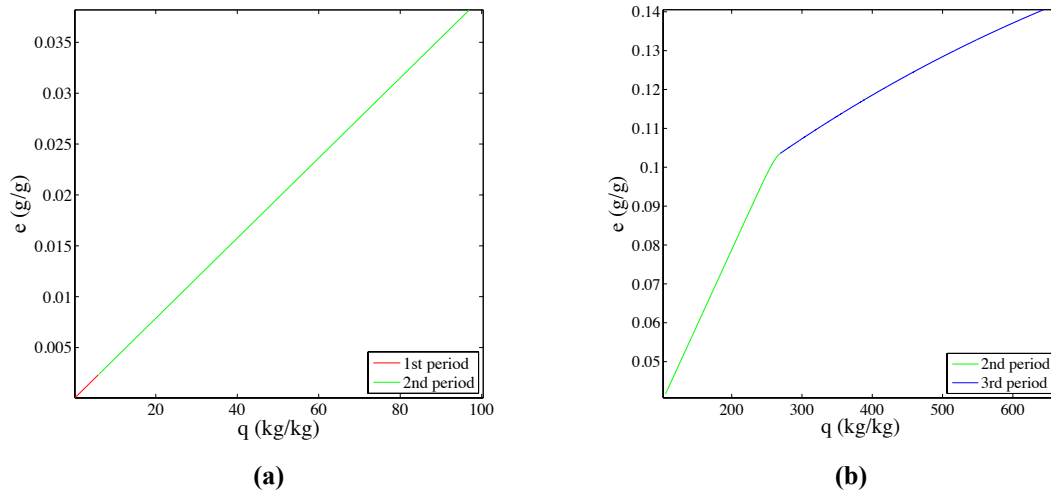
Figure 3.6: *Enlargement of the first part of the extraction (a) and of the end of the second extraction period (b) of the complete model.*

is evident, from Figure 3.6b, how little is the curved part of the second extraction period, so that it can be assumed a totally straight line. The reason of this behavior can be found in the second period equation where the value of the second term is so little that can be neglected.

Another observation is that the first period equation is able to describe the same behavior of the second one. In fact, neglecting the second part of this latter equation, the only difference between the two expressions is the presence of the external mass transfer resistance in the first equation. This behavior has been observed in all the experimental curves fitted at different operative conditions (see Chapter 4). Therefore, it can be inferred that only the external mass transfer resistance affects this part of the extraction, and then the first equation is sufficient to describe also the transition period.

In conclusion, the second extraction period can be fully described by the first equation, giving also a minor residual function, calculated as the average absolute relative deviation (AARD):

$$AARD(\%) = \frac{100}{n} \times \sum_{1}^{n} \left| \frac{e_{calc} - e_{exp}}{e_{exp}} \right| , \qquad (3.31)$$

where n is the number of experimental points, e_{calc} is the calculated extraction yield and e_{exp} is the experimental extraction yield.

The end of the first equation period will correspond to the beginning of the third extraction period, and the relative amount of passed solvent will be calculated matching the two equations (Eqs. 3.27 and 3.29). The extraction curve is represented in Figure 3.7 and it is pretty much the same of the extraction curve obtained with three periods.
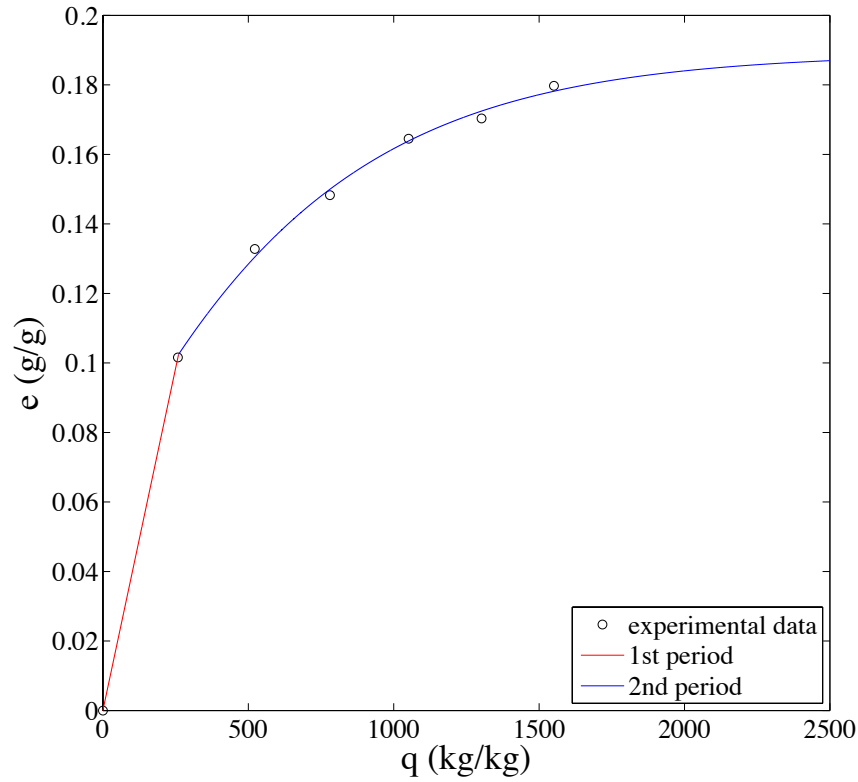
Figure 3.7: *Complete model with two extraction periods applied to the $SCCO_2$ extraction of oil from microalgae at 30 MPa and 45°C.*

3.7 Simplified model based on characteristic times

Until now the reported equations have always been written with the extraction yield as a function of the relative amount of passed solvent. Another formulation allows to calculate the yield as a function of the time, giving as result an extraction curve with the time on the horizontal axis instead of the passed solvent.

This simplified model was also proposed by Sovová [Sovová, 2012], and permits to evaluate the characteristic times of the extraction process. Like in the simplified model, there are two extraction periods and two equations are used:

$$e' = t y_s \left[1 - \exp\left(-\frac{1}{\theta_f} \right) \right] q' , \qquad\qquad for\ t \leq t_1 , \qquad (3.32)$$

$$e' = c_u \left[1 - (1 - G) \exp\left(-\frac{t - t_1}{t_i} \right) \right] , \qquad\qquad for\ t > t_1 , \qquad (3.33)$$

where e' is the extraction yield expressed as E/N, q' is the specific flow rate (equal to $\dot{Q}/N$), t_1 is the extraction time at the end of the first period, θ_f is the external mass transfer resistance, t_i is the characteristic time of the solid phase mass transfer and G is the initial fraction of
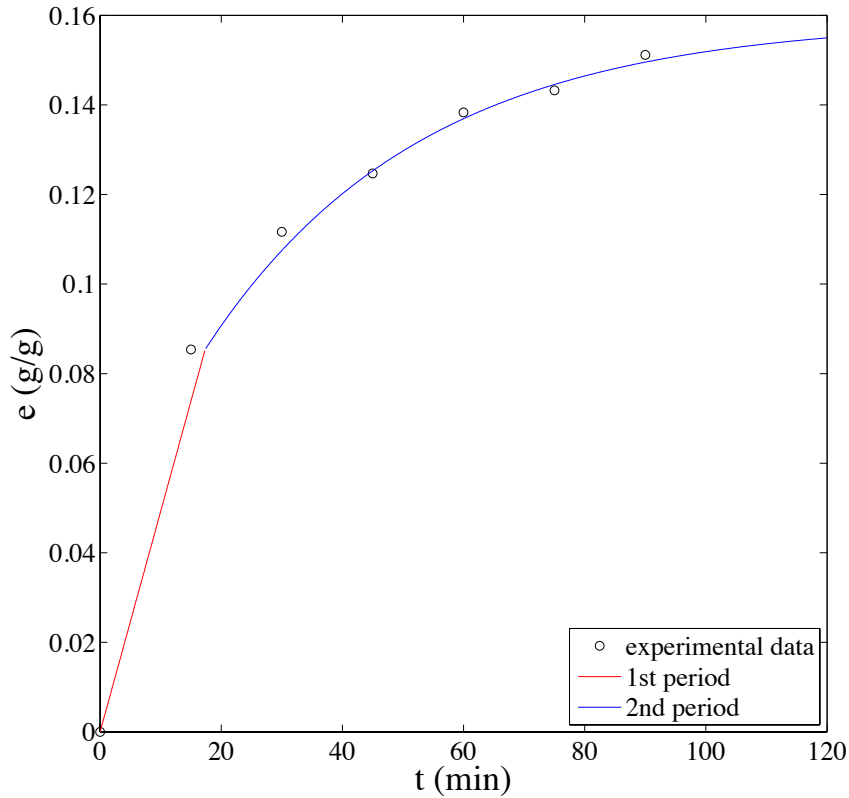
Figure 3.8: *Simplified model based on characteristic times applied to the $SCCO_2$ extraction of oil from microalgae at 30 MPa and 45 °C; fitted values: $G = 0.54$, $\theta_f = 0.025$, $t_i = 35.46\ min$.*

solute in open cells.

In this model, the external mass transfer resistance, θ_f, the characteristic time of the internal mass transfer, t_i, and the initial fraction of solute in the open cells, G, are the unknown parameters.

Defining the extraction yield at the end of the first extraction period as:

$$e'(t_1) = Gc_u \ , \tag{3.34}$$

the characteristic time of the first extraction period is calculated as:

$$t_1 = \frac{Gc_u}{y_s q' \left[1 - \exp\left(1 - \frac{1}{\theta_f} \right) \right]} \ . \tag{3.35}$$

The resulting extraction curve is shown in Figure 3.8.

This model appears less precise than the previous one because the extraction yield is expressed as a function of time and the specific flow rate is the average of the flow rate, that may change during the process. Otherwise, in the previous models it is considered the actual

value of the flow rate at each step, removing the error caused by the use of an average flow rate, that influences not only the first period equation but also the formulation of t_1.

Chapter 4

Results and discussions

This research work was divided in two parts: the experimental part, where all the data were collected, and the modeling part, where the kinetics and the solubility were modeled. This chapter is focused on experimental results and on the application of the model of broken and intact cells, while the behavior of solubility will be amply discussed in the next chapter. Furthermore, the profile of lipids composition is discussed, comparing different techniques, different microalgae strains and different operative conditions in supercritical CO_2 extraction.

4.1 Experimental results

The first experiments were carried out at constant pressure and temperature to find the most suitable extraction time and to understand the role of ethanol, particle size and microalgae humidity. The CO_2 flow rate was kept constant in all the experiments.

The extraction time depends mainly on the mass of microalgae initially loaded into the extractor. With 0.5 g of load, the adequate extraction time was 90 minutes, while with 3 g more than 3 hours were needed. Afterwards, the role of ethanol was investigated, testing different percentages with respect to the CO_2 flow rate. The best result was obtained with 6% in mass, namely 5 ml/min for a constant CO_2 flow rate of 0.4 kg/h.

The particle size is also an important parameter, since the smaller the particles, the greater the contact surface. Indeed, higher yields were achieved with smaller particles.

Several experiments were performed with the same conditions but with different microalgae humidity (8% and 20%), to understand its influence. However, no substantial differences were observed, proving that when the humidity is less than 20% there are no changes in the extraction process, as reported in literature [Crampon *et al.*, 2013].

As a result of all the experimental runs, the conditions selected as optimal were:

Mass of microalgae loaded into the extractor $= 0.5$ g;

Extraction time = 90 min;

CO_2 flow rate = 0.4 kg/h;

Ethanol flow rate = 0.5 ml/min;

Particle size = less than 0.5 mm;

Micoralgae humidity = 8%.

Keeping fixed these variables, pressure and temperature were changed at each experiment to obtain the highest extraction yield. At first, pressure was varied in a range between 15 MPa and 30 MPa, at constant temperature; then, temperature was varied between 45 °C and 65 °C, at constant pressure. Table 4.1 shows the experimental data that were used to fit the model of broken and intact cells. Comments about these data are discussed in the next sections.

Table 4.1: *Experimental data collected during tests.*

(a) *05/28/2013 - Scenedesmus obliquus, 30 MPa, 45 °C.*

t	$V_{CO_2}^{IN}$	$V_{CO_2}^{FIN}$	E	e
min	m^3	m^3	g	-
0	0	0	0	0
5	312.1330	312.1510	0.0270	0.0658
10	312.1691	312.1847	0.0129	0.0973
15	312.2032	312.2215	0.0096	0.1207
20	312.2395	312.2567	0.0074	0.1387
25	312.2755	312.2931	0.0065	0.1546
30	312.3131	312.3322	0.0059	0.1690
35	312.3511	312.3715	0.0058	0.1831
40	312.3890	312.4072	0.0033	0.1912
45	312.4244	312.4410	0.0025	0.1973
50	312.4600	312.4753	0.0017	0.2014
55	312.4936	312.5135	0.0008	0.2034

t, time; $V_{CO_2}^{IN}$, initial CO_2 volume; $V_{CO_2}^{FIN}$, final CO_2 volume; E, mass of extract; e, yield (E/N_m).

(b) *05/30/2013 - Scenedesmus obliquus, 30 MPa, 35 °C.*

t	$V_{CO_2}^{IN}$	$V_{CO_2}^{FIN}$	E	e
min	m^3	m^3	g	-
0	0	0	0	0
15	313.0544	313.1159	0.0235	0.0559
30	313.1360	313.1893	0.0192	0.1015
45	313.2087	313.2662	0.0108	0.1272
60	313.2861	313.3424	0.0043	0.1374
75	313.3633	313.4185	0.0024	0.1431
90	313.4381	313.4958	0.0013	0.1462

t, time; $V_{CO_2}^{IN}$, initial CO_2 volume; $V_{CO_2}^{FIN}$, final CO_2 volume; E, mass of extract; e, yield (E/N_m).

Table 4.1: *Experimental data collected during tests (Continued).*

(a) *05/31/2013 - Scenedesmus obliquus, 20 MPa, 35 °C.*

t	$V_{CO_2}^{IN}$	$V_{CO_2}^{FIN}$	E	e
min	m^3	m^3	g	-
0	0	0	0	0
15	313.5223	313.5782	0.0204	0.0500
30	313.5954	313.6502	0.0200	0.0990
45	313.6678	313.7272	0.0060	0.1137
60	313.7453	313.8076	0.0069	0.1306
75	313.8215	313.8898	0.0033	0.1387
90	313.8972	313.9512	0.0030	0.1461

t, time; $V_{CO_2}^{IN}$, initial CO_2 volume; $V_{CO_2}^{FIN}$, final CO_2 volume; E, mass of extract; e, yield (E/N_m).

(b) *06/03/2013 - Nannochloropsis salina, 30 MPa, 45 °C.*

t	$V_{CO_2}^{IN}$	$V_{CO_2}^{FIN}$	E	e
min	m^3	m^3	g	-
0	0	0	0	0
15	313.9832	314.0376	0.0439	0.1577
30	314.0608	314.1163	0.0136	0.2066
45	314.1460	314.1968	0.0107	0.2450
60	314.2251	314.2780	0.0078	0.2731
75	314.3065	314.3603	0.0048	0.2903
90	314.3894	314.4454	0.0037	0.3036

t, time; $V_{CO_2}^{IN}$, initial CO_2 volume; $V_{CO_2}^{FIN}$, final CO_2 volume; E, mass of extract; e, yield (E/N_m).

(c) *06/05/2013 - Scenedesmus obliquus, 15 MPa, 55 °C.*

t	$V_{CO_2}^{IN}$	$V_{CO_2}^{FIN}$	E	e
min	m^3	m^3	g	-
0	0	0	0	0
15	314.4748	314.5297	0.0233	0.0564
30	314.5543	314.6063	0.0157	0.0945
45	314.6311	314.6851	0.0088	0.1158
60	314.7112	314.7558	0.0043	0.1262
75	314.7818	314.8270	0.0025	0.1323
90	314.8526	314.9089	0.0011	0.1349

t, time; $V_{CO_2}^{IN}$, initial CO_2 volume; $V_{CO_2}^{FIN}$, final CO_2 volume; E, mass of extract; e, yield (E/N_m).

Table 4.1: *Experimental data collected during tests (Continued).*

(a) *06/06/2013 - Scenedesmus obliquus, 25 MPa, 40 °C.*

t min	$V_{CO_2}^{IN}$ m^3	$V_{CO_2}^{FIN}$ m^3	E g	e -
0	0	0	0	0
15	314.9332	314.9886	0.0358	0.0911
30	315.0114	315.0667	0.0117	0.1209
45	315.0932	315.1489	0.0070	0.1387
60	315.1760	315.2260	0.0049	0.1511
75	315.2526	315.2973	0.0037	0.1606
90	315.3235	315.3693	0.0028	0.1677

t, time; $V_{CO_2}^{IN}$, initial CO_2 volume; $V_{CO_2}^{FIN}$, final CO_2 volume; E, mass of extract; e, yield (E/N_m).

(b) *06/07/2013 - Scenedesmus obliquus, 30 MPa, 45 °C.*

t min	$V_{CO_2}^{IN}$ m^3	$V_{CO_2}^{FIN}$ m^3	E g	e -
0	0	0	0	0
15	315.4014	315.4576	0.0400	0.1015
30	315.4852	315.5428	0.0123	0.1328
45	315.5705	315.6269	0.0061	0.1482
60	315.6511	315.7100	0.0064	0.1645
75	315.7376	315.7922	0.0023	0.1703
90	315.8197	315.8739	0.0037	0.1797

t, time; $V_{CO_2}^{IN}$, initial CO_2 volume; $V_{CO_2}^{FIN}$, final CO_2 volume; E, mass of extract; e, yield (E/N_m).

(c) *06/10/2013 - Chlorella protothecoides, 30 MPa, 45 °C.*

t min	$V_{CO_2}^{IN}$ m^3	$V_{CO_2}^{FIN}$ m^3	E g	e -
0	0	0	0	0
15	315.9127	315.9698	0.0128	0.0313
30	315.9961	316.0520	0.0129	0.0629
45	316.0798	316.1354	0.0075	0.0813
60	316.1589	316.2142	0.0088	0.1028
75	316.2412	316.3030	0.0067	0.1192
90	316.3306	316.3877	0.0046	0.1305

t, time; $V_{CO_2}^{IN}$, initial CO_2 volume; $V_{CO_2}^{FIN}$, final CO_2 volume; E, mass of extract; e, yield (E/N_m).

Table 4.1: *Experimental data collected during tests (Continued).*

(a) *07/22/2013 - Scenedesmus obliquus, 15 MPa, 45 °C.*

t	$V_{CO_2}^{IN}$	$V_{CO_2}^{FIN}$	E	e
min	m^3	m^3	g	-
0	0	0	0	0
15	317.5862	317.6422	0.0219	0.0470
30	317.6631	317.7186	0.0141	0.0773
45	317.7412	317.7957	0.0102	0.0992
60	317.8181	317.8728	0.0054	0.1108
75	317.8950	317.9486	0.0055	0.1226
90	317.9719	318.0280	0.0039	0.1310

t, time; $V_{CO_2}^{IN}$, initial CO_2 volume; $V_{CO_2}^{FIN}$, final CO_2 volume; E, mass of extract; e, yield (E/N_m).

(b) *07/25/2013 - Scenedesmus obliquus, 25 MPa, 55 °C.*

t	$V_{CO_2}^{IN}$	$V_{CO_2}^{FIN}$	E	e
min	m^3	m^3	g	-
0	0	0	0	0
15	319.5086	319.5596	0.0304	0.0653
30	319.5854	319.6378	0.0340	0.1383
45	319.6642	319.7144	0.0156	0.1718
60	319.7410	319.7910	0.0101	0.1935
75	319.8179	319.8728	0.0087	0.2122
90	319.8995	319.9557	0.0022	0.2169

t, time; $V_{CO_2}^{IN}$, initial CO_2 volume; $V_{CO_2}^{FIN}$, final CO_2 volume; E, mass of extract; e, yield (E/N_m).

(c) *10/03/2013 - Chlorella protothecoides, 25 MPa, 55 °C.*

t	$V_{CO_2}^{IN}$	$V_{CO_2}^{FIN}$	E	e
min	m^3	m^3	g	-
0	0	0	0	0
15	324.9316	324.9746	0.0256	0.0686
30	324.9746	325.0224	0.0177	0.1161
45	325.0224	325.0729	0.0127	0.1501
60	325.0729	325.1194	0.0071	0.1691
75	325.1194	325.1691	0.0045	0.1812
90	325.1691	325.2215	0.0030	0.1892

t, time; $V_{CO_2}^{IN}$, initial CO_2 volume; $V_{CO_2}^{FIN}$, final CO_2 volume; E, mass of extract; e, yield (E/N_m).

Table 4.1: *Experimental data collected during tests (Continued).*

(a) *10/08/2013 - Scenedesmus obliquus, 30 MPa, 55 °C.*

t min	$V_{CO_2}^{IN}$ m^3	$V_{CO_2}^{FIN}$ m^3	E g	e -
0	0	0	0	0
15	327.2783	327.3204	0.0322	0.0840
30	327.3204	327.3794	0.0220	0.1415
45	327.3794	327.4145	0.0115	0.1715
60	327.4145	327.4691	0.0089	0.1947
75	327.4691	327.5244	0.0017	0.1992
90	327.5244	327.5679	0.0010	0.2018

t, time; $V_{CO_2}^{IN}$, initial CO_2 volume; $V_{CO_2}^{FIN}$, final CO_2 volume; E, mass of extract; e, yield (E/N_m).

(b) *10/10/2013 - Scenedesmus obliquus, 30 MPa, 45 °C.*

t min	$V_{CO_2}^{IN}$ m^3	$V_{CO_2}^{FIN}$ m^3	E g	e -
0	0	0	0	0
15	328.8623	328.9098	0.0407	0.1108
30	328.9138	328.9637	0.0345	0.2047
45	328.9970	329.0487	0.0127	0.2392
60	329.0487	329.1003	0.0015	0.2433
75	329.1003	329.1544	0.0009	0.2458
90	329.1544	329.2081	0.0007	0.2477

t, time; $V_{CO_2}^{IN}$, initial CO_2 volume; $V_{CO_2}^{FIN}$, final CO_2 volume; E, mass of extract; e, yield (E/N_m).

(c) *10/11/2013 - Chlorella protothecoides, 25 MPa, 45 °C.*

t min	$V_{CO_2}^{IN}$ m^3	$V_{CO_2}^{FIN}$ m^3	E g	e -
0	0	0	0	0
15	329.3644	329.4100	0.0285	0.0726
30	329.4128	329.4502	0.0271	0.1416
45	329.4831	329.5329	0.0148	0.1793
60	329.5390	329.5843	0.0032	0.1874
75	329.5843	329.6251	0.0010	0.1900
90	329.6251	329.6863	0.0010	0.1925

t, time; $V_{CO_2}^{IN}$, initial CO_2 volume; $V_{CO_2}^{FIN}$, final CO_2 volume; E, mass of extract; e, yield (E/N_m).

Table 4.1: *Experimental data collected during tests (Continued).*

(a) *10/15/2013 - Scenedesmus obliquus, 15 MPa, 45 °C.*

t min	$V_{CO_2}^{IN}$ m^3	$V_{CO_2}^{FIN}$ m^3	E g	e -
0	0	0	0	0
15	330.4375	330.4879	0.0261	0.0660
30	330.4879	330.5419	0.0210	0.1190
45	330.5419	330.5958	0.0063	0.1350
60	330.5958	330.6466	0.0043	0.1458
75	330.6466	330.7022	0.0020	0.1509
90	330.7022	330.7610	0.0025	0.1572

t, time; $V_{CO_2}^{IN}$, initial CO_2 volume; $V_{CO_2}^{FIN}$, final CO_2 volume; E, mass of extract; e, yield (E/N_m).

(b) *10/16/2013 - Scenedesmus obliquus, 30 MPa, 65 °C.*

t min	$V_{CO_2}^{IN}$ m^3	$V_{CO_2}^{FIN}$ m^3	E g	e -
0	0	0	0	0
15	331.8920	331.9307	0.0317	0.0875
30	331.9307	331.9709	0.0298	0.1697
45	331.9709	332.0168	0.0097	0.1964
60	332.0168	332.0668	0.0073	0.2166
75	332.0668	332.1104	0.0076	0.2376
90	332.1104	332.1628	0.0033	0.2467

t, time; $V_{CO_2}^{IN}$, initial CO_2 volume; $V_{CO_2}^{FIN}$, final CO_2 volume; E, mass of extract; e, yield (E/N_m).

(c) *10/17/2013 - Chlorella protothecoides, 25 MPa, 65 °C.*

t min	$V_{CO_2}^{IN}$ m^3	$V_{CO_2}^{FIN}$ m^3	E g	e -
0	0	0	0	0
15	333.2042	333.2500	0.0233	0.0592
30	333.2500	333.2937	0.0247	0.1220
45	333.2937	333.3347	0.0144	0.1587
60	333.3347	333.3758	0.0056	0.1729
75	333.3758	333.4312	0.0033	0.1813
90	333.4312	333.4771	0.0006	0.1828

t, time; $V_{CO_2}^{IN}$, initial CO_2 volume; $V_{CO_2}^{FIN}$, final CO_2 volume; E, mass of extract; e, yield (E/N_m).

Table 4.1: *Experimental data collected during tests (Continued).*

(a) *10/18/2013 - Scenedesmus obliquus, 20 MPa, 65 °C.*

t min	$V_{CO_2}^{IN}$ m^3	$V_{CO_2}^{FIN}$ m^3	E g	e -
0	0	0	0	0
15	334.7822	334.8038	0.0324	0.0847
30	334.8038	334.8298	0.0184	0.1328
45	334.8298	334.8499	0.0114	0.1626
60	334.8499	334.8935	0.0094	0.1872
75	334.8935	334.9426	0.0044	0.1987
90	334.9426	334.9907	0.0030	0.2065

t, time; $V_{CO_2}^{IN}$, initial CO_2 volume; $V_{CO_2}^{FIN}$, final CO_2 volume; E, mass of extract; e, yield (E/N_m).

(b) *10/21/2013 - Scenedesmus obliquus, 20 MPa, 55 °C.*

t min	$V_{CO_2}^{IN}$ m^3	$V_{CO_2}^{FIN}$ m^3	E g	e -
0	0	0	0	0
15	335.1112	335.1562	0.0221	0.0533
30	335.1562	335.1947	0.0195	0.1004
45	335.1947	335.2398	0.0079	0.1195
60	335.2398	335.2884	0.0043	0.1298
75	335.2884	335.3311	0.0037	0.1388
90	335.3311	335.3729	0.0020	0.1436

t, time; $V_{CO_2}^{IN}$, initial CO_2 volume; $V_{CO_2}^{FIN}$, final CO_2 volume; E, mass of extract; e, yield (E/N_m).

(c) *10/22/2013 - Chlorella protothecoides, 15 MPa, 65 °C.*

t min	$V_{CO_2}^{IN}$ m^3	$V_{CO_2}^{FIN}$ m^3	E g	e -
0	0	0	0	0
15	335.5192	335.5633	0.0132	0.0345
30	335.5633	335.6111	0.0097	0.0599
45	335.6111	335.6620	0.0078	0.0803
60	335.6620	335.7128	0.0059	0.0958
75	335.7128	335.7652	0.0051	0.1091
90	335.7652	335.8180	0.0022	0.1149

t, time; $V_{CO_2}^{IN}$, initial CO_2 volume; $V_{CO_2}^{FIN}$, final CO_2 volume; E, mass of extract; e, yield (E/N_m).

Table 4.2: *Extraction process parameters evaluated with the simplified model.*

Species	P	T	C_1	$C_2 \cdot 10^2$	r	$k_s a_s \cdot 10^5$	q_c	AARD
-	MPa	°C	-	-	-	$m^{-1}s^{-1}$	-	%
S. o.	15	45	1.27	0.35	0.22	7.40	282.46	1.41
S. o.	15	55	1.24	0.31	0.17	7.01	256.89	1.25
S. o.	15	65	1.01	0.16	0.15	3.29	218.88	2.21
S. o.	25	45	1.91	0.53	0.34	8.35	400.37	0.88
S. o.	25	55	1.01	0.22	0.22	4.32	235.91	1.97
S. o.	25	65	1.60	0.41	0.38	6.01	467.43	1.96
S. o.	30	45	0.69	0.16	0.44	2.71	258.78	0.92
S. o.	30	55	1.01	0.27	0.25	5.31	211.46	2.40
S. o.	30	65	1.01	0.27	0.32	4.36	293.83	4.53
C. p.	30	45	1.03	0.11	0.25	2.78	545.74	2.99
N. s.	30	45	0.77	0.11	0.36	2.56	344.44	0.99

S. o., *Scenedesmus obliquus*; C. p., *Chlorella protothecoides*; N. s., *Nannochloropsis salina*; P, pressure; T, temperature; C_1, first adjustable parameter; C_2, second adjustable parameter; r, grinding efficiency; $k_s a_s$, internal mass transfer coefficient times the specific area between the region of broken and intact cells; q_c, relative amount of passed solvent at the end of the first extraction period; AARD, average absolute relative deviation.

4.2   Application of the model

The extraction curve were fitted using the models described in Chapter 3: the simplified model, the complete model and the model based on characteristic times. It can be seen from the results that the simplified model already gives very good results, while the model based on characteristic times is less accurate but still valid for determining the characteristic times of the extraction process. The complete model is the most accurate, and even if it is characterized by three extraction periods, two periods are sufficient to describe the extraction curve.

4.2.1   Results of the simplified model

The simplified model (Eqs. 3.18 and 3.19) was applied to estimate the adjustable parameters C_1 and C_2, used then to calculate the grinding efficiency and the internal mass transfer coefficient (r and $k_s a_s$), using Eqs 3.20 and 3.21. Table 4.2 shows the results at every pressure and temperature for *S. obliquus*, and at 30 MPa and 45 °C for the other species. The residual function is also reported, calculated as the average absolute relative deviation (AARD, Eq. 3.31), as well as the relative amount of passed solvent at the end of the first extraction period, q_c. The results are of the same order of magnitude as those reported in literature [Mouahid *et al.*, 2013].

The extraction curve can be evaluated for each pressure and temperature, as shown in Figure 4.1, indicating with different colors the two extraction periods. The extraction process

(a) *S. o., 15 MPa, 45 °C.*

(b) *S. o., 15 MPa, 55 °C.*

(c) *S. o., 15 MPa, 65 °C.*

(d) *S. o., 25 MPa, 45 °C.*

(e) *S. o., 25 MPa, 55 °C.*

(f) *S. o., 25 MPa, 65 °C.*

Figure 4.1: *Results of the simplified model at different pressures and temperatures and with different types of microalgae (e, extraction yield; q, relative amount of passed solvent; S. o., Scenedesmus obliquus; N. s., Nannochloropsis salina; C. p., Chlorella protothecoides). The red color indicates the first extraction period, the blue color indicates the second one.*
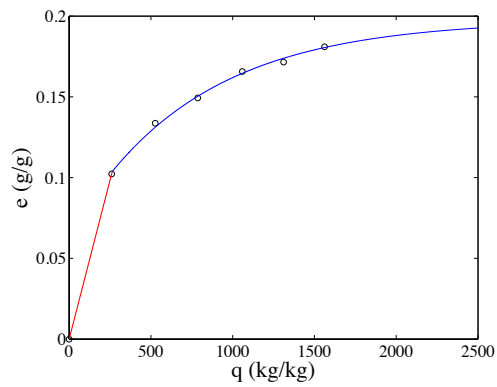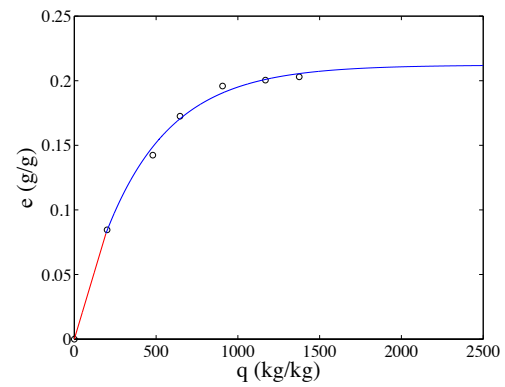
(g) *S. o., 30 MPa, 45 °C.*

(h) *S. o., 30 MPa, 55 °C.*
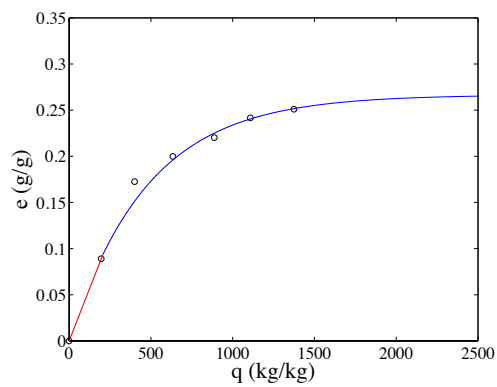
(i) *S. o., 30 MPa, 65 °C.*

(j) *N. s., 30 MPa, 45 °C.*
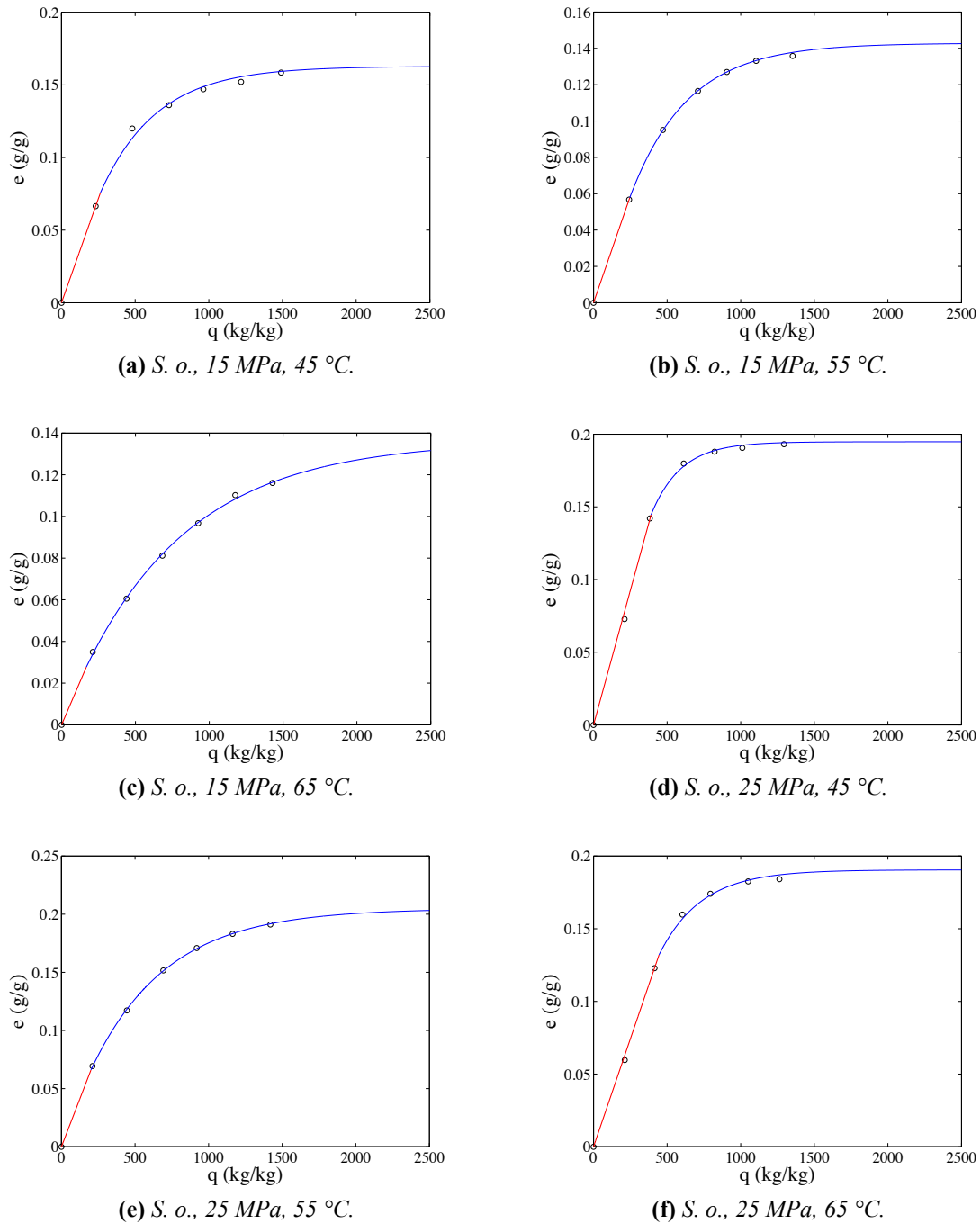
(k) *C. p., 30 MPa, 45 °C.*

Figure 4.1: *Results of the simplified model at different pressures and temperatures and with different types of microalgae (Continued).*

Table 4.3: *Extraction process parameters evaluated with the complete model.*

Species	P	T	r	$k_f a_0$	$k_s a_s \cdot 10^4$	$\theta_e \cdot 10^2$	θ_i	G	q_s	AARD
-	MPa	°C	-	$m^{-1}s^{-1}$	$m^{-1}s^{-1}$	-	-	-	-	%
S. o.	15	45	0.23	1.88	1.29	3.03	60.08	0.49	262.67	2.58
S. o.	15	55	0.18	1.96	1.21	3.29	75.52	0.43	250.44	0.76
S. o.	15	65	0.14	1.78	0.57	3.75	148.53	0.28	208.68	0.60
S. o.	25	45	0.36	1.84	1.90	2.36	32.03	0.75	385.53	3.60
S. o.	25	55	0.18	1.84	0.79	2.61	79.72	0.36	209.87	0.34
S. o.	25	65	0.25	1.83	1.75	2.66	38.66	0.68	417.69	2.76
S. o.	30	45	0.44	1.96	0.54	2.76	143.73	0.54	260.16	1.01
S. o.	30	55	0.20	1.81	1.00	2.60	64.98	0.38	185.59	1.46
S. o.	30	65	0.24	1.77	0.94	2.57	65.32	0.46	250.76	4.37
C. p.	30	45	0.16	2.04	0.64	2.80	141.28	0.38	458.60	1.33
N. s.	30	45	0.37	1.73	0.46	3.72	171.44	0.48	347.81	0.50

S. o., *Scenedesmus obliquus*; C. p., *Chlorella protothecoides*; N. s., *Nannochloropsis salina*; P, pressure; T, temperature; r, grinding efficiency; $k_f a_0$, external mass transfer coefficient times the specific surface area per unit volume of extraction bed; $k_s a_s$, internal mass transfer coefficient times the specific area between the region of broken and intact cells; θ_e, external mass transfer resistance; θ_i, internal mass transfer resistance; G, initial fraction of solute in intact cells; q_s, relative amount of passed solvent at the end of the first extraction period; AARD, average absolute relative deviation.

takes 90 minutes and the samples are collected every 15 minutes. It can be observed that in most experiments after $45 \div 60$ minutes, the slope of the extraction curve is very slight. At this time, indeed, the yield increases very slowly, gaining no more than 1% every 15 minutes. This is the beginning of the second extraction period, indicated with blue color, while the first extraction period lasts always $15 \div 30$ minutes and is indicated with red color.

The graphs in Figure 4.1 show that the simplified model gives already good results despite its parameters are a first estimation.

4.2.2   Results of the complete model

The complete model allows to evaluate the external mass transfer coefficient, k_f, the grinding efficiency, r, and the internal mass transfer coefficient multiplied by the specific area between the region of broken and intact cells, $k_s a_s$. These results are reported in Table 4.3 for each pressure, temperature and microalgae species, as well as the external and internal mass transfer resistances, θ_e and θ_i, obtained with Eqs. 3.23 and 3.22. The value of k_f is multiplied with the specific surface area per unit volume of extraction bed, a_0. It can be seen that the internal mass transfer coefficient is several orders of magnitude smaller than the external mass transfer coefficient, as expected [Sovová, 2005]. The table also shows the initial fraction of solute in open cells, G, calculated with Eq. 3.30, and the value of q_s, defined as the relative amount of passed solvent at the end of the first extraction period when only
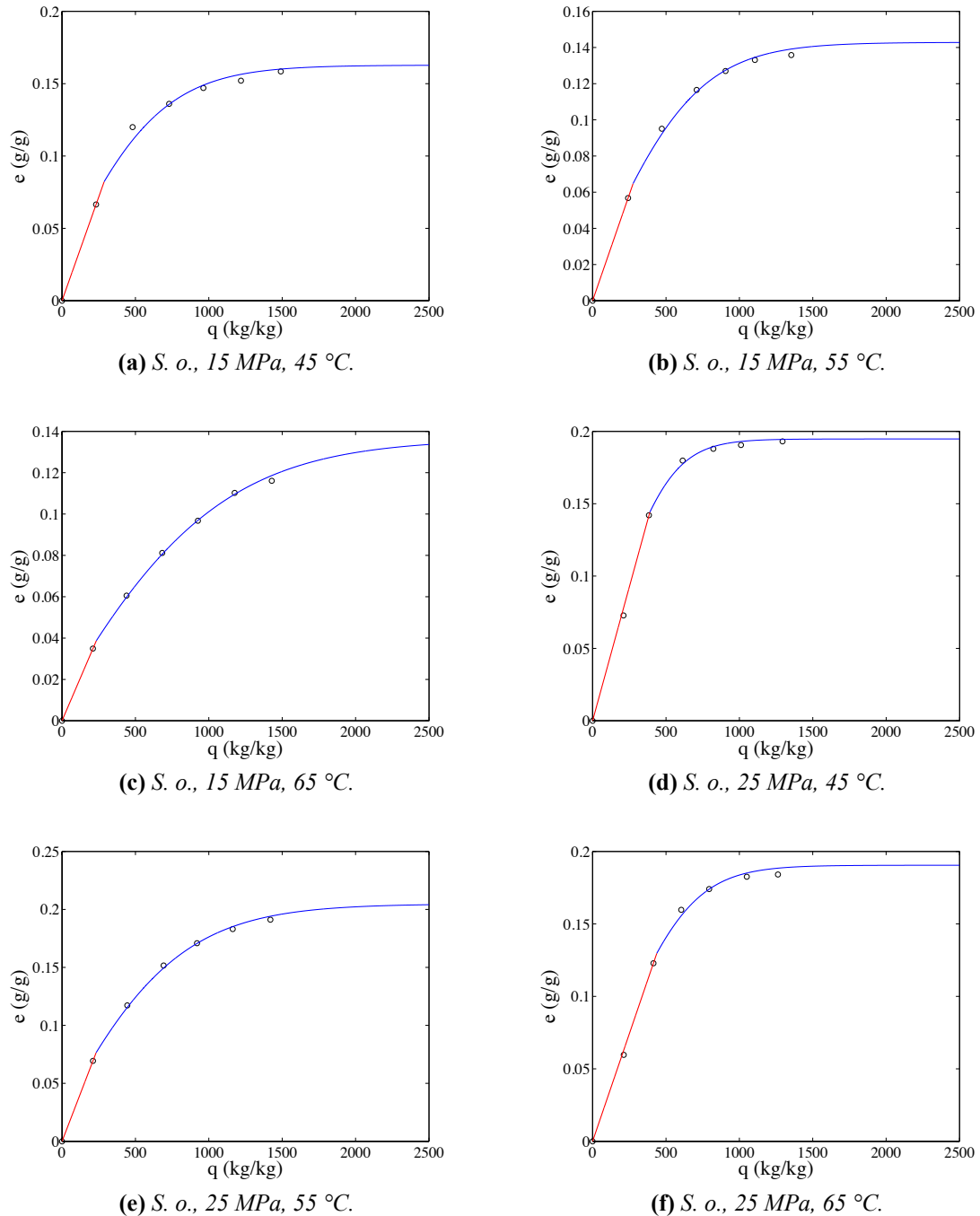
Figure 4.2: *Results of the complete model with two equations at different pressures and temperatures and with different types of microalgae (e, extraction yield; q, relative amount of passed solvent; S. O., Scenedesmus Obliquus; N. S., Nannochloropsis Salina; C. P., Chlorella Protothecoides). The red color indicates the first extraction period, the blue color indicates the second one.*
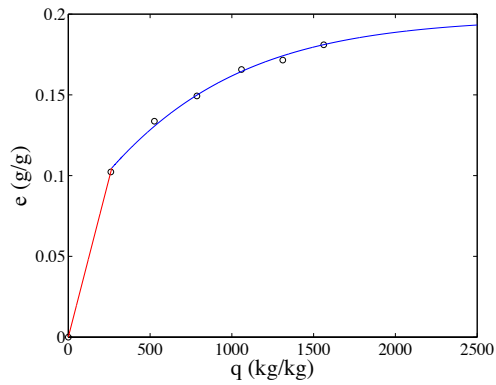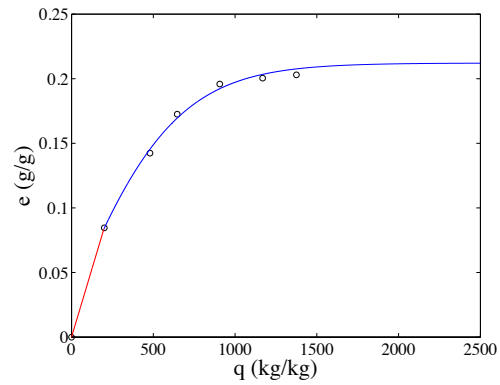
(g) *S. o., 30 MPa, 45 °C.*

(h) *S. o., 30 MPa, 55 °C.*
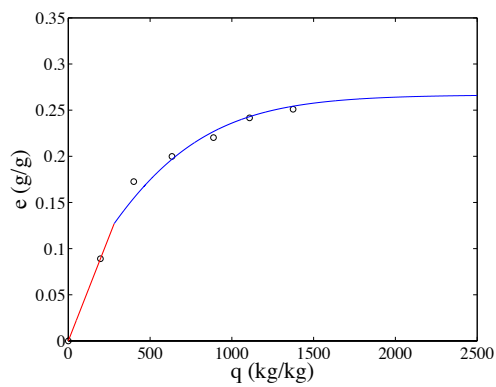
(i) *S. o., 30 MPa, 65 °C.*
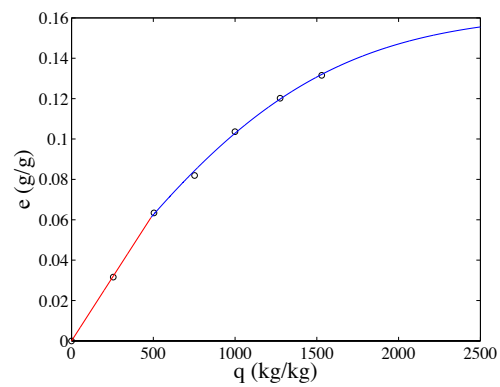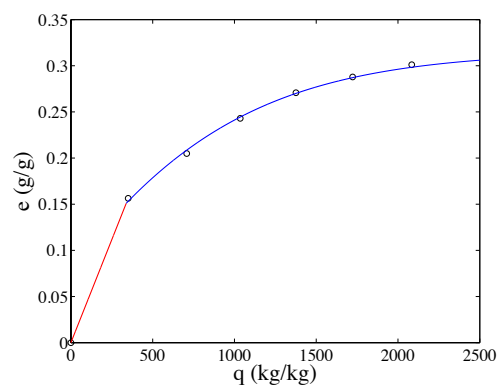
(j) *N. s., 30 MPa, 45 °C.*
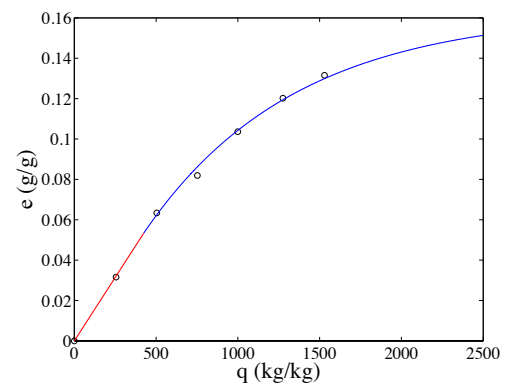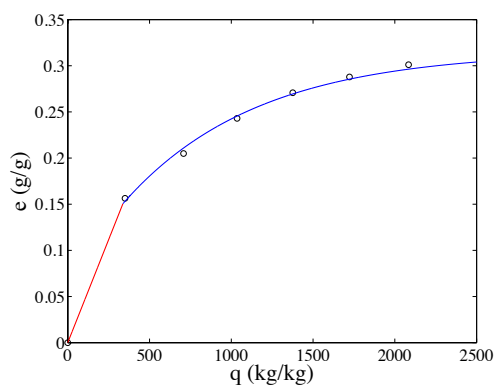

(k) *C. p., 30 MPa, 45 °C.*

Figure 4.2: *Results of the complete model with two equations at different pressures and temperatures and with different types of microalgae (Continued).*

two periods are considered, the first one and the third one. This parameter is comparable with q_c in the simplified model and, indeed, their values are very similar. Furthermore, the comparison between the two models residual functions (in Tables 4.2 and 4.3) confirms that the simplified model already gives a good approximation of r and $k_s a_s$. Once again, results are similar to those reported in literature [Mouahid *et al.*, 2013].

Figure 4.2 shows the extraction curves obtained using the complete model, considering only the first extraction period equation and the third one (Eqs. 3.27 and 3.29), since the second extraction period can be completely described with the first equation. As in the simplified model, the extraction periods are indicated with different colors and the experimental data are represented with circled marks.

4.2.3   Results of the model based on characteristic times

This model is slightly different from the others because the yield is expressed as the ratio between the mass of extract, E, and the solid loaded into the extractor, N, instead of the mass of insoluble solid, N_m. These quantities are linked by Eq. 3.11, therefore in the extraction process equations the value of c_u ($\text{kg}_{\text{solute}}/\text{kg}_{\text{solid}}$) will appear, instead of that of x_u ($\text{kg}_{\text{solute}}/\text{kg}_{\text{insoluble solid}}$). The extraction yield will be expressed as a function of time, while in the other models it is a function of the relative amount of passed solvent. Similarly, the initial fraction of solute in open cells, G, will be the unknown quantity, instead of the fraction of broken cells, r.

Table 4.4 shows the results of the fitting obtained with Eqs. 3.32 and 3.33, that represent the first and the second extraction periods. The adjustable parameters are the initial fraction of oil in intact cells, the external mass transfer resistance, θ_f, and the characteristic time of the solid phase mass transfer, t_i. Then, Eqs. 3.34 and 3.35 are used to calculate the yield and the time at the end of the first extraction period.

From the values of θ_f, it seems that the external mass transfer resistance does not change at the different operative conditions. This is probably due to the lack of experimental points in the first extraction period. However, the curve fits properly the experimental data and the order of magnitude is equal to that reported in literature. The higher residual function confirms what it has already been explained in the previous chapter about the lesser accuracy of this model compared to the other two.

Figure 4.3 represents the extraction curve at the different operative conditions. In these graphs, the lesser precision can be seen, especially around the switching time between the first and the second extraction period.
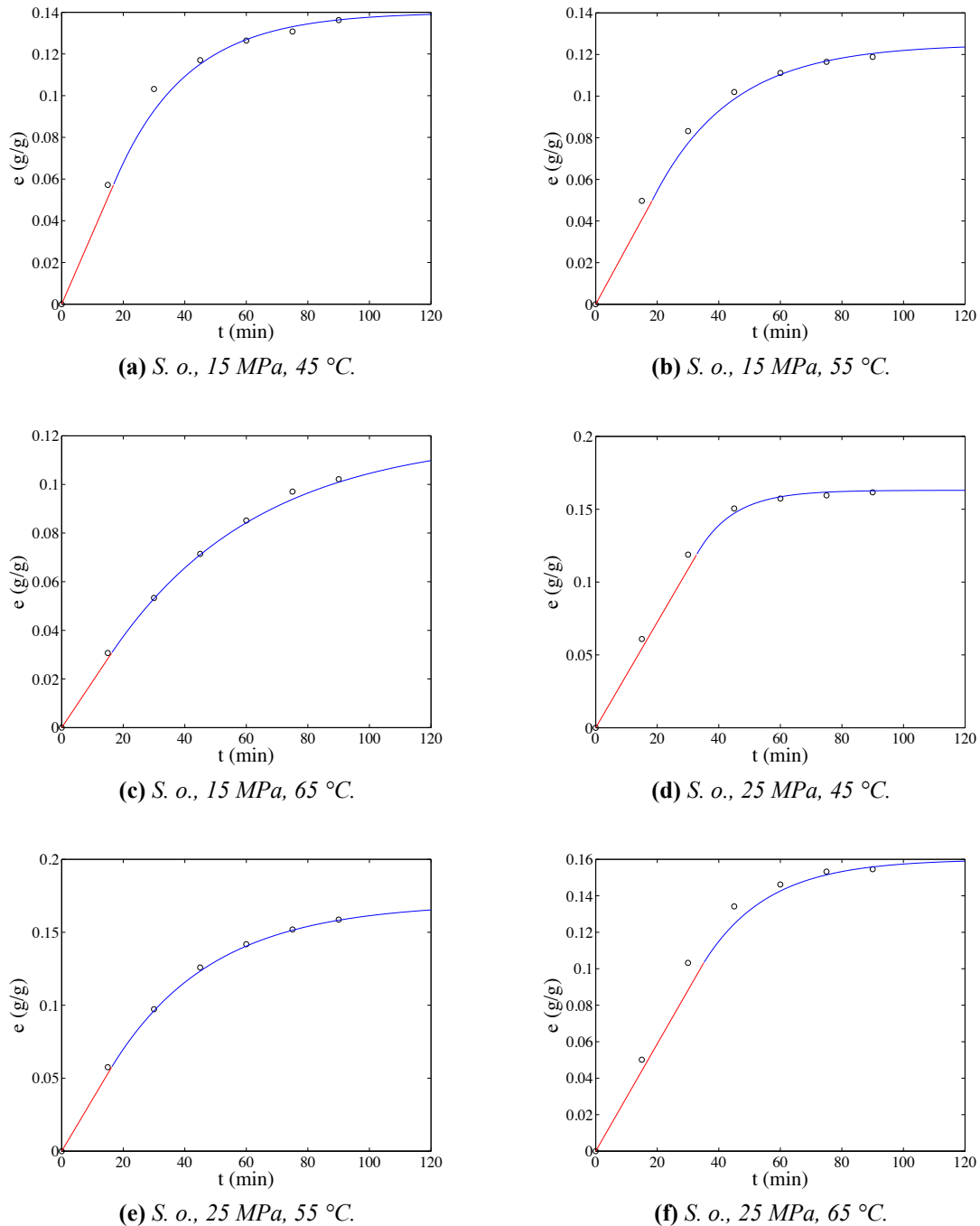
(a) *S. o., 15 MPa, 45 °C.*

(b) *S. o., 15 MPa, 55 °C.*

(c) *S. o., 15 MPa, 65 °C.*

(d) *S. o., 25 MPa, 45 °C.*

(e) *S. o., 25 MPa, 55 °C.*

(f) *S. o., 25 MPa, 65 °C.*

Figure 4.3: *Results of the model based on characteristic times at different pressures and temperatures and with different types of microalgae (e, extraction yield; t, extraction time; S. o., Scenedesmus obliquus; N. s., Nannochloropsis salina; C. p., Chlorella protothecoides). The red color indicates the first extraction period, the blue color indicates the second one.*
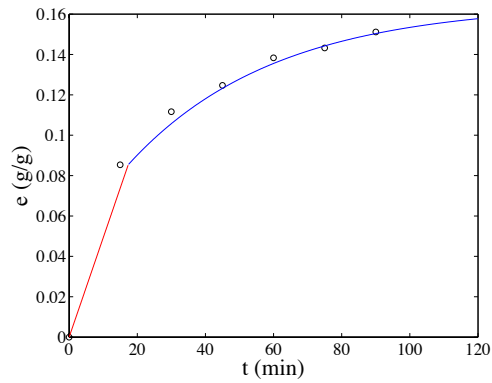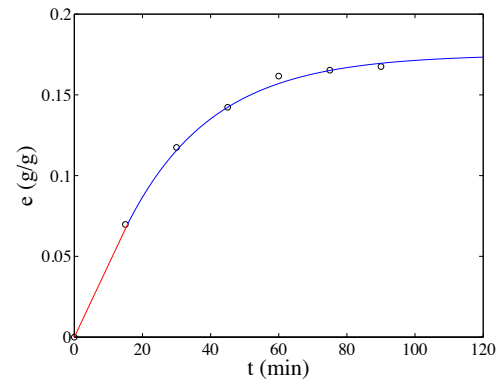
(g) *S. o., 30 MPa, 45 °C.*

(h) *S. o., 30 MPa, 55 °C.*
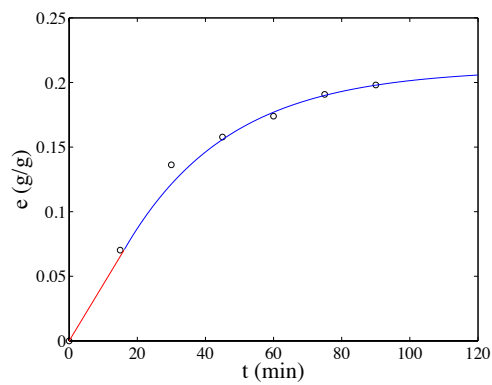
(i) *S. o., 30 MPa, 65 °C.*
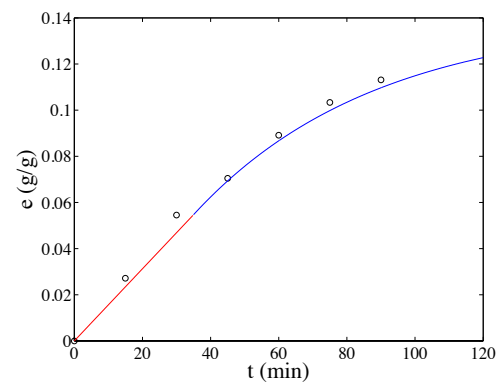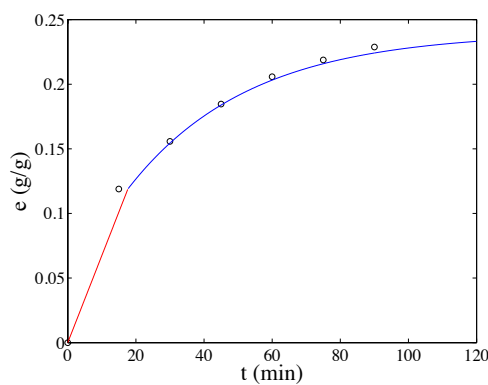
(j) *N. s., 30 MPa, 45 °C.*

(k) *C. p., 30 MPa, 45 °C.*

Figure 4.3: *Results of the model based on characteristic times at different pressures and temperatures and with different types of microalgae (Continued).*

Table 4.4: *Extraction process parameters evaluated with the model based on characteristic times.*

| Species	P	T	G	$\theta_f \cdot 10$	t_i	e_1	t_1	AARD
-	MPa	°C	-	-	min	%	min	%
S. o.	15	45	0.43	0.25	17.19	5.72	16.83	10.94
S. o.	15	55	0.42	0.25	21.70	4.97	18.32	18.14
S. o.	15	65	0.28	0.25	39.61	3.07	16.24	8.05
S. o.	25	45	0.74	0.25	10.46	11.89	32.80	9.66
S. o.	25	55	0.36	0.25	28.02	5.75	16.23	7.69
S. o.	25	65	0.67	0.25	16.08	10.32	35.10	13.26
S. o.	30	45	0.54	0.25	35.46	8.55	17.35	13.56
S. o.	30	55	0.41	0.25	23.20	6.98	15.61	4.04
S. o.	30	65	0.36	0.25	20.33	7.03	16.11	7.27
C. p.	30	45	0.41	0.25	51.47	5.45	34.89	14.09
N. s.	30	45	0.48	0.25	39.21	11.89	17.65	15.01

S. o., *Scenedesmus obliquus*; C. p., *Chlorella protothecoides*; N. s., *Nannochloropsis salina*; P, pressure; T, temperature; G, initial fraction of solute in intact cells; θ_f, external mass transfer resistance; t_i, characteristic time of the solid phase mass transfer; e_1, yield at the end of the first extraction period; t_1, time at the end of the first extraction period; AARD, average absolute relative deviation.

4.3   Pressure and Temperature effects on the extraction

The experiments were performed at different pressure and temperature to understand the role of the density in the extraction process. In Table 4.5 both density of CO_2 and density of the mixture CO_2 and ethanol are reported, the former calculated with the Bender equation of state (Eq. 1.1) and the latter with Eq. 3.13. It can be seen that the difference is very small, being the ethanol only 6% of the CO_2 flow rate.

As shown in this table, the solvent density increases with pressure and decreases with temperature. Since the solvent power of the CO_2 is strictly related to the density, the yield is expected to increase with it. However, while the higher the pressure, the higher the extraction yield, the latter increases with temperature only at 30 MPa. Instead, at lower pressures, the higher the temperature, the lower the extraction yield. These results suggest the presence of a cross-over pressure value between 25 and 30 MPa, indicating that the yield is not always enhanced with increasing the density. This behavior can be explained considering the competitive effect of the solvent power and the solute vapor pressure: at constant pressure, the first one decreases increasing the temperature while the other one increases. As a result, at lower temperatures the solute vapor pressure is so low that it does not affect the extraction, while at higher temperatures its effect becomes more relevant and produces an increase of the yield. The highest extraction yield was then obtained at 30 MPa and 65 °C.

The cross-over point is clearly visible in Figure 4.4, at around 25 MPa. The cross-over

Table 4.5: *CO_2 density and mixture ($CO_2 + EtOH$) density at different pressures and temperatures.*

P MPa	T °C	CO_2 Density kg/m^3	Mixture Density kg/m^3	e %
15	45	741.22	742.75	15.72
15	55	651.72	657.26	13.49
15	65	553.27	562.06	11.49
20	45	812.87	810.01	15.95
20	55	754.30	755.09	14.36
20	65	691.16	694.35	13.81
25	45	857.59	851.61	19.25
25	55	810.83	807.46	18.92
25	65	761.85	761.03	18.28
30	45	890.88	882.39	17.97
30	55	850.59	844.41	20.18
30	65	809.09	805.17	24.67

P, pressure; T, temperature; e, extraction yield.
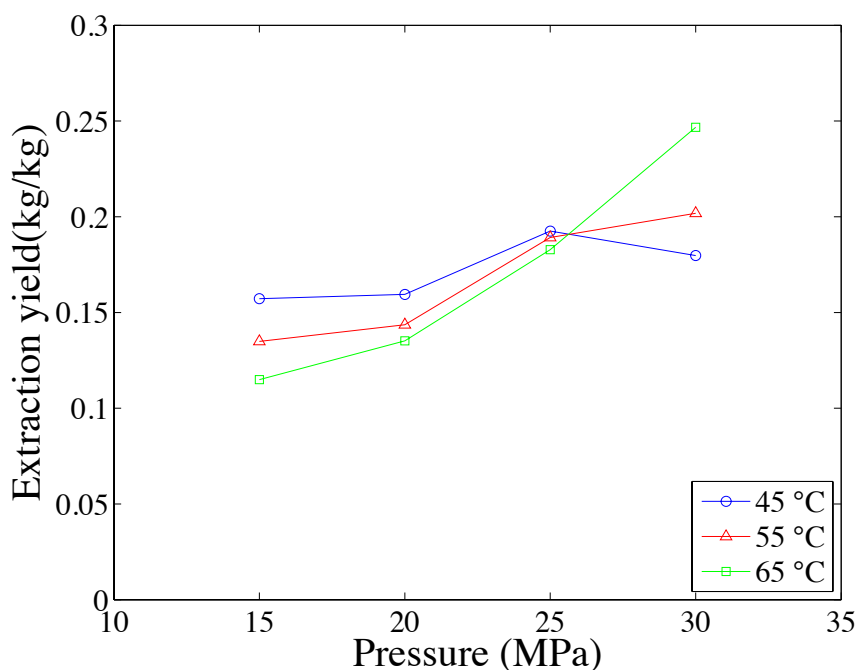
Figure 4.4: *Extraction yield of S. obliquus after 90 min of extraction as a function of the pressure with parametric temperature.*

phenomenon has also been reported in literature by other authors [Asghari-Kiavi *et al.*, 2004; Setianto *et al.*, 2009; Vatanara *et al.*, 2005]. This particular characteristic of the system will be investigated more extensively in Chapter 5 where the behavior of solubility as a function of pressure and temperature will be discussed as well.
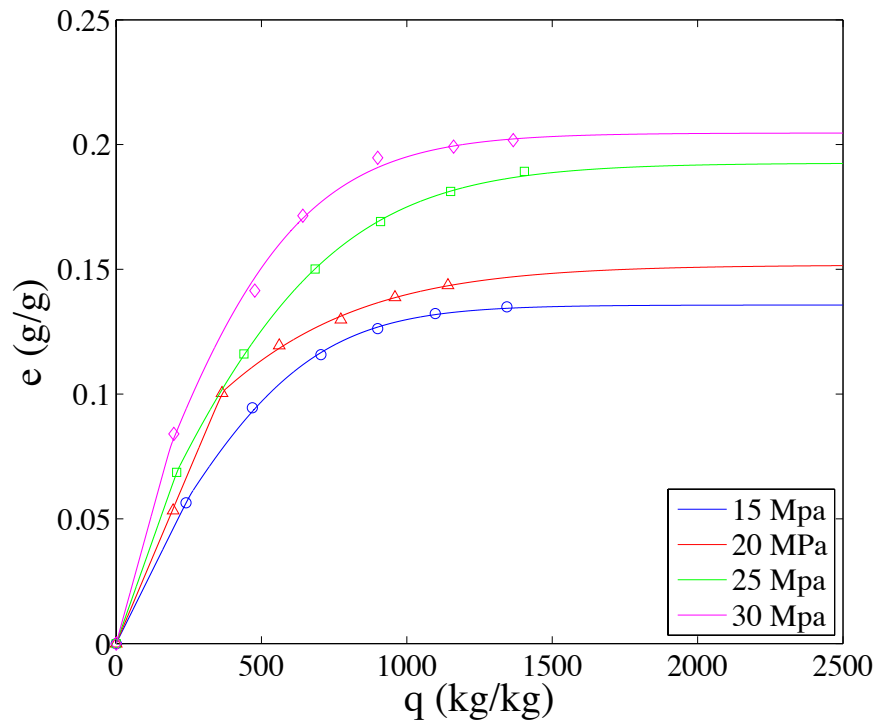
Figure 4.5: *Complete model applied on S. obliquus at the constant temperature of* $55°C$, *at different pressures.*
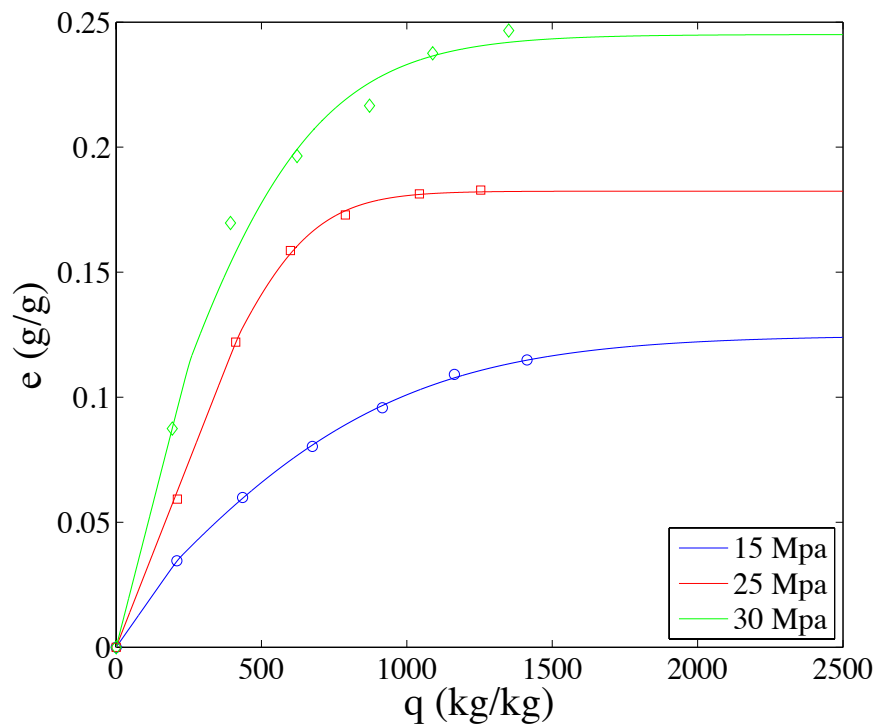
Figure 4.6: *Complete model applied on S. obliquus at the constant temperature of* $65°C$, *at different pressures.*
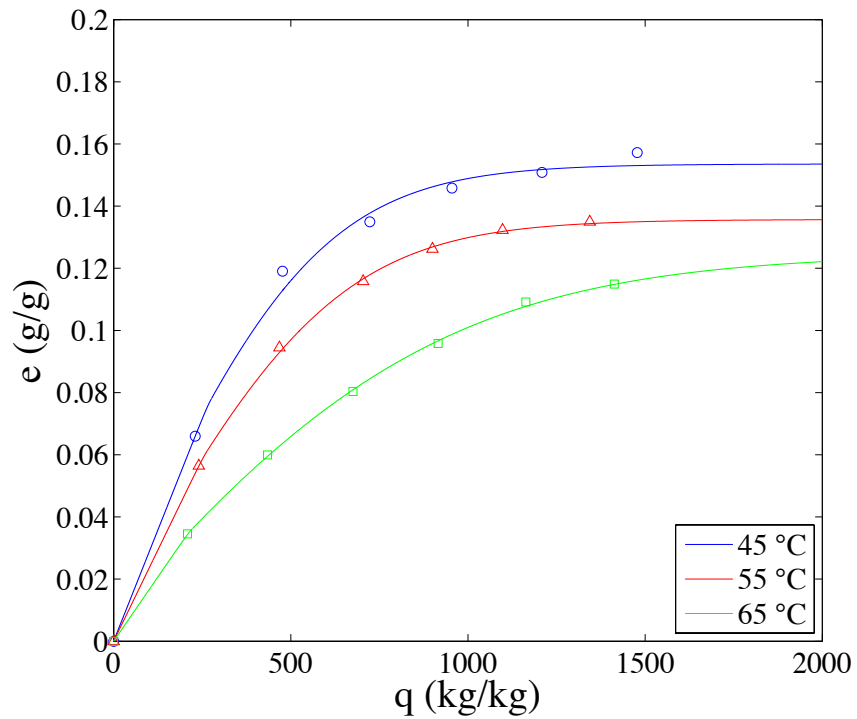
Figure 4.7: *Complete model applied on S. obliquus at the constant pressure of 15 MPa, at different temperatures.*
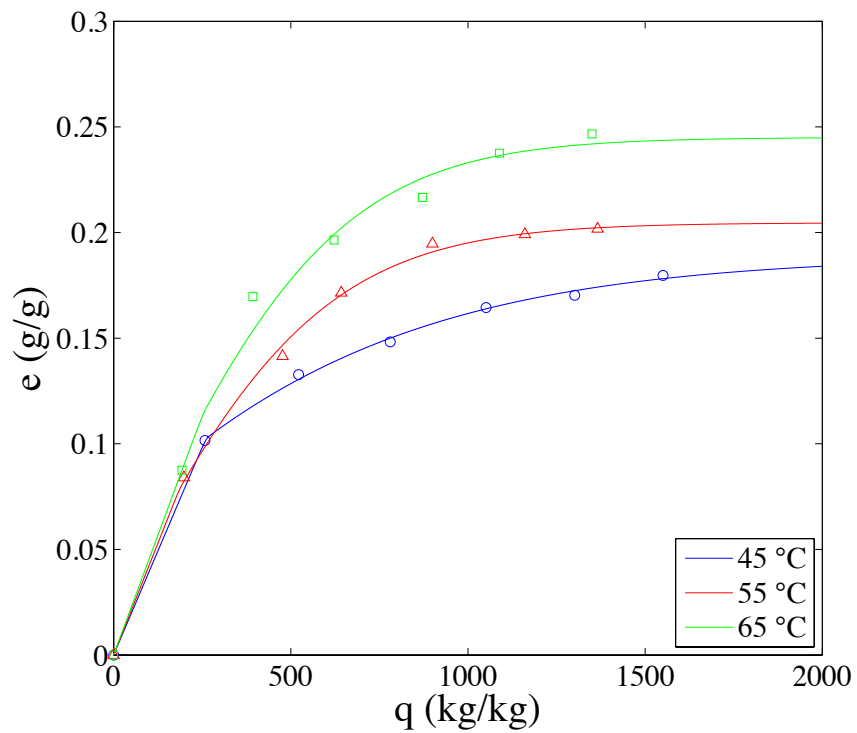
Figure 4.8: *Complete model applied on S. obliquus at the constant pressure of 30 MPa, at different temperatures.*

Figures 4.5 and 4.6 show that the yield always increases with pressure at constant temperature, since the solvent power is always enhanced by pressure. Figures 4.7 and 4.8 show the combining effect of solvent power and solute vapor pressure.

4.4 Lipids profile analysis

The lipids profile is influenced by many factors including not only the type of the extraction and its operative conditions, but also some microalgae characteristics such as the strain and the cultivation methods. Therefore, some strains are richer in saturated fatty acids and other strains have a greater quantity of polyunsaturated fatty acids [Halim *et al.*, 2012]. Cultivation methods, instead, could change the lipids content by varying for example the nutrients distributed during their growth [Lv *et al.*, 2010; Mairet *et al.*, 2011].

In this section a comparison between different extraction methods and microalgae species is presented, as well as an analysis of pressure and temperature effect on lipids composition when supercritical extraction is used. Attention will be paid mainly to the polyunsaturated fatty acids (PUFA) content, since some of them, like the essential oils (linoleic acid, α-linolenic acid and others), are considered high-value products. More detailed informations about microalgae lipids composition are in Chapter 1, section 1.3.

The analysis of lipids profiles resulted compatible with those available in literature [Crampon *et al.*, 2013; Santana *et al.*, 2012].

4.4.1 Soxhlet vs Supercritical CO_2 extraction

Owing to the disadvantages of solvent extraction (toxic solvents, traces of metals or solvent in the final product, high temperatures, etc.), supercritical CO_2 extraction has become very attractive as it could be a valuable alternative thanks to the numerous advantages already discussed in Chapter 1.

Soxhlet extraction was performed in a laboratory scale apparatus using a mixture of chloroform and methanol 1:2 as the solvent. The extraction time was 18 hours at a constant temperature of 105 °C, for 0.5 g of strain. First, *Scenedesmus Obliquus* extraction was studied. The yield obtained, defined as the mass of extract divided by the mass of insoluble solid, was 29.03%, higher than the one measured with supercritical CO_2 extraction at 300 MPa and 65 °C (best conditions), 24.67 %. These results are reported in Table 4.6.

To compare the lipids composition of both methods, the *Free Fatty Acids (FFA) conversion* and the *Lipid Yield* are introduced. The first one is defined as:

$$FFA\ conversion = \frac{mass\ of\ fatty\ acids}{mass\ of\ microalgae\ extract} \times 100 \,, \qquad (4.1)$$

Table 4.6: *Comparison between supercritical CO_2 extraction and solvent extraction on lipid yield and free fatty acids content.*

Method	Extraction time	Temperature	Extraction yield	FFA conversion	Lipid Yield
-	h	°C	wt.%	wt.%	wt.%
Soxhlet	18	105	29.03	51.13	14.84
SCCO$_2$	1.5	65	24.67	73.57	18.15

Extraction yield = (mass of microalgae extract/mass of insoluble solid)×100; FFA conversion = (mass of fatty acids/ mass of microalgae extract)×100; Lipid yield = (Extraction yield×FFA conversion)/100.

while the second one is expressed as:

$$Lipid\,Yield = \frac{Extraction\,Yield \times FFA\,conversion}{100} \, . \qquad (4.2)$$

As shown in Table 4.6, the *FFA conversion* is 73.57% with SCCO$_2$ extraction, and 51.13% with Soxhlet. These results lead to a *Lipid Yield* of 14.84% with Soxhlet and 18.15% with supercritical extraction. Furthermore, the higher temperature of the Soxhlet extraction with respect to supercritical CO_2 extraction could degrade the lipids and the solvent is not only toxic, unlike the CO_2, but it also extracts non-target compounds, like waxes and impurities, that increase the yield but decrease the quality.

Table 4.7 reports the fatty acids composition of the oil obtained at different experimental conditions. Although the FFA conversion is higher with supercritical CO_2 extraction, these results prove that there are no substantial differences on the FFA composition between the two methods. This means that the effect of temperature have not influenced the FFA composition, but SCCO$_2$ is faster, more selective and does not require a toxic solvent. Table 4.8 reports the percentage of saturated fatty acids (SFA), monounsaturated fatty acids (MUFA) and polyunsaturated fatty acids (PUFA), with a particular attention on the $\omega6/\omega3$ ratio. As can be seen, *Scenedesmus obliquus* has a higher quantity of omega-3 fatty acids than omega-6 fatty acids, but no significant difference can be observed between Soxhlet extraction and SCCO$_2$ extraction from these data.

4.4.2 Microalgae species and lipids composition

Three species of microalgae were compared: *Scenedesmus obliquus, Chlorella protothecoides* and *Nannochloropsis salina*. Supercritical CO_2 extractions were carried on for 90 minutes at 30 MPa and 45 °C. *Nannochloropsis salina* has been reported to have a high lipids content [Mohammady *et al.*, 2005], and indeed the highest yield was obtained with these microalgae species. In Figure 4.9, the model of broken and intact cells is applied to fit the extraction curves of the three different microalgae strains. It shows that, at the same opera-
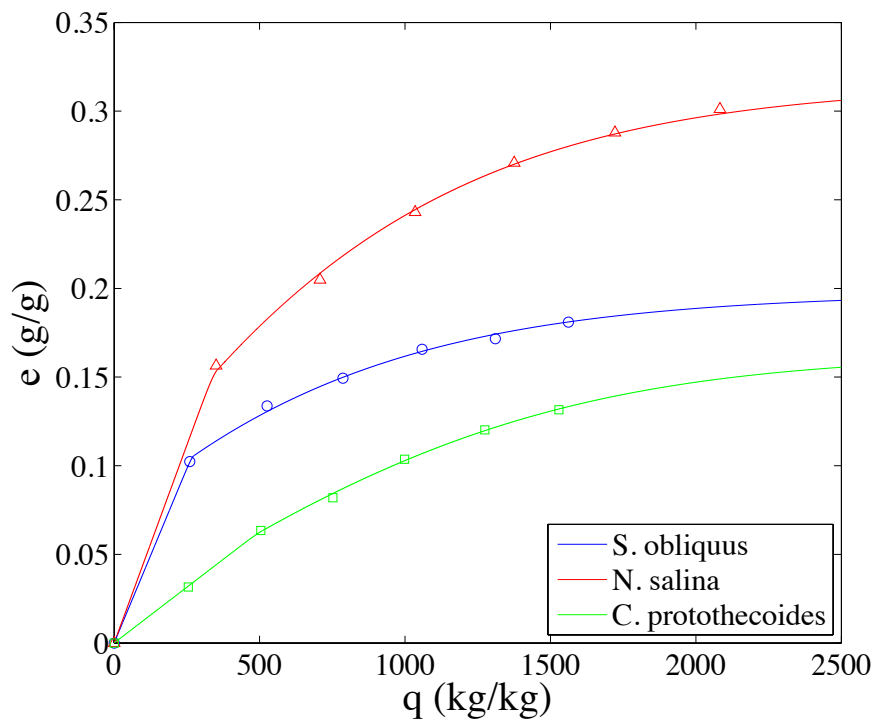
Figure 4.9: *Comparison between different species of microalgae.*

tive conditions, the yield reached was 30.36% with *N. salina*, 17.97% with *S. obliquus* and 13.30% with *C. protothecoides*.

As shown in Figure 4.10, the saturated fatty acids content in *N. salina* is 61%, while the unsaturated fatty acids percentage is 39%. The other strains, *S. obliquus* and *C. protothecoides* are richer in unsaturated fatty acids (approximately 65% the first one and 75% the second one). It is brought to attention that, even if the strain *C. protothecoides* has more unsaturated fatty acids than the strain *S. obliquus*, *C. protothecoides* and *N. salina* have a higher value of the $\omega6/\omega3$ ratio (see Table 4.8). This means that *S. obliquus* is the strain with the highest content of omega-3 fatty acids, that are the most valued ones in food and farmaceuticals industries, since the human body requires them for good health but is not able to synthesize them [Rubio-Rodríguez *et al.*, 2010]. As shown in Table 4.7, α-linolenic acid (ALA) is the most abundant omega-3 fatty acid and linoleic acid (LA) is the most abundant omega-6 fatty acid. *N. salina* has a low content in α-linolenic and linoleic acids (0.30% and 1.19% respectively), while the other microalgae species are richer in these FFA: *S. obliquus* has 9.34% of LA and 13.40% of ALA, while *C. protothecoides* has 23.59% of LA and 7.12% of ALA. The highest yield was then achieved with *Nannochloropsis Salina*, while the highest $\omega3/\omega6$ ratio (namely the lowest $\omega6/\omega3$ ratio), was obtained with *Scenedesmus Obliquus*.

It should be noted that *S. obliquus* has also a fair amount of C16:0 and C18:1 fatty acids, while *N. salina* is richer in C16:0 and C16:1cis fatty acids. This is desirable for biodiesel
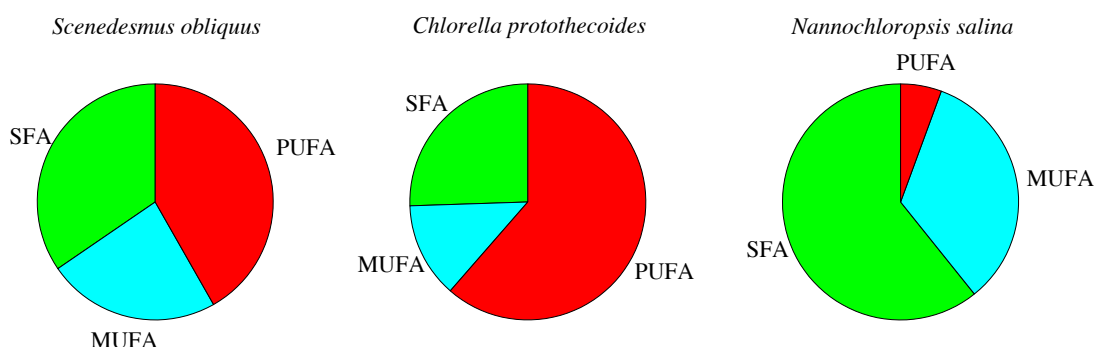
Figure 4.10: *Fatty acids content in different types of microalgae.*

production, since these compounds have higher oxidation stability than PUFA [Halim *et al.*, 2012]. However, to verify that a microalgae strain is suitable for biodiesel production more analyses should be made, such as the amount of cis-isomers, that are favorable for biodiesel production since they have advantageous cold flow properties (like freezing at a much lower temperature than other lipids) [Halim *et al.*, 2012].

4.4.3 SFE conditions and lipids composition

The influence of pressure, temperature and extraction time on lipid composition was investigated with the microalgae strain of *S. Obliquus*.

As mentioned above, the highest yield (24.7%) is obtained at 30 MPa, 65 °C and an extraction time of 90 minutes. However, these conditions do not correspond to those that give the lowest $\omega6/\omega3$ ratio. Table 4.8 shows that the lowest ratio, equal to 0.25, is achieved at the lowest temperature (45 °C), the lowest pressure (15 MPa) and the shortest extraction time (30 min).

Figure 4.11 shows the influence of the extraction conditions on α-linolenic acid (ALA) and linoleic acid (LA) content, while Table 4.7 reports their percentages. The graphs show clearly that, while linoleic acid is poorly influenced by the extraction conditions, α-linolenic acid is adversely influenced by them. Figure 4.11a shows that pressure poorly influences the free fatty acids content, lowering the ALA content of only 2% (from 21.5% at 15 MPa to 19.4% at 30 MPa). Figure 4.11b illustrates that the higher the temperature, the more significant is its effect on the linolenic acid. The extraction time is the most relevant parameter on omega-3 fatty acid ALA (Figure 4.11c), as it decreases from 20.1% to 13.4% when the extraction time is varied from 30 to 90 minutes, respectively.

To sum up, the highest yield is reached at higher pressure, temperature and extraction time, while for the omega-3 fatty acids content the opposite is true. Therefore, a compromise

should be sought between high yield and high $\omega 3/\omega 6$ ratio. An economic evaluation could be useful to find the best extraction conditions, since the energy consumption due to the heating and the pressurization is substantial to determine the process profitability.

Table 4.7: *Fatty acids composition of microalgae oil as a function of the extraction method, species and SFE conditions adopted.*

	Soxhlet	S. Obliquus								C. Protothecoides	N. Salina
		$SCCO_2$								$SCCO_2$	$SCCO_2$
Pressure (MPa)	1	30	30	30	15	25	30	30	30	30	30
Temperature (°C)	105	45	45	45	45	45	50	55	60	45	45
Extraction time (min)	1080	30	60	90	30	30	30	30	30	90	90
Saturated											
C14:0	0.54	0.47	0.51	0.82	0.42	0.45	0.49	0.51	0.55	0.76	3.87
C16:0	24.10	19.83	23.53	29.91	18.03	18.89	20.35	21.39	23.68	21.12	52.41
C18:0	0.93	1.10	1.39	1.87	0.97	1.01	1.15	1.45	1.06	1.46	2.29
Monounsaturated											
C16:1 ω9	3.00	2.65	2.73	4.11	2.15	2.45	2.78	2.77	3.19	4.80	0.24
C16:1cis ω7	0.30	0.26	0.36	0.51	0.17	0.24	0.28	0.29	0.34	1.58	29.17
C18:1 ω9	14.22	15.50	14.01	16.22	14.56	14.90	15.62	16.21	16.07	3.54	3.18
Polyunsaturated											
C16:2 ω6	2.23	2.03	2.12	0.00	1.98	2.00	2.22	2.19	2.53	0.00	0.00
C16:2	2.63	2.04	2.53	2.89	2.00	2.02	2.62	2.62	2.99	21.32	0.11
C16:3 ω3	4.03	4.20	4.09	3.83	4.00	4.10	4.02	4.39	3.95	7.60	0.11
C16:4 ω3	11.16	12.31	10.72	7.83	8.89	10.60	11.55	10.63	9.81	0.31	0.18
C18:2 ω6 (LA)	8.91	9.80	8.45	9.34	10.33	10.10	9.59	9.47	9.61	23.59	1.19
C18:3 ω3 (ALA)	18.08	20.10	17.02	13.40	21.47	21.01	19.36	18.86	17.18	7.12	0.30
C18:4 ω3	2.22	2.50	2.15	1.40	3.00	2.75	2.47	2.30	1.94	0.04	0.08
C18:5 ω3	0.74	0.01	1.92	0.00	0.00	0.01	1.11	0.95	0.83	0.00	0.00
C20:5 ω3 (EPA)	0.01	0.59	0.00	0.00	0.01	0.14	0.01	0.00	0.01	0.03	1.50

Table 4.8: *Microalgae lipid classes as a function of extraction method, species and SFE conditions adopted.*

	Soxhlet	S. Obliquus								C. Protothecoides	N. Salina
		$SCCO_2$								$SCCO_2$	$SCCO_2$
Pressure (MPa)	1	30	30	30	15	25	30	30	30	30	30
Temperature (°C)	105	45	45	45	45	45	50	55	60	45	45
Extraction time (min)	1080	30	60	90	30	30	30	30	30	90	90
SFA	27.38	22.75	26.90	34.59	20.33	21.33	23.40	24.65	26.71	25.68	61.25
MUFA	19.95	20.25	19.78	23.69	20.99	20.86	20.93	21.27	22.00	13.12	33.89
PUFA	52.67	57.44	53.32	41.80	58.84	58.08	55.67	54.08	51.28	61.77	5.66
Omega-3	36.32	40.90	36.01	26.59	41.86	41.10	38.63	37.24	33.76	15.13	0.77
Omega-6	11.20	11.00	10.61	9.34	10.65	10.46	11.86	11.71	12.20	23.63	2.32
Omega-6/Omega-3	0.31	0.27	0.29	0.35	0.25	0.25	0.31	0.31	0.36	1.56	3.02

(a) *Extraction pressure influence on free fatty acids content.*

(b) *Extraction temperature influence on free fatty acids content.*

(c) *Extraction time influence on free fatty acids content.*

Figure 4.11: *Influence of pressure, temperature and extraction time on lipids composition in supercritical CO_2 extraction.*

4.5   Concluding remarks

The results of this chapter can be summarized in these following points:

- The experimental total lipids extraction profiles are compatible with those available in literature.

- The model of broken and intact cells fits properly the extraction curves with the simplified model, but the complete model is often more accurate and allows to better characterize the system parameters. Furthermore, two extraction periods instead of three are sufficient to describe completely the system. The model based on characteristic times is less accurate but useful to understand the relation between extraction yield and extraction time.

- The analysis of the oil extracted with supercritical CO_2 extraction showed no substantial differences with the oil extracted with Soxhlet. This demonstrates that $SCCO_2$ is able to extract the same amount of oil extracted with solvent extraction, with advantages such as no use of toxic solvent, lower impurities content and less extraction time.

- The highest omega-3 content was obtained with *Scenedesmus Obliquus* while the highest yield was reached with *Nannochloropsis Salina*.

- The highest yield was achieved at 30 MPa and 65 °C for an extraction time of 90 minutes, while the highest $\omega3/\omega6$ ratio was reached at 15 MPa and 45 °C with an extraction time of 30 minutes.

- In any case, an economic evaluation would be necessary to find the optimal conditions.

Chapter 5

The modeling of solubility in supercritical CO_2 extraction

The solubility has a key role in supercritical fluid extraction since it determines how much oil can be dissolved into the solvent. Microalgae lipids composition changes from species to species but is mainly characterized by neutral and polar lipids [Halim *et al.*, 2012]. A mixture of supercritical CO_2 and ethanol is then suitable for the extraction since CO_2 has a great affinity with non polar and low polar compounds, and ethanol increases the affinity with polar compounds [Lam and Lee, 2013; Mendes *et al.*, 2006].

These affinities leads to a quite good solubility, therefore, it is important to understand the solubility behavior in supercritical extraction, and its relation with density. The relation between solubility and density has already been studied by many authors that have proposed different equations. One of the most famous equations has been developed by Chrastil, followed by other modified equations introduced later on. In this chapter, three equations will be examined and fitted to experimental data: Chrastil equation [Chrastil, 1982], Del Valle-Aguilera equation [Del Valle and Aguilera, 1988], and Adachi-Lu equation [Adachi and Lu, 1983].

5.1 The cross-over point

In supercritical systems solubility depends on density, which in turn depends on temperature and pressure. Therefore, changing these two variables, the final yield is affected considerably. Usually, an increase in pressure causes a solubility enhancement while increasing the temperature the solubility decreases. However, in some cases the solute vapor pressure, that increases with temperature, can influence the system enough to determine an increase in solubility even if the solvent power is not favored. Therefore, the same effect that was shown
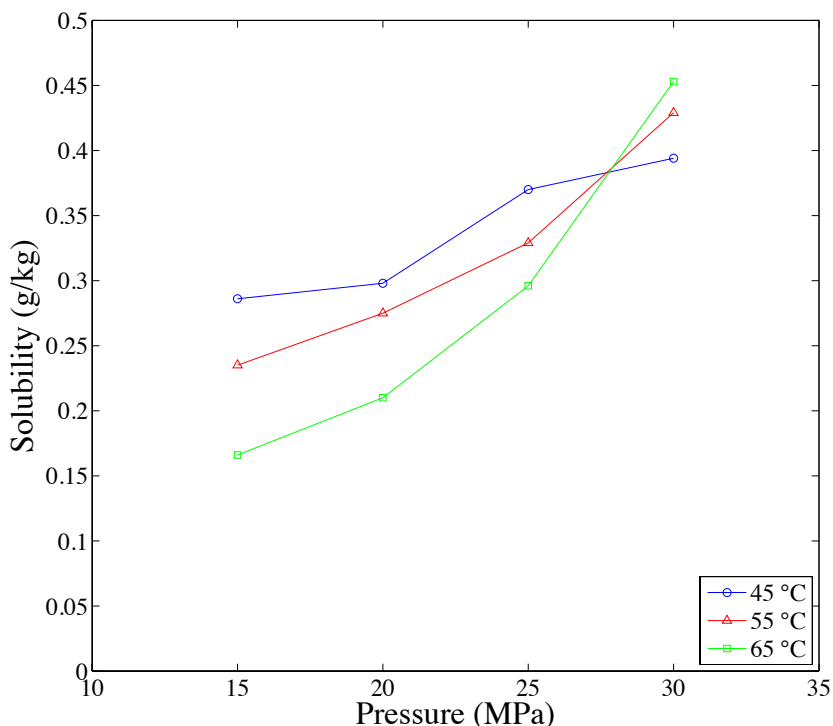
Figure 5.1: *Oil solubility in supercritical carbon dioxide at different pressures and temperatures.*

when the yield was plotted against pressure, in Figure 4.4, can also be observed when the solubility is plotted against pressure, in Figure 5.1. Below the cross-over value, solubility decreases with temperature, while above it solubility is raised. The highest solubility is then registered at 30 MPa and 65 °C, while the lowest one at 15 MPa and 65 °C. The cross-over lays between 25 and 30 MPa. The values of solubility at different pressures and temperatures are reported in Table 5.1, together with CO_2 density values.

The cross-over phenomenon can be explained more in detail considering that density does not have a linear dependence on temperature. Indeed, there is a difference between the region near the critical point and the region far from it. Above the critical point, at lower pressures the solubility decreases with temperature because the solvent density decreases rapidly with increasing the temperature near the critical pressure. Density is then the dominating factor and prevails on the solute vapor pressure, which is quite low in the case of microalgal oil. Nevertheless, at higher pressures the density changes are more tempered, consequently vapor pressure becomes the prevailing factor, leading the solubility to increase with temperature. The separation between these two regions above the critical point is indicated by the cross-over point represented in Figure 5.1.

Table 5.1: CO_2 *density and solubility at different pressures and temperatures.*

| P | T | ρ_f | y_s |
MPa	°C	kg/m³	g/kg
15	45	741.22	0.286
15	55	651.72	0.235
15	65	553.27	0.166
20	45	812.87	0.298
20	55	754.30	0.275
20	65	691.16	0.210
25	45	857.59	0.370
25	55	810.83	0.329
25	65	761.85	0.296
30	45	890.88	0.394
30	55	850.59	0.423
30	65	809.09	0.453

P, pressure; T, temperature; ρ_f, CO_2 density; y_s, solubility.

5.2 Solubility equations

In 1982, Chrastil published an equation to correlate the solubility of solids and liquids in dense gases as a function of density and temperature [Chrastil, 1982]. Afterwards, Del Valle-Aguilera and Adachi-Lu modified this equation adding one parameter the first one, and two parameters the second one [Adachi and Lu, 1983; Del Valle and Aguilera, 1988]. In this work, all of these equations were fitted to experimental data and the unknown parameters were calculated.

5.2.1 The Chrastil Equation

The Chrastil equation [Chrastil, 1982] is derived from the study of the equilibrium between a solute and a dense gas solvent. The dissolution of the solute in the solvent occurs when the molecules of the solute associate with the gas molecules to form a "solvato complex". One molecule of a solvato complex can be described as one molecule of solute A associated with k molecules of solvent B. Under equilibrium conditions, there is a relation between A (the solute molecule), kB (the solvent molecules) and AB_k (the solvato complex molecule), expressed as:

$$A + k B \rightleftharpoons AB_k .$$ (5.1)

The equilibrium constant, K_{eq}, will be then:

$$K_{eq} = \frac{[AB_k]}{[A][B]^k} \tag{5.2}$$

where [A] is the solute concentration, [B] is the solvent concentration, [AB] is the concentration of the solvato complex and k is an association number. The expression above can be written using the logarithmic base:

$$\ln K_{eq} + \ln [A] + k \ln [B] = ln[AB]_k . \tag{5.3}$$

The logarithm of the equilibrium constant is equal to:

$$\ln K_{eq} = \frac{\Delta H_{solv}}{RT} + q_s , \tag{5.4}$$

where ΔH_{solv} is the heat of solvation, R is the ideal gas constant, T is the absolute temperature, and q_s is a constant.

The logarithm of the solute vapor concentration can be approximated by the Clausius-Clapeyron equation:

$$\ln [A] = \frac{\Delta H_{vap}}{RT} + q_v , \tag{5.5}$$

where ΔH_{vap} is the heat of vaporization of the solute and q_v is a constant.

Equations 5.4 and 5.5 can be used in Eq. 5.3 to obtain:

$$\frac{\Delta H}{RT} + q + k \ln [B] = \ln[AB_k] , \tag{5.6}$$

where ΔH is the total reaction heat: $\Delta H = \Delta H_{solv} + \Delta H_{vap}$ and q is a constant equal to: $q = q_s + q_v$.

Furthermore, the concentrations can be divided by the molecular weight to pass from mol/L to g/L:

$$[AB]_k = \frac{S}{MW_A + kMW_B} , \tag{5.7}$$

$$[B] = \frac{\rho}{MW_B} . \tag{5.8}$$

where M_B and MW_B are the molecular weight of A and B respectively, S is the concentration of the solute in the solvent, and ρ is the solvent density, both expressed in g/L.

Equations 5.7 and 5.8 are included in Eq. 5.6 to obtain:

$$\frac{\Delta H}{RT} + q + k \ln \rho - k \ln MW_B = \ln S - \ln(MW_A + kMW_B) , \tag{5.9}$$

which rearranged gave the Chrastil equation:

$$S = \rho^k \exp\left(\frac{a}{T} + b\right) , \tag{5.10}$$

where S is the solubility of the solute in the dense gas, expressed in g/L, ρ is the solvent density in g/L, k is the association number, T is the temperature in K, a is the heat of reaction as the solute associates with the solvent, and b is a relationship between the molecular weights of the solute and the solvent. They are expressed as:

$$a = \frac{\Delta H}{R} , \tag{5.11}$$

$$b = \ln(M_A + kMW_B) + q - k\ln MW_B . \tag{5.12}$$

The parameters to be evaluated are the association number, k, and the values of a and b. The experimental data of solubility, density and temperature were used to fit the values of these parameters.

5.2.2 Del Valle-Aguilera equation

The equation of Del Valle-Aguilera [Del Valle and Aguilera, 1988] adds one parameter to the Chrastil equation, in order to describe more in detail the dependence of the solubility on temperature. These authors introduced an empirical modification in the Chrastil equation to compensate the variation of ΔH_{vap} with temperature.

According to the Chrastil equation, the plot of $\ln S$ as a function of $\ln \rho$ should give a straight line with slope k and intercept I for: $\rho = 1$ g/mL. Furthermore, the intercept can be plotted as a function of temperature at constant density of 1 g/mL. The result is again a straight line with slope m and intercept b:

$$I = b + \frac{m}{T} . \tag{5.13}$$

The modification introduced by Del Valle and Aguilera changes Eq. 5.13 above from a first degree equation to a second degree equation:

$$I = b + \frac{m}{T} + \frac{n}{T^2} . \tag{5.14}$$

The resulting equation of the solubility as a function of density and temperature becomes:

$$S = \rho^k \exp\left(\frac{a}{T} + b + \frac{c}{T^2}\right) , \tag{5.15}$$

where all the variables are defined as in the Chrastil model except c which is the empirical modification introduced by Del Valle-Aguilera.

The fitting to experimental data will be used to obtain four parameters instead of three, namely the association number, k, and the values of a, b, and c.

5.2.3   Adachi-Lu equation

The Adachi-Lu model [Adachi and Lu, 1983] changes the dependence of the solubility with respect to density, adding two parameters in the exponential term of density. The Chrastil equation becomes:

$$S = \rho^{k+c\rho+d\rho^2} + exp\left(\frac{a}{T} + b\right) , \qquad (5.16)$$

where all the variables are defined as in the Chrastil model except d and e, which depend on the modification introduced by Adachi and Lu.

The unknown parameters are: k, a, b, c, and d, and are adjusted by fitting to experimental data.

5.3   Solubility modeling

The three equations recalled in the previous section were fitted to the experimental data reported in Table 5.1, in order to estimate which model is more accurate.

CO_2 density is calculated with the Bender equation of state (Eq. 1.1). The presence of ethanol was neglected, since the difference between the CO_2 density and the mixture density is low. The solubility is calculated from the initial slope of the extraction curve, namely the ratio between the mass of extract collected in the first extraction period and the amount of solvent passed in this period. The first extraction period is, indeed, the one where the solubility corresponds to the phase equilibrium value. Finally, the solubility obtained is multiplied by the density to converts the units from g/kg to g/L.

The models of Chrastil, Del Valle-Aguilera and Adachi-Lu were fitted to experimental data using MATLAB®. The functions and scripts are reported in Appendix C, section C.2.

5.3.1   Pressure effects

To evaluate the parameters of each model and compare them, the data obtained at constant temperature and different pressures were considered. The temperature was maintained at 55 °C and the pressure was varied from 15 MPa to 30 MPa. The results are represented in Figures 5.2 and 5.3, which show the solubility as a function of pressure, and as a function of the density, respectively. The curve trend is very similar in all the three cases considered.
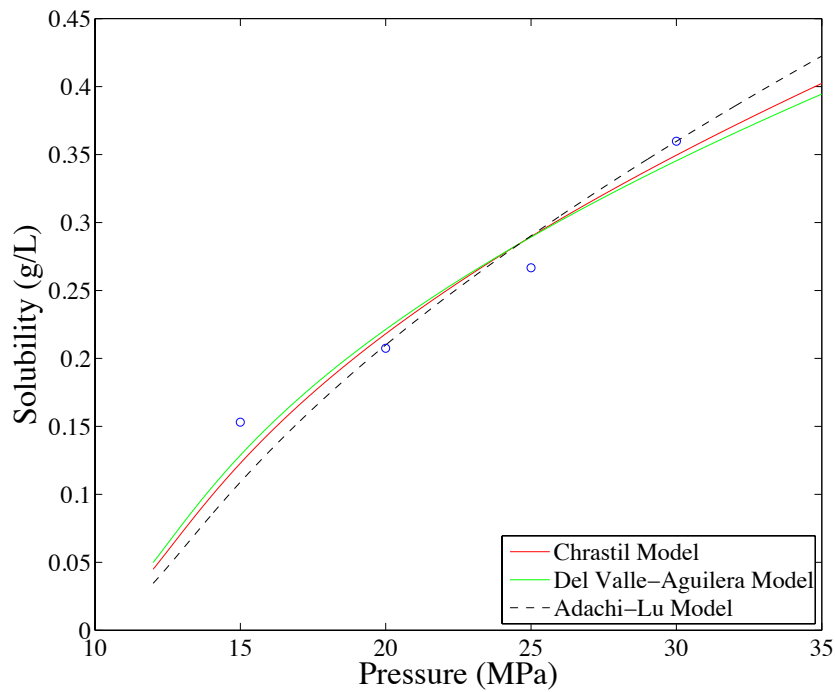
Figure 5.2: *Oil solubility in supercritical carbon dioxide as a function of the pressure at constant temperature.*
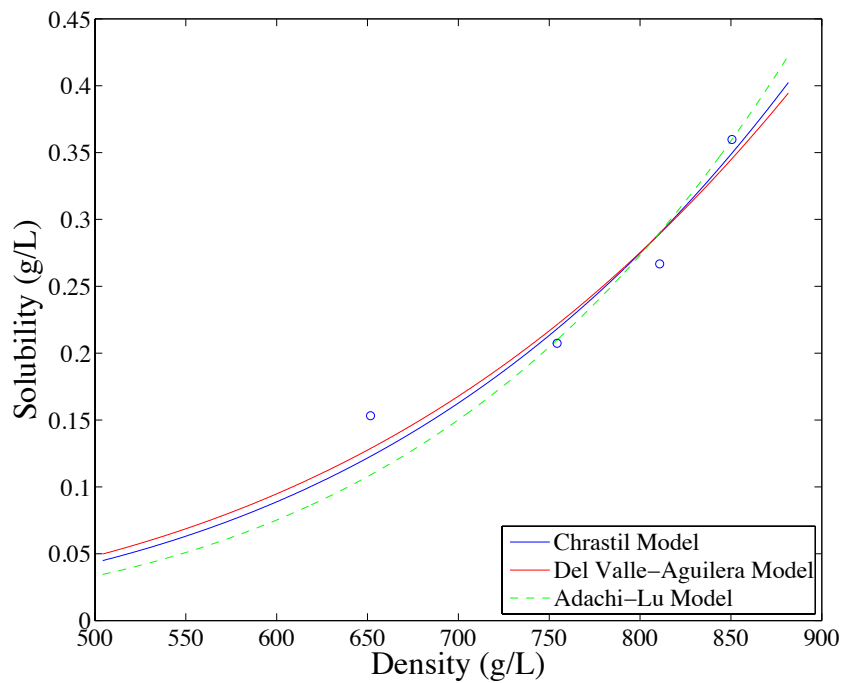
Figure 5.3: *Oil solubility in supercritical carbon dioxide as a function of the density at constant temperature.*

Table 5.2: *Calculated parameters for the solubility models of Chrastil, Del Valle-Aguilera and Adachi-Lu.*

Parameters	Chrastil	Del Valle-Aguilera	Adachi-Lu
A	3.9265	3.7059	4.4849
B	17.7140	-19.0766	-25.0568
C	-1.4850×10^4	-2.3248×10^3	-2.0411×10^3
D		1.0587×10^4	
E			1.04×10^{-10}
F			1.08×10^{-12}
AARD (%)	9.09	8.77	9.71

AARD, average absolute relative deviation.

To simplify the comparison between the parameters, they are called A, B, C, D, E, and F, and the equations are expressed as:

$$S = \rho^A \exp\left(B + \frac{C}{T} \right) , \tag{5.17}$$

$$S = \rho^A \exp\left(B + \frac{C}{T} + \frac{D}{T^2} \right) , \tag{5.18}$$

$$S = \rho^{A+E\rho+F\rho^2} + exp\left(B + \frac{C}{T} \right) . \tag{5.19}$$

It can be seen that A, B, and C (the parameters of the Chrastil model) are present in all the three equations, while D is the parameter added in the Del Valle-Aguilera model and E and F are the parameters added in the Adachi-Lu model.

The parameter values are summarized in Table 5.2, together with the residual function of each model. The model of Del Valle-Aguilera resulted the most accurate, while the Adachi-Lu model has the values of the parameters E and F so small that its form leads back to the Chrastil equation.

Being the most accurate (with an AARD of 8.77%), the model of Del Valle-Aguilera was chosen to represent the other isotherm curves. Figure 5.4 shows the cross-over point, that occurs after 25 MPa, as in Figure 5.1. Table 5.3 shows the parameters obtained fitting the curves at each temperature. The lack of precision (from 4.31% to 18.88%) is probably due to the lack of experimental points. Furthermore, the pressure does not directly appear in the formula, but it is present in the density equation, so the dependence on it is less marked. However, Figure 5.4 confirms that the solubility always increase with pressure.

Figure 5.4: *Del Valle-Aguilera model applied to show the microalgae oil solubility in supercritical carbon dioxide as a function of the pressure, with parametric temperature.*

Table 5.3: *Calculated parameters for the solubility model of Del Valle-Aguilera at different temperatures.*

Parameters	Temperature (°C)		
	45	55	65
A	2.8635	3.7059	6.0190
B	-13.5717	-19.0766	-5.7725
C	-2.2412×10^3	-2.3248×10^3	-1.2049×10^4
D	1.0563×10^4	1.0587×10^4	1.0649×10^4
AARD (%)	4.31	8.77	18.88

AARD, average absolute relative deviation.

5.3.2 Temperature effects

The behavior of solubility with respect to temperature was also investigated at constant pressure. The Chrastil model was applied, since the residual function is very low and the precision is greater than that one of the previous fitting. The temperature, indeed, appears directly in the equation inside the exponential term, and indirectly inside the density equation, where it has a more important role (Eq. 1.1). The curves of solubility versus temperature are represented in Figure 5.5, at three different pressures. The parameters and the residual function for each isobaric curve are reported in Table 5.4. The curve trend at 30 MPa shows that the

Figure 5.5: *Chrastil model applied to show the microalgae oil solubility in supercritical carbon dioxide as a function of the temperature, with parametric pressure.*

Table 5.4: *Calculated parameters for the solubility model of Chrastil at different pressures.*

Parameters	Pressure (MPa)		
	15	25	30
A	0.0019	3.5332	4.3397
B	6.07×10^{-4}	-21.5453	-26.9687
C	-3.4037×10^2	-1.0645×10^3	-1.1169×10^3
AARD (%)	0.72	1.23	1.75

 AARD, average absolute relative deviation.

solubility increases with temperature, being increased by the solute vapor pressure, while at 15 MPa and 25 MPa it decreases with the increasing of temperature.

5.3.3   Density effects

The results obtained in the previous sections can be used to plot the solubility as a function of density. For example, from Table 5.1 it can be seen that below the cross-over point the solubility always increases with density, so it could be interesting to observe the profile of solubility versus density.

The density trend with respect to temperature and pressure can be observed in Figure 5.6,

(a) CO_2 *density as a function of temperature with parametric pressure.*

(b) CO_2 *density as a function of pressure with parametric temperature.*
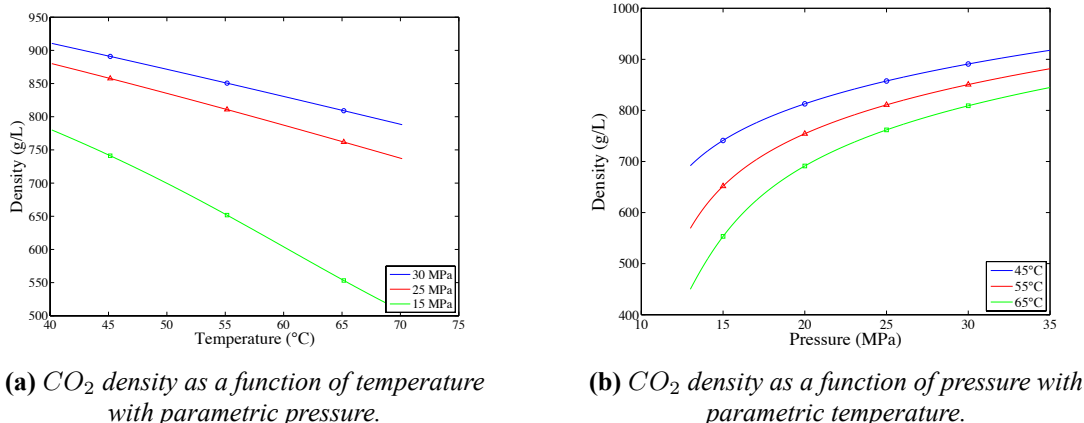
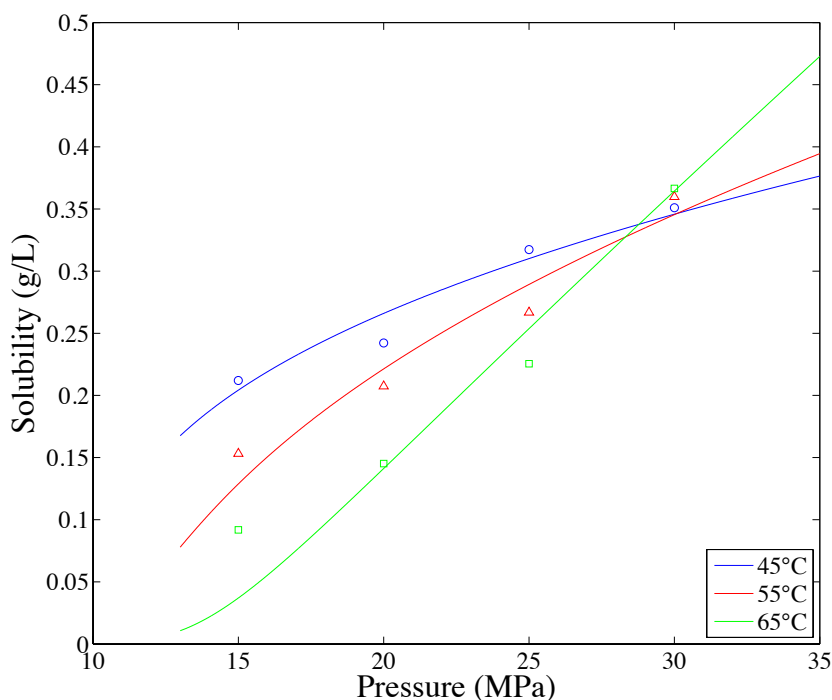**Figure 5.6:** *Influence of pressure and temperature on CO_2 density.*
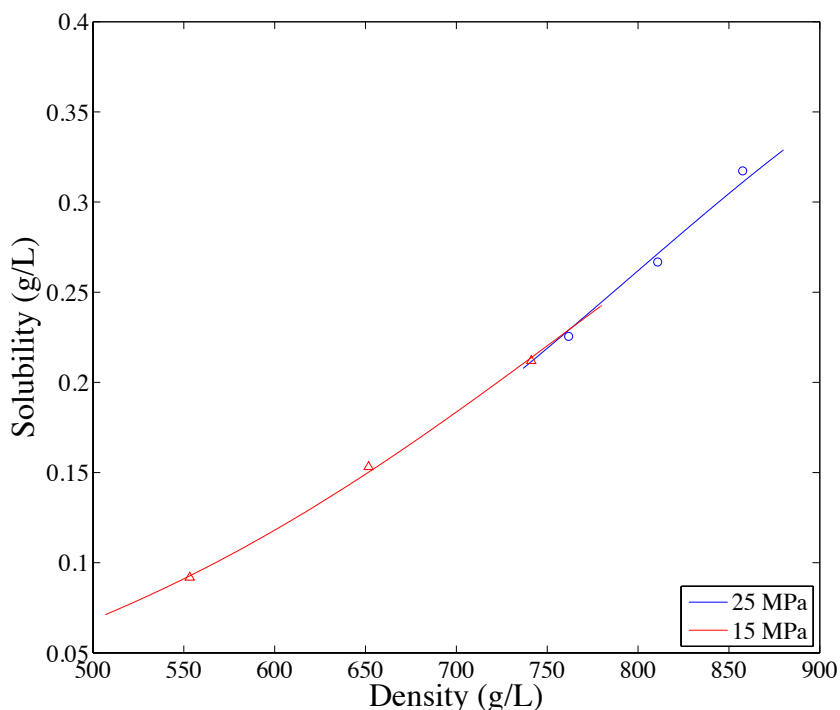
Figure 5.7: *Chrastil model applied to show the microalgae oil solubility in supercritical carbon dioxide as a function of the density, with parametric pressure.*

where, once again, it can be observed that density decreases with temperature, and increases with pressure. Furthermore, it is clearly visible how density decreases rapidly at the lowest pressure (15 MPa).

To understand the relation between density and solubility, the data obtained with the Chrastil model were used (Table 5.4). Figure 5.7 shows a linear trend, similar to the results obtained by Chrastil when investigating the relation between the solubility of several compounds and the CO_2 density [Chrastil, 1982].
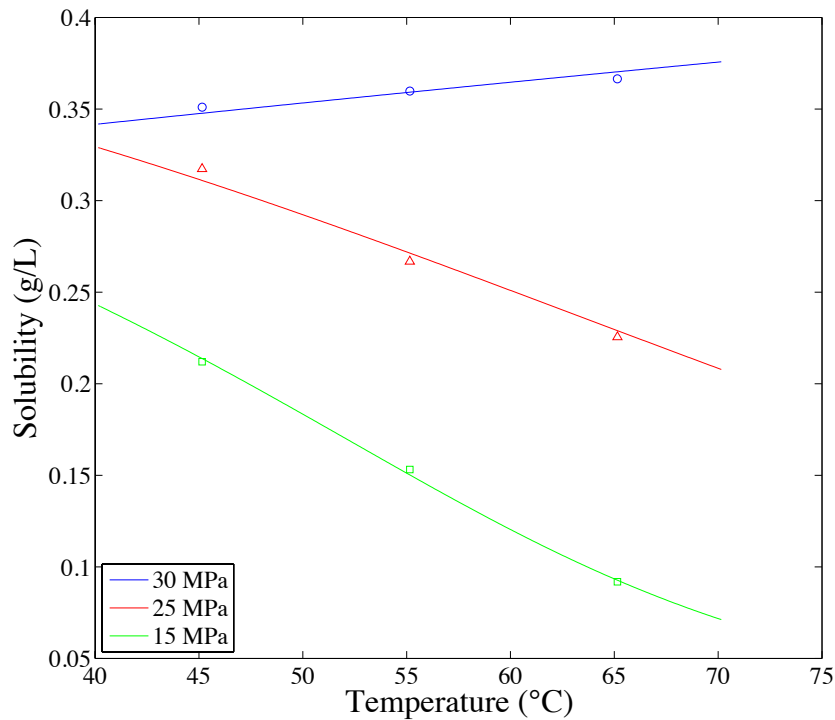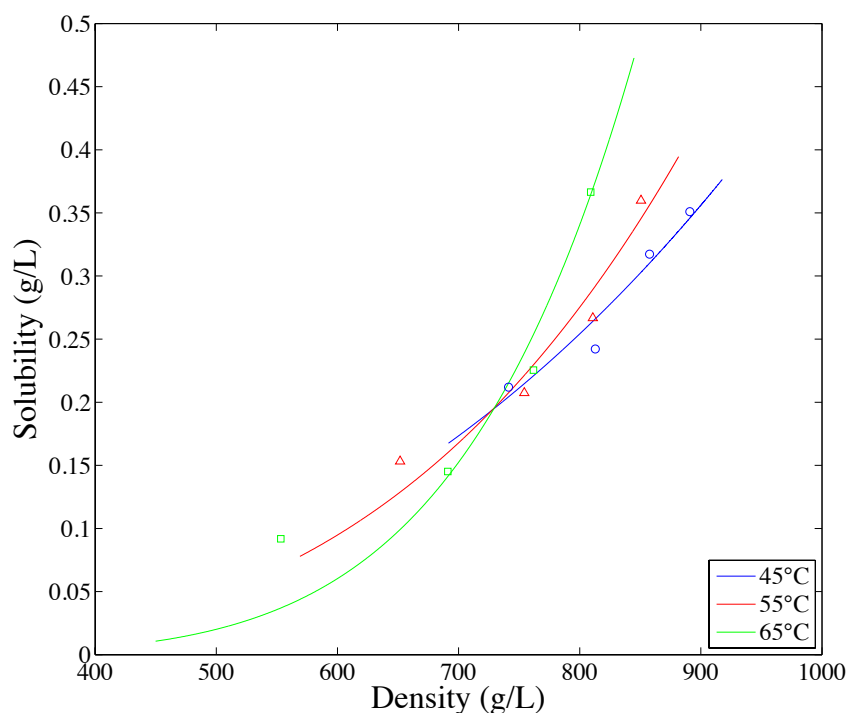
Figure 5.8: *Chrastil model applied to show the microalgae oil solubility in supercritical carbon dioxide as a function of the density, with parametric temperature.*

Furthermore, the data obtained with the model of Del Valle-Aguilera can be used to plot the solubility as a function of density, at constant pressure. The result is shown in Figure 5.8: here a cross-over point between 25 and 30 MPa is present, as already seen in the other Figures that show the cross-over, but this curve trend is not confirmed by the literature, in which the curves at different temperatures never intersect each other. The density, indeed, does not have a linear dependence on the pressure, so even if the cross-over point appears in the function of solubility against pressure, it should not appear in the function of solubility versus density. The lack of experimental points could be the reason of this behavior.

The existence of cross-over points is reported by several authors. For example, Setianto et al. (2009) calculating the phase equilibria of cashew nut shell liquid and CO_2 system, found a cross-over around 24 MPa [Setianto *et al.*, 2009]. Asghari-Khiavi et al. (2004) analyzed the extraction of medroxyprogesterone and cyproterone acetate with supercritical carbon dioxide and reported the presence of a cross-over point between 22 MPa and 30 MPa [Asghari-Kiavi *et al.*, 2004]. These and other similar cases [Setianto *et al.*, 2012; Vatanara *et al.*, 2005] demonstrate that the cross-over phenomenon is well documented in literature and it is important to investigate it for each type of solute, since the solubility is a key parameter in supercritical fluid extraction.

5.4 Other thermodynamic models

The Chrastil model, the Del Valle-Aguilera model and the Adachi-Lu model are based on semi-empirical correlations between solubility and density. This modeling approach is called "density-based" approach. In particular, the Chrastil equation, is considered the most successful one. However, the downside of this approach is that, due to the empirical nature of the equations, they are unable to predict phase equilibria [Sovová and Stateva, 2011].

Besides the density-based approach, there are other three approaches: the dense gas approach, the expanded liquid approach and the solubility parameter approach (that will not be discussed). They are based on a molecular thermodynamic description of the system, which is made of two phases: the supercritical phase (the solvent) and the solid phase (solid solute). The thermodynamic equilibrium is achieved when, for all the components, the fugacity in a phase is equal to the fugacity in the other phase:

$$f_i^S = f_i^F \, , \tag{5.20}$$

where f_i^S is the fugacity of component i in the solid phase and f_i^F is the fugacity of component i in the supercritical phase.

The dense gas and the expanded liquid approach differ in the description of the supercritical phase, that in the first case is considered as a gas, while in the second case as a liquid. Both of them express the fugacity of the solute (component 2) in the solid phase using a fluid-phase reference state:

$$f_2^S = P_2^S \varphi_2^S \exp \int_{P_2^S}^{P} \frac{v_2^S}{RT} \, \mathrm{d}P \, , \tag{5.21}$$

where P_2^S is the sublimation pressure of the pure solid, φ_2^S is the fugacity coefficient at sublimation pressure, v_2^S is the molar volume of the solid, R is the ideal gas constant, P is the pressure and T is the temperature.

If the supercritical fluid is considered as a gas, the fugacity coefficient will be expressed as:

$$f_2^G = y_2 P \varphi_2^G \, , \tag{5.22}$$

where y_2 is the solubility of the solute in the supercritical fluid, P is the pressure and φ_2^G is the fugacity coefficient of the solute in the supercritical phase.

Equating these two expressions, the solubility is obtained as:

$$y = \frac{P_2^S}{P} \frac{\varphi_2^S \exp\left[\frac{v_2^S(P - P_2^S)}{RT}\right]}{\varphi_2^G} \, . \tag{5.23}$$

For an ideal gas, the solubility is equal to the ratio of the two pressures, P_2^S and P, since the fugacity coefficients, φ_2^S and φ_2^G, and the exponential term, that is the Poynting factor, are equal to 1. For real components these corrections factors cannot be neglected and become dominant, since the fugacity coefficients consider the deviation from the ideal case and the Poynting factor considers the effect of pressure. In particular, the fugacity coefficient of the solute in the solid phase, φ_2^S, differs little from the unity, since the sublimation pressure is quite small, and the Poynting factor is usually below 2 or 3. The most important factor is certainly the fugacity coefficient in the supercritical phase, φ_2^G, that is usually far from unity. The only possibility to calculate this term accurately is to use an equation of state approach. Unfortunately, cubic equations of state, for which interaction parameter values are often available, have often a poor behavior in the supercritical region.

The expanded liquid approach considers the supercritical fluid as a liquid, therefore the activity coefficient must be determined. This means that, while the dense gas approach needs one parameter (the fugacity coefficient, φ_2^G), the expanded liquid approach has to determine two parameters: the activity coefficient and the partial molar volume of the solute at infinite dilution.

The main problem of these approaches is that the thermodynamic model has to describe a very complex system with several difficulties. For example, the solubility depends much on vapor (sublimation) pressure, but this data is often unavailable for low volatile compounds. Many thermodynamic models have also some difficulties in describing the anomalous behavior of the system near the critical point, due to rapid density changes. Furthermore, the supercritical fluid solutions are often highly non-ideal mixture, since the molecular sizes and the interaction strengths of solute and solvent usually differs very much. Therefore, since the systems in supercritical fluid extraction are complex, they can be described accurately only with a robust and reliable structure that comprehends: thermodynamic parameters for pure components and binary interaction parameters, a proper mixture model, and numerical techniques that can solve the equilibrium relations [Sovová and Stateva, 2011].

Conclusions

The aim of this work was to investigate the kinetics and the solubility of supercritical CO_2 extraction of lipids from microalgae both experimentally and theoretically.

The experiments were performed with a laboratory plant assembled for the purpose. Three microalgae strains were used: *Scenedesmus obliquus*, *Chlorella protothecoides*, and *Nannochloropsis salina*. At first, particle size, moisture content and co-solvent flow rate were optimized. It is reported that the smaller the particle size, the higher the yield. Therefore, after drying the microalgae, they were milled and sieved with a filter to obtain a diameter below 0.5 mm. Microalgae were dried to reduce the moisture content since water could reduce the surface contact between solvent and solute. Ethanol was used as co-solvent to increase the yield of polar compounds, using 6% by weight with respect to CO_2 flow rate.

The second part of experiments was focused on finding the optimal operative conditions. Since the solubility of oil in supercritical CO_2 depends on density, pressure and temperature were varied to affect density and, therefore, the solubility. The extractions were carried out at pressures of 15, 20, 25, and 30 MPa, and temperatures of 45, 55, and 65 °C. CO_2 flow rate was kept fixed at 0.4 kg/h, with an extraction time of 90 minutes for 0.5 g of microalgae charged into the extractor. Samples were collected every 15 minutes, in order to obtain the extraction curve.

Lipids composition was also analyzed to determine the operative conditions that brings higher ratio $\omega 3/\omega 6$ and to compare supercritical fluid extraction with the traditional solvent extraction. The free fatty acids profile of the three different species of microalgae was also compared.

The model of broken and intact cells [Sovová, 2005] was used to obtain the values of the parameters that govern the process with a fitting to experimental data. This model, built to describe the supercritical fluid extraction of vegetable oil from plant materials, resulted equally suitable for the extraction of lipids from microalgae. The system was considered as a plug flow with no solute-matrix interaction, and the process was divided in two periods: in the first one the extraction yield is controlled by phase equilibrium, in the second one by internal mass transfer resistance. The extraction curve equations were fitted to experimental

data for each experiment, to adjust the unknown values of the grinding efficiency (or also the fraction of broken cells), r, the external mass transfer coefficient, k_f, and the internal mass transfer coefficient multiplied by the specific area between the regions of intact and broken cells, $k_s a_s$. A simplified model was used to evaluate a first estimation of r and $k_s a_s$, and another simplified model was fitted to calculate the characteristic times of the process. The extraction curve was plotted for each experiment, showing that the simplified model is able to fit properly the extraction curves, giving satisfactory results. The main difference with respect to the complete model is that the latter evaluates an extra parameter, namely k_f. Furthermore, it was shown that the transition period, that appears only in the complete model, can be neglected since the equation of the first period is able to describe it. The model based on characteristic times is slightly less precise than the other ones but gives valid results as well. For all the models, the parameters values were similar to those reported in literature [Mouahid *et al.*, 2013; Sovová, 2005, 2012].

The modeling of solubility was also investigated, to understand its relation with density. The solubility of oil in supercritical CO_2 is, indeed, strictly dependent on density, and therefore on pressure and temperature. Changing them, the solubility can be therefore fine-tuned to increase the process efficiency. To link the solubility with CO_2 density, the Chrastil model [Chrastil, 1982] was applied and compared with other two models, developed by Del Valle-Aguilera [Del Valle and Aguilera, 1988] and Adachi-Lu [Adachi and Lu, 1983], which modified the first one adding one and two parameters, respectively. The model of Del Valle-Aguilera resulted the most accurate, while the Adachi-Lu model gives the value of the additional parameters very small, leading back to the Chrastil equation. However, all the three models give satisfactory results, with the limit that they cannot predict phase equilibria, since they are empirical correlations.

The oil collected after the experiments was analyzed to observe the lipids profile at different operative conditions and to compare different strains and different techniques (solvent extraction and supercritical CO_2 extraction). Attention was paid on free fatty acids composition, in particular on the content of omega-3 and omega-6 fatty acids.

Supercritial CO_2 extraction has many advantages with respect to solvent extraction: carbon dioxide is cheap, easily available, not toxic, not flammable and in its supercritical state has high selectivity, high diffusivity and low viscosity. Comparing the lipids composition of this technique with respect to solvent extraction it can be seen that there are no substantial differences. This demonstrates that supercritical CO_2 is able to extract the same amount of oil extracted with solvent extraction, with the advantages of ensuring a free-solvent process, faster and more selective.

The comparison of the three microalgae strains reported a different fatty acids composition, as expected. *Scenedesmus obliquus* and *Chlorella protothecoides* are richer in polyunsaturated fatty acids, while *Nannochloropsis salina* resulted richer in saturated fatty acids. Therefore, while the highest yield was obtained with *N. salina*, which has indeed a higher lipids content, the highest omega-3 fatty acids content was obtained with *S. obliquus*. The ratio between omega-3 and omega-6 fatty acids was also analyzed, and *S. obliquus* resulted to have the highest value of this ratio.

Comparing the extraction yield at different operative conditions, the highest yield was obtained at 30 MPa and 65 °C with an extraction time of 90 minutes, while the highest omega-3 fatty acids content was achieved at 15 MPa and 45 °C after 30 minutes of extraction. This shows that increasing pressure, temperature and extraction time mostly, the omega-3 fatty acids content diminishes. Furthermore, pressure and temperature effects on yield showed the presence of a cross-over point between 25 and 30 MPa, and the same behavior was observed with solubility. This means that yield and solubility are favored by temperature only at higher pressures, while near the critical point, increasing temperature, density changes are so rapid that negatively affect solubility and yield. The cross-over phenomenon is common in the extraction processes, and varies with the type of material and solute. The knowledge of this point is important to optimize the operative conditions of the process.

The results obtained in this work show that supercritical fluid extraction can be a competitive technique, but an economic evaluation should be done to verify its feasibility, particularly at large scale. The model of broken and intact cells turns out to be a general and versatile model which gave satisfactory results with microalgae, even if built for plant materials. Solubility modeling with empirical equations that relates it with density, gives also good results, but other models should be investigated that can predict phase equilibria, using an adequate equation of state and proper mixing rules.

Appendix A

The Bender equation of state

The Bender equation of state (Eq. 1.1) calculates the pressure as a function of temperature and density using a 20 parameters expression, fitted on property data. These parameters, that allow to calculate the constants B, C, D, E, F, G, and H, are:

$$
\begin{aligned}
a_1 &= 0.22488558; & a_{11} &= 0.12115286; \\
a_2 &= 0.1371796 \cdot 10^3; & a_{12} &= 0.10783386 \cdot 10^3; \\
a_3 &= 0.1443021 \cdot 10^5; & a_{13} &= 0.43962336 \cdot 10^2; \\
a_4 &= 0.2963049 \cdot 10^7; & a_{14} &= -0.36505545 \cdot 10^8; \\
a_5 &= 0.20606039 \cdot 10^9; & a_{15} &= 0.1949051 \cdot 10^{11}; \\
a_6 &= 0.45554393 \cdot 10^{-1}; & a_{16} &= -0.29186718 \cdot 10^{13}; \\
a_7 &= 0.77042840 \cdot 10^2; & a_{17} &= 0.24358627 \cdot 10^8; \\
a_8 &= 0.40602371 \cdot 10^5; & a_{18} &= -0.37546530 \cdot 10^{11}; \\
a_9 &= 0.40029509; & a_{19} &= 0.11898141 \cdot 10^{14}; \\
a_{10} &= -0.39436077 \cdot 10^3; & a_{20} &= 0.5000000 \cdot 10;
\end{aligned}
\tag{A.1}
$$

The additional 7 parameters, necessary to calculate the enthalpy with Eq. 1.4, are:

$$
\begin{aligned}
e_1 &= 0.185312 \cdot 10^{-3}; \\
e_2 &= -0.8552719 \cdot 10^{-2}; \\
e_3 &= 0.1450667; \\
e_4 &= -1.068975; \\
e_5 &= 5.219996; \\
e_6 &= 1.833078; \\
e_7 &= -0.5882021;
\end{aligned}
\tag{A.2}
$$

The derivatives of B, C, D, E, F, G, and H, that appear in Eq. 1.4, are defined as:

$$
\begin{aligned}
T\frac{\mathrm{d}B}{\mathrm{d}T} &= a_1 T + \frac{a_3}{T} + \frac{2a_4}{T^2} + \frac{3a_5}{T^3} \; ; \\
T\frac{\mathrm{d}C}{\mathrm{d}T} &= a_6 T + \frac{a_8}{T} \; ; \\
T\frac{\mathrm{d}D}{\mathrm{d}T} &= a_9 T \; ; \\
T\frac{\mathrm{d}E}{\mathrm{d}T} &= a_{11} T \; ; \\
T\frac{\mathrm{d}F}{\mathrm{d}T} &= 0 \; ; \\
T\frac{\mathrm{d}G}{\mathrm{d}T} &= -\frac{2a_{14}}{T^2} - \frac{3a_{15}}{T^3} - \frac{4a_{16}}{T^4} \; ; \\
T\frac{\mathrm{d}H}{\mathrm{d}T} &= -\frac{2a_{17}}{T^2} - \frac{3a_{18}}{T^3} - \frac{4a_{19}}{T^4} \; ;
\end{aligned}
\tag{A.3}
$$

The Matlab program that solves the Bender equation (Eq. 1.1), given pressure and temperature, is:

```
function ro = benderro(P, T)

R = 0.188918;

a1  = 0.22488558;
a2  = 0.13717965e3;
a3  = 0.14430214e5;
a4  = 0.29630491e7;
a5  = 0.20606039e9;
a6  = 0.45554393e-1;
a7  = 0.77042840e2;
a8  = 0.40602371e5;
a9  = 0.40029509;
a10 = -0.39436077e3;
a11 = 0.12115286;
a12 = 0.10783386e3;
a13 = 0.43962336e2;
a14 = -0.36505545e8;
a15 = 0.19490511e11;
a16 = -0.29186718e13;
a17 = 0.24358627e8;
a18 = -0.37546530e11;
a19 = 0.11898141e14;
a20 = 0.50000000e1;

B = a1.*T-a2-a3./T-a4./T^2-a5./T^3;
C = a6.*T+a7+a8./T;
```

```matlab
   D = a9.*T+a10;
   E = a11.*T+a12;
30 F = a13;
   G = a14./T^2+a15./T^3+a16./T^4;
   H = a17./T^2+a18./T^3+a19./T^4;

   Fx=('R.*T.*x+B.*x.^2+C.*x.^3+D.*x.^4+E.*x.^5+F.*x.^6+(G+H.*x.^2).*x.^3.*
       exp(-a20.*x.^2)-P');
35 a=0;
   c=1;
   e=0.000001;
   x=a;
   Fa=eval(Fx);
40 x=c;
   Fc=eval(Fx);
   while abs(c-a)>e
       b=(a+c)/2;
       x=b;
45     Fb=eval(Fx);
       if Fa*Fb<=0
           c=b;
           Fc=Fb;
       else
50         a=b;
           Fa=Fb;
       end
   end
   ro = b;
55 end
```

The program that solves Eq. 1.4, to obtain the enthalpy, is:

```matlab
   function h = benderh(ro, T)

   T0 = 298.15;
   R = 0.188918;

5

   TB = 1000;

   a1  = 0.22488558;
   a2  = 0.13717965e3;
10 a3  = 0.14430214e5;
   a4  = 0.29630491e7;
   a5  = 0.20606039e9;
   a6  = 0.45554393e-1;
```

```
   a7  = 0.77042840e2;
15 a8  = 0.40602371e5;
   a9  = 0.40029509;
   a10 = -0.39436077e3;
   a11 = 0.12115286;
   a12 = 0.10783386e3;
20 a13 = 0.43962336e2;
   a14 = -0.36505545e8;
   a15 = 0.19490511e11;
   a16 = -0.29186718e13;
   a17 = 0.24358627e8;
25 a18 = -0.37546530e11;
   a19 = 0.11898141e14;
   a20 = 0.50000000e1;


   e1 = 0.1853128e-3;
30 e2 = -0.8552719e-2;
   e3 = 0.1450667;
   e4 = -1.068975;
   e5 = 5.219996;
   e6 = 1.833078;
35 e7 = -0.5882021;


   B = a1.*T-a2-a3./T-a4./T.^2-a5./T.^3;
   C = a6.*T+a7+a8./T;
   D = a9.*T+a10;
40 E = a11.*T+a12;
   F = a13;
   G = a14./T.^2+a15./T.^3+a16./T.^4;
   H = a17./T.^2+a18./T.^3+a19./T.^4;

45 TdBdT = a1.*T+a3./T+2.*a4./T.^2+3.*a5./T.^3;
   TdCdT = a6.*T-a8./T;
   TdDdT = a9.*T;
   TdEdT = a11.*T;
   TdFdT = 0;
50 TdGdT = -2*a14./T.^2-3*a15./T.^3-4*a16./T.^4;
   TdHdT = -2*a17./T.^2-3*a18./T.^3-4*a19./T.^4;


   h0 = 0;
   h = h0 + R.*TB.*(-e1/3.*((T./TB).^(-3)-(T0./TB).^(-3)) ...
55     -e2/2.*((T./TB).^(-2)-(T0./TB).^(-2)) ...
       -e3.*((T./TB).^(-1)-(T0./TB).^(-1)) ...
       +e4*log(T./T0) + e5.*((T./TB)-(T0./TB)) ...
```

```
     +e6/2.*((T./TB).^2-(T0./TB).^2) ...
     +e7/3.*((T./TB).^3-(T0./TB).^3)) ...
60   +(2.*B-TdBdT).*ro+1/2.*(3.*C-TdCdT).*ro.^2 ...
     +1/3.*(4.*D-TdDdT).*ro.^3+1/4.*(5.*E-TdEdT).*ro.^4 ...
     +1/5.*(6.*F-TdFdT).*ro.^5+(G+H.*ro.^2).*ro.^2.*exp(-a20.*ro.^2) ...
     +(G-TdGdT).*1/(2.*a20).*(1-exp(-a20.*ro.^2)) ...
     +(H-TdHdT).*1/(2.*a20.^2).*(1-(a20.*ro.^2+1).*exp(-a20.*ro.^2)) ...
65   +R.*(T-T0);
end
```

Finally, the following function is used to recall the previous ones:

```
function [ro, h] = density(P, T)

P = P/10;
T = T+273.15;
5 m = length(P);

ro = zeros(1,m);

for i=1:m
10    ro(i) = benderro(P(i), T(i));
end

h = benderh(ro, T);

15 end
```

Appendix B

The extractor

The extractor is made of stainless steel, with two pieces that are screwed one with the other. The microalgae chamber has a length of 12 mm. A teflon o-ring with 3 mm of thickness and an internal diameter of 15 mm was placed in the empty cavity to obtain an extraction chamber with a diameter of 15 mm and a length of 15 mm. Therefore, a length of 15 mm was obtained. Figure B.1 show the geometries of the pieces.
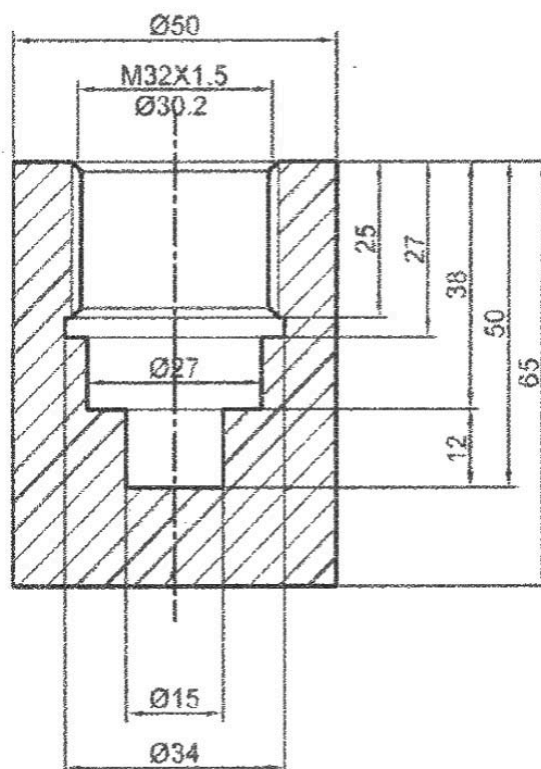
(a) *External piece.*

Figure B.1: *Geometric specification of the reactor.*
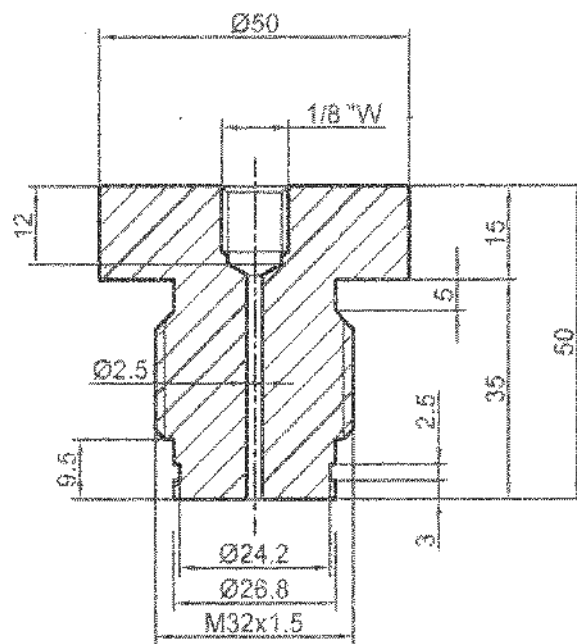
(b) *Internal piece.*
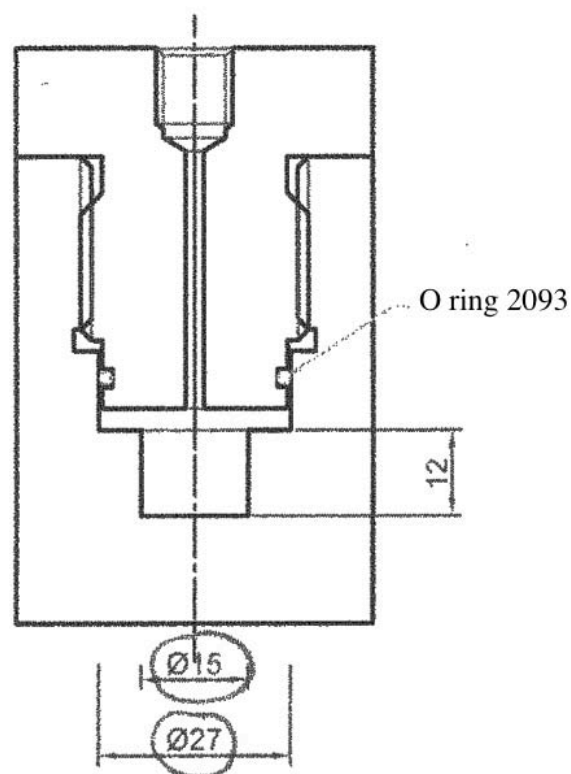
(c) *Joined pieces.*

Figure B.1: *Geometric specification of the reactor (Continued).*

Appendix C

Kinetics and solubility models in Matlab

The models applied to evaluate the kinetics extraction and the correlation between solubility and density were implemented in MATLAB®. This Appendix show the scripts and functions built for the fitting to experimental data.

C.1   Kinetics modeling

To model the kinetics of each test, the experimental data were reported in a file text with this scheme:

```
0       0          0            0            0.5125     300
15      0.0400     315.4014     315.4576     8.6        45
30      0.0123     315.4852     315.5428     0.5        2
45      0.0061     315.5705     315.6269     0.1650     0
60      0.0064     315.6511     315.7100     0.891      0
75      0.0023     315.7376     315.7922     0          0
90      0.0037     315.8197     315.8739     0          0
```

This file is loaded in the script that solve the fittings of simplified model, complete model and model based on characteristic times. The script is:

```
% This program allows to calculate the extraction curve of SFE of oil
% from microalgae using the  Sovov Model. The functions "nlinfit" and
% "fminsearch" will be used to fit the calculated curve to experimental
% data, varying some parameters in each equation.
% In the initial part the experimental data are loaded and the required
% variables are calculated. A simplified model will follow, for a first
% estimation of two adjustable parameters (r and ksas). Then, another
% simplified model will be fitted to evaluate the characteristic times of
% the process. Finally, the complete model will be used to optimize the
% parameters that govern the extraction process (r, ksas, kf).
```

```matlab
clear all; clc;
close all

% Load data

filename = input('File with experimental data: ');
FID = fopen(filename);
A = fscanf(FID,'%g %g %g %g %g %g', [6 inf]);
A = A';

% Definition of the loaded data

t = A(:,1);              % [min] cumulative time
m_oil = A(:,2);          % [g] oil mass obtained at each sample i
CO2_in = A(:,3);         % [m3] initial CO2 volume at each sample i
CO2_fin = A(:,4);        % [m3] final CO2 volume at each sample i
CO2 = CO2_fin - CO2_in;  % [m3] passed CO2 volume at each sample i
m_in = A(1,5);           % [g] wet microalgae mass
moisture = A(2,5);       % [%] microalgae moisture
EtOH = A(3,5);           % [ml/min] EtOH flow rate
P = A(1,6);              % [bar] pressure
T = A(2,6);              % [°C] temperature
n = A(3,6);              % point corresponding to the end of the 1st
    extraction period
m = length(t);           % number of experimental points

cu = fitcu(A);

% Computation of the solid dried mass

Ng = m_in-(m_in*moisture/100);% [g] total dried mass(oil+insoluble solid)
N = Ng/1000;                  % [kg]   " "
Nmg = (1-cu)*Ng;              % [g] mass of insoluble solid
Nm = Nmg/1000;                % [kg]   " "
xu = cu*N/Nm;                 % [kg/kg] concentration of oil in the
    untreated solid (oil/insoluble solid)

% Computation of the CO2 density

ro_CO2 = density(P, T)*10^3;  % [kg/m3] CO2 density

% Computation of the EtOH density

cost = [1.6288 0.27469 514 0.23178];
```

```matlab
PM_EtOH=46.068;                                          % [kg/kmol]
ro_EtOH=PM_EtOH*cost(1)/cost(2)^(1+(1-(T+273)/cost(3))^cost(4));% [kg/m3]


% Computation of the total density (CO2+EtOH)


rorec = 0.94/ro_CO2 + 0.06/ro_EtOH;
ro = 1/rorec;                    % [kg/m3] total density


% Computation of the bed porosity


D = 0.015;                       % [m] reactor diameter
L = 0.015;                       % [m] reactor length
Areatt = pi*D^2/4;               % [m2] reactor area
Vreatt = Areatt*L;               % [m3] reactor volume
dr = 1554;                       % [kg/m3] microalgae real density
da = m_in*10^(-3)/Vreatt;        % [kg/m3] microalgae apparent density
porosity = 1 - da/dr;            % [-] bed porosity


% Computation of the specific area per unit volume of extraction bed


dp = 0.4*10^(-3);                        % [m] particle diameter
a0 = 6*(1-porosity)/dp;                  % [1/m] specific area per unit
     volume of extraction bed
Patm = 1.01325;                          % [bar] atmospheric pressure
Troom = 25;                              % [°C] room temperature
ro_CO2_std = density(Patm, Troom)*10^3;% [kg/m3] CO2 density at standard
     conditions
gam = ro*porosity/(dr*(1-porosity));   % [-] CO2 to solid ratio in the
     bed


% Computation of: cumulative CO2 volume, cumulative EtOH volume and total
% volume


V_CO2 = zeros(1,m);
V_CO2(1) = CO2(1);
for i=2:m
    V_CO2(i) = V_CO2(i-1)+CO2(i);
end
V_CO2 = V_CO2';        % [m3] cumulative volume of the passed CO2
M = V_CO2*ro_CO2_std; % [kg] cumulative mass of the passed CO2


Q = M./(t*60);        % [kg/s] CO2 flow rate
Q(1) = 0;
Qaver = mean(Q);      % [kg/s] average CO2 flow rate
```

```matlab
q = M./Nm;              % [kg/kg] relative amount of the passed CO2 (kg_CO2
      /kg_insoluble solid)

% Computation of the cumulative experimental yield

yield100 = zeros(1,m);
yield100(1) = m_oil(1)/Nmg*100;
for i=2:m
    yield100(i) = yield100(i-1)+m_oil(i)/Nmg*100;
end
yield100 = yield100';   % [g/g(%)] percental yield = 100*oil/insoluble
      solid
yield = yield100/100;   % [g/g] yield = oil/insoluble solid
yieldstar = yield*Nm/N; % [g/g(%)] yield = oil/solid

% Computation of the oil solubility

p = polyfit(q(1:n), yield(1:n), 1);
ys = p(1);              % [g/kg*10^(-3)] solubility (oil/CO2)

% SIMPLIFIED MODEL

% Adjustable parameters of the simplified model:
% r1    = first estimation of the grinding efficiency
% ksas1 = first estimation of the product ks*as (ks = internal mass
% transfer coefficient, as = specific area between the regions of broken
% and intact cells)

alfa =  [0.4 10e-5]; % initial values of r1 and ksas1
options = statset('MaxIter', 1e10, 'Tolfun', 1e-10, 'Robust', 'on'); %
      options for nlinfit
c = nlinfit(q, yield, @(alfa, x)sm(alfa, x, xu), alfa, options);     %
      fitting for c(1) and c(2)
c1 = c(1);
c2 = c(2);

qc0 = 400;
options = optimset('TolFun', 1e-10, 'Display', 'Off');
qc = fsolve(@calcoloqc, qc0, options, xu, c1, c2, ys);

% Creation of the vector of the horizontal axis

q1c = 0:0.1:qc;
```

```matlab
135  q2c = (qc+0.1):0.1:2500;

     % Computation of the yield at each q of the horizontal axis

     e1c = q1c*ys;                % [g/g] calculated yield of the 1st
          extraction period
140  e2c = xu*(1-c1*exp(-c2*q2c)); % [g/g] calculated yield of the 2nd
          extraction period

     % Computation of the first estimation of r and ksas from the simplified
     % model

145  r1 = 1 - c1*exp(-c2*qc/2);               % [-] first estimation of r
     ksas1 = (1-r1)*(1-porosity)*(Qaver)*c2/Nm; % [1/(s*m)] first estimation
          of ksas

     % Computation of G with the simplified model

150  eqc = qc*ys;
     G_sm = eqc/xu;

     % Computation of the residual function of the Simplified Model

155  y2 = yield(n:m);             % [g/g] experimental yield of the 2nd
          extraction period
     q2 = q(n:m);                 % [kg/kg] experimental q of the 2nd
          extraction period
     e2 = xu*(1-c1*exp(-c2*q2));

     res_sm = 100.*sum(abs((e2-y2)./y2))./length(y2);
160
     % SIMPLIFIED MODEL BASED ON CHARACTERISTIC TIMES

     % Adjustable parameters of the model based on characteristic times:
     % G = initial fraction of extract in open cells
165  % tetaf = external mass transfer resistance
     % ti    = characteristic time of the internal mass transfer

     % In this model will be calculated also the yield at the end of the first
     % extraction period (eprimo) and the time at the end of the first
170  % extraction period (tprimo).

     t1 = t(2:n);          % [min] time of the 1st extraction period
     t2 = t(n:m);          % [min] time of the second extraction period
```

```
     qspec = Qaver/N*60; % [1/min] specific flow rate (CO2/(solid*s))
175
     % First extraction period

     y1 = yield(2:n); % [g/g] experimental yield of the 1st extraction period
     Y1 = y1*Nm/N;    % [g/g] experimental yield of the 1st extraction period
180  delta0 = 1;       % initial value of tetaf
     options = optimset('TolFun', 1e-10);
     [tetaf, res_tm1] = fminsearch(@modeltime1f, delta0, options, t1, Y1, ys,
         qspec);


     % Second extraction period
185
     Y2 = y2*Nm/N;      % [g/g] experimental yield of the 2nd extraction period
     zeta0 = [30 0.1]; % initial value of ti
     [ink, res_tm2] = fminsearch(@modeltime2f, zeta0, [], t2, Y2, cu, t1); % [
         min] characteristic time of the 2nd extraction period
     ti = ink(1);
190  G = ink(2);
     eprimo = G*cu; % [g/g] yield at the end of the 1st extraction period
     tprimo = eprimo/(ys*qspec*(1-exp(-1/tetaf))); % [min] time at the end of
         the 1st extraction period
     tc1 = 0:0.1:tprimo; % [min] time vector for the horizontal axis
     E1c = ys.*qspec.*tc1.*(1-exp(-1./tetaf));    % [g/g] yield calculated at
         each time of the horizontal axis
195
     tc2 = (tprimo+0.1):0.1:120; % [min] calculated time for the horizontal
         axis
     E2 = cu.*(1-(1-G).*exp(-(tc2-tprimo)./ti));  % [g/g] calculated yield of
         the 2nd extraction period


     % Residual function of the simplified model based on characteristic times
200
     res_tm = sqrt(res_tm2^2+res_tm1^2);


     % COMPLETE MODEL


205  % Adjustable parameters of the complete model:
     % kf   = external mass transfer coefficient
     % r    = grinding efficiency
     % ksas = internal MT coefficient multiplied by specific area between the
     %        regions of intact and broken cells
210  % kf will be estimated using the equation of the first extraction period,
     % r and ksas will be evaluated using the equations of the second and
```

```matlab
% third extraction period.
% r1 and ksas1, the results of the simplified model fitting, are used as
% initial values of the second fitting.

% First extraction period

q1 = q(2:n);
iota0 = 0.001; % initial value of kf
options = optimset('MaxFunEvals', 1e10); % options for nlinfit
kf = fminsearch(@modcomplete1f, iota0, options, q1, y1, a0, gam, porosity
    , Qaver, Nm, ys); % [1/s] external MT coefficient
tetae = porosity*Qaver/(gam*kf*a0*Nm); % [-] external MT resistance
kfa0 = kf*a0;

% Second and third extraction period

qp = q(n:m);
yp = yield(n:m);
csi = [r1 ksas1]; % initial values of r and ksas
options = statset('MaxIter', 3000, 'Tolfun', 1e-10, 'Robust', 'on', '
    WgtFun', 'fair');
CSI = nlinfit(qp, yp, @(csi, x)mc3(csi, x, kf, xu, ys, porosity, Qaver,
    gam, Nm, a0), csi, options);

r = CSI(1);         % [-] grinding efficiency
ksas = CSI(2);      % [1/(s*m)] product ks*as
qm = r*xu*tetae/ys; % q at the end of the 1st extraction period
tetai = (1-porosity)*Qaver/(gam*ksas*Nm); % [-] internal MT resistance
betam = gam*tetai*ys/xu; % coefficient
qn = qm + gam*tetai*log(1-r+r*exp(1/betam)); % q at the end of the second
    extraction period

% Computation of the residual function

q1exp = q(2:n);
e1exp = yield(2:n);
e1calc = q1exp.*ys.*(1-exp(-1./tetae));
q2exp = q(2:n);
e2exp = yield(2:n);
e2calc = ys.*q2exp - r.*xu.*tetae.*exp((betam./tetae).*log(1+(1./r).*(exp
    ((q2exp-qm)./(gam.*tetai))-1))-1./tetae); % [-] yield of the 2nd
    extraction period
q3exp = q(n:m);
e3exp = yield(n:m);
```

```matlab
e3calc = xu.*(1-betam.*log(1+(1-r).*(exp(1./betam)-1).*exp(-(q3exp-qm)./(
    gam.*tetai))));


err1 = 100*sum(abs((e1calc-e1exp)./e1exp))./length(e1exp);
err2 = 100*sum(abs((e2calc-e2exp)./e2exp))./length(e2exp);
err3 = 100*sum(abs((e3calc-e3exp)./e3exp))./length(e3exp);


res_cm = sqrt(err1^2+err3^2);


% Creation of the vector of the horizontal axis

qmc1 = 0:0.1:qm;            % [kg/kg] q of the 1st extraction period
qmc2 = (qm+0.1):0.1:qn;   % [kg/kg] q of the 2nd extraction period
qmc3 = (qn+0.1):0.1:2500; % [kg/kg] q of the 3rd extraction period

% Computation of the yield at each q of the horizontal axis

YIELD1 = qmc1.*ys.*(1-exp(-1./tetae));


    % [-] yield of the 1st extraction period
YIELD2 = ys.*qmc2-r.*xu.*tetae.*exp((betam./tetae).*log(1+(1./r).*(exp((
    qmc2-qm)./(gam.*tetai))-1))-1./tetae); % [-] yield of the 2nd
    extraction period
YIELD3 = xu.*(1-betam.*log(1+(1-r).*(exp(1./betam)-1).*exp(-(qmc3-qm)./(
    gam.*tetai))));                              % [-] yield of the 3rd
    extraction period

% Complete model with 2 equations (first and third period)

options = optimset('TolFun', 1e-10, 'TolX', 1e-12, 'Display', 'Off');
qs0 = 400;
qs = fsolve(@calcoloqs, qs0, options, ys, tetae, xu, betam, r, qm, gam,
    tetai);


qm1 = 0:0.1:qs;
qm2 = qs:0.1:2500;

EY1 = qm1.*ys.*(1-exp(-1./tetae));
EY2 = xu.*(1-betam.*log(1+(1-r).*(exp(1./betam)-1).*exp(-(qm2-qm)./(gam.*
    tetai))));

% Computation of G with the complete model

eqs = qs*ys*(1-exp(-1/tetae));
```

```matlab
285  G_cm = eqs/xu;

     % FIGURES

     % Plot of the experimental data
290  plot(q, yield, 'o');
     legend('experimental data', 'Location', 'SouthEast');
     % Plot of the simplified model
     figure;
     plot(q, yield, 'ok');
295  hold on
     plot(q1c, e1c, 'r');
     plot(q2c, e2c, 'b');
     xlabel('q (kg/kg)');
     ylabel('e (g/g)');
300  legend('experimental data', '1st period', '2nd period', 'Location', '
         SouthEast');
     % Plot of the simplified model based on characteristic times
     figure;
     plot(t, yieldstar, 'ok');
     hold on
305  plot(tc1, E1c, 'r');
     plot(tc2, E2, 'b');
     xlabel('t (min)');
     ylabel('e (g/g)');
     legend('experimental data', '1st period', '2nd period', 'Location', '
         SouthEast');
310  % Plot of the complete model
     figure;
     plot(q, yield, 'ok');
     hold on
     plot(qmc1, YIELD1, 'r');
315  plot(qmc2, YIELD2, 'c');
     plot(qmc3, YIELD3, 'b');
     xlabel('q (kg/kg)');
     ylabel('e (g/g)');
     legend('experimental data', '1st period', '2nd period', '3rd period', '
         Location', 'SouthEast');
320  %Plot of the complete model with 2 equations
     figure;
     plot(q, yield, 'ok');
     hold on
     plot(qm1, EY1, 'r');
325  plot(qm2, EY2, 'b');
```

```matlab
xlabel('q (kg/kg)');
ylabel('e (g/g)');
legend('experimental data', '1st period', '2nd period', 'Location', '
    SouthEast');
% Enlargments
figure;
plot(qmc1, YIELD1, 'r');
hold on
plot(qmc2(1:1000), YIELD2(1:1000), 'c');
xlabel('q (kg/kg)');
ylabel('e (g/g)');
legend('1st period', '2nd period', 'Location', 'SouthEast');
figure;
plot(qmc2(1000:length(qmc2)), YIELD2(1000:length(YIELD2)), 'c');
hold on
plot(qmc3(1:5000), YIELD3(1:5000), 'b');
xlabel('q (kg/kg)');
ylabel('e (g/g)');
legend('2nd period', '3rd period', 'Location', 'SouthEast');

% Closing data file
fclose(FID);
```

The functions recalled in this script are listed below:

- Computation of the CO_2 density with the Bender equation of state: see Appendix A;

- Second extraction period of the simplified model (the first one does not have adjustable parameters):

```matlab
function y = sm(alfa, x, xu)

y = xu.*(1-alfa(1).*exp(-alfa(2).*x));

end
```

- Computation of the relative amount of passed solvent at the end of the first extraction period:

```matlab
function qc = calcoloqc(x, xu, c1, c2, ys)

qc = xu*(1-c1*exp(-c2*x))-x*ys;

end
```

- First extraction period of the model based on characteristic times:

```matlab
function err = modeltime1f(delta, t1, Y1, ys, qspec)


y = ys*qspec.*t1.*(1-exp(-1./delta));
err = 100*sum(abs((y-Y1)./Y1))./length(Y1);


end
```

- Second extraction period of the model based on characteristic times:

```matlab
function err = modeltime2f(zeta, t2, Y2, cu, t1)


y = cu*(1-(1-zeta(2))*exp(-(t2-t1(length(t1)))/zeta(1)));
err = 100*sum(abs((y-Y2)./Y2))./length(Y2);


end
```

- First extraction period of the complete model:

```matlab
function err = modcomplete1f(iota, q1, y1, a0, gam, porosity, Qaver,
        Nm, ys)


y = q1.*ys.*(1-exp(-1./(porosity*Qaver/(gam*iota*a0*Nm))));
err = 100*sum(abs((y-y1)./y1))./length(y1);


end
```

- Second and third extraction periods of the complete model:

```matlab
function y = mc3(csi, x, kf, xu, ys, porosity, Qaver, gam, Nm, a0)


tetae = porosity*Qaver/(gam*kf*a0*Nm);
qm = csi(1)*xu*tetae/ys;
tetai = (1-porosity)*Qaver/(gam*csi(2)*Nm);
betam = gam*tetai*ys/xu;


y = xu.*(1-betam.*log(1+(1-csi(1)).*(exp(1./betam)-1).*exp(-(x-qm)
        ./(gam.*tetai))));


end
```

- Computation of the relative amount of passed solvent at the end of the first extraction period of the complete model when only the first and the third periods are considered:

```
function qs = calcoloqs(x, ys, tetae, xu, betam, r, qm, gam, tetai)

qs = xu.*(1-betam.*log(1+(1-r).*(exp(1./betam)-1).*exp(-(x-qm)./(gam
     .*tetai)))) ...
     -x.*ys.*(1-exp(-1./tetae));

end
```

- Second extraction period of the simplified model with c_u as addictional parameter:

```
function y = smcu(alfa, x, Ng)

cu = alfa(3)/(1+alfa(3));
N = Ng/1000;
Nmg = (1-cu)*Ng;
Nm = Nmg/1000;

y = alfa(3).*(1-alfa(1).*exp(-alfa(2).*x))*Nm/N;

end
```

- Second extraction period of the model based on characteristic times with c_u as addictional parameter (the first one does not change):

```
function err = modeltime2fcu(zeta, t2, Y2, t1)

y = zeta(3)*(1-(1-zeta(2))*exp(-(t2-t1(length(t1)))/zeta(1)));
err = 100*sum(abs((y-Y2)./Y2))./length(Y2);

end
```

- First extraction period of the complete model with c_u as addictional parameter:

```
function err = modcomplete1fcu(iota, q1, y1, a0, gam, porosity,
     Qaver, Ng, ys, xup)

cu = xup/(1+xup);
N = Ng/1000;
Nmg = (1-cu)*Ng;
Nm = Nmg/1000;

y = q1.*ys.*(1-exp(-1./(porosity*Qaver/(gam*iota(1)*a0*Nm))))*Nm/N;
err = 100*sum(abs((y-y1)./y1))./length(y1);
end
```

- Second and third extraction period of the complete model with c_u as addictional parameter:

```matlab
function y = mc3cu(csi, x, kf, ys, porosity, Qaver, gam, a0, Ng)

cu = csi(3)/(1+csi(3));
N = Ng/1000;
Nmg = (1-cu)*Ng;
Nm = Nmg/1000;

tetae = porosity*Qaver/(gam*kf*a0*Nm);
qm = csi(1)*csi(3)*tetae/ys;
tetai = (1-porosity)*Qaver/(gam*csi(2)*Nm);
betam = gam*tetai*ys/csi(3);

y = csi(3).*(1-betam.*log(1+(1-csi(1)).*(exp(1./betam)-1).*exp(-(x-
    qm)./(gam.*tetai)))).*Nm./N;

end
```

C.2   Solubility modeling

The modeling of solubility was performed with three equations developed by Chrastil, Del Valle-Aguilera and Adachi-Lu. The script that fits these expressions with experimental data is:

```matlab
% Solubility modeling

clear all; clc;
close all;


T = [55 55 55 55];
TK = T(1)+273.15;
P = [150 200 250 300];
SexpA = [0.0235 0.0275 0.0329 0.0423]*10;    % g(oil)/kg
ro = density(P, T)*1000;                      % g/L
Sexp = SexpA.*ro*10^(-3);                     % g/L

alfa0 = [20 -10000 15];
A0 = chrastilP(alfa0, ro, Sexp, TK);
options = optimset('MaxIter', 1e20,'MaxFunEvals', 2000,'TolFun', 1e-10);
A = fminsearch(@chrastilP, alfa0, options, ro, Sexp, TK);
k1 = A(1);
```

```matlab
a1 = A(2);
a2 = A(3);
disp(A);


Sc = ro.^k1.*exp(a1./TK+a2);
resc = 100.*sum(abs((Sc-Sexp)./Sexp))./length(Sexp);


Pc = 120:0.1:350;
Tc = zeros(1, length(Pc));
for i = 1:length(Pc)
    Tc(i) = 55;
end
roc = density(Pc, Tc)*1000;
Scalc = roc.^(k1).*exp(a1./(TK)+a2);


figure1 = figure;
axes1 = axes('Parent',figure1,'FontSize',18,'FontName','Times New Roman')
    ;
box(axes1,'on');
hold(axes1,'all');
plot(Pc/10, Scalc, 'r');
hold on


beta0 = [10 10000 -2000 -15];
B0 = valleP(beta0, ro, Sexp, TK);
options = optimset('TolFun', 1e-10);
B = fminsearch(@valleP, beta0, options, ro, Sexp, TK);
k1 = B(1);
a1 = B(2);
a2 = B(3);
a3 = B(4);
disp(B);


Sv = ro.^k1.*exp(a1./TK.^2+a2./TK+a3);
resv = 100.*sum(abs((Sv-Sexp)./Sexp))./length(Sexp);


Scalv = roc.^k1.*exp(a1./TK.^2+a2./TK+a3);
plot(Pc/10, Scalv, 'g');


g0 = [10 1e-10 1e-12 -2000 -20];
G0 = adachiP(g0, ro, Sexp, TK);
options = optimset('MaxFunEvals', 3000, 'TolFun', 1e-10);
G = fminsearch(@adachiP, g0, options, ro, Sexp, TK);
a1 = G(1);
```

```matlab
a2 = G(2);
a3 = G(3);
a4 = G(4);
a5 = G(5);
disp(G);


Sa = ro.^(a1+a2.*ro+a3.*ro.^2).*exp(a4./TK+a5);
resa = 100.*sum(abs((Sa-Sexp)./Sexp))./length(Sexp);


Scala = roc.^(a1+a2.*roc+a3.*roc.^2).*exp(a4./TK+a5);
plot(Pc/10, Scala, 'k--');
plot(P/10, Sexp, 'o');
legend('Chrastil Model','Del Valle-Aguilera Model','Adachi-Lu Model','
    Location','SouthEast');
xlabel('Pressure (MPa)','FontSize',24,'FontName','Times New Roman');
ylabel('Solubility (g/L)','FontSize',24,'FontName','Times New Roman');


figure1 = figure;
axes1 = axes('Parent',figure1,'FontSize',18,'FontName','Times New Roman')
    ;
box(axes1,'on');
hold(axes1,'all');
plot(roc, Scalc, 'b');
hold on
plot(roc, Scalv, 'r');
plot(roc, Scala, 'g--');
plot(ro, Sexp, 'o');
legend('Chrastil Model','Del Valle-Aguilera Model','Adachi-Lu Model','
    Location','SouthEast');
xlabel('Density (g/L)','FontSize',24,'FontName','Times New Roman');
ylabel('Solubility (g/L)','FontSize',24,'FontName','Times New Roman');

disp('Chrastil error');
disp(resc);
disp('Del Valle error');
disp(resv);
disp('Adachi error');
disp(resa);
```

The recalled functions are:

- Chrastil equation:

```matlab
function S = chrastilP(alfa, ro, Sexp, TK)
```

```
Scalc = ro.^(alfa(1)).*exp(alfa(2)./TK+alfa(3));
S = norm((Scalc-Sexp)/Sexp);

end
```

- Del Valle-Aguilera equation:

```
function S = valleP(beta, ro, Sexp, TK)

Scalc = ro.^beta(1).*exp(beta(2)./TK.^2+beta(3)./TK+beta(4));
S = norm((Scalc-Sexp)/Sexp);

end
```

- Adachi-Lu equation:

```
function err = adachiP(g, ro, Sexp, TK)

Scalc = ro.^(g(1)+g(2).*ro+g(3).*ro.^2).*exp(g(4)./TK+g(5));
err = norm((Scalc-Sexp)/Sexp);

end
```

The script that fits only the equation of Del Valle-Aguilera to model the solubility as a function of pressure, with parametric temperature, is:

```
% Model solubility

clear all; clc;
close all;

T = [45 45 45 45];
TK = T(1)+273.15;
P = [150 200 250 300];
Sexp1 = [0.0286 0.0298 0.0370 0.0394]*10;
ro1 = density(P, T)*1000;
Sexp1 = Sexp1.*ro1.*10^(-3);

beta0 = [10 10000 -2000 -10];
B0 = valleP(beta0, ro1, Sexp1, TK);
options = optimset('MaxFunEvals', 2000);
B1 = fminsearch(@valleP, beta0, options, ro1, Sexp1, TK);
k1 = B1(1);
a1 = B1(2);
```

```matlab
a2 = B1(3);
a3 = B1(4);
disp(B1);

Sv1 = ro1.^k1.*exp(a1./TK.^2+a2./TK+a3);
res1 = 100.*sum(abs((Sv1-Sexp1)./Sexp1))./length(Sexp1);
disp('res1');
disp(res1);

Pc = 130:0.1:350;
Tc = zeros(1, length(Pc));
for i = 1:length(Pc)
    Tc(i) = 45;
end
roc1 = density(Pc, Tc)*1000;
Scalv1 = roc1.^k1.*exp(a1./TK.^2+a2./TK+a3);


T = [55 55 55 55];
TK = T(1)+273.15;
P = [150 200 250 300];
Sexp2 = [0.0235 0.0275 0.0329 0.0423]*10;
ro2 = density(P, T)*1000;
Sexp2 = Sexp2.*ro2.*10^(-3);


beta0 = [10 10000 -2000 -15];
B0 = valleP(beta0, ro2, Sexp2, TK);
options = optimset('MaxFunEvals', 2000);
B2 = fminsearch(@valleP, beta0, options, ro2, Sexp2, TK);
k1 = B2(1);
a1 = B2(2);
a2 = B2(3);
a3 = B2(4);
disp(B2);

Sv2 = ro2.^k1.*exp(a1./TK.^2+a2./TK+a3);
res2 = 100.*sum(abs((Sv2-Sexp2)./Sexp2))./length(Sexp2);
disp('res2');
disp(res2);

Tc = zeros(1, length(Pc));
for i = 1:length(Pc)
    Tc(i) = 55;
end
roc2 = density(Pc, Tc)*1000;
```

```matlab
Scalv2 = roc2.^k1.*exp(a1./TK.^2+a2./TK+a3);

T = [65 65 65 65];
TK = T(1)+273.15;
P = [150 200 250 300];
Sexp3 = [0.0166 0.0210 0.0296 0.0453]*10;
ro3 = density(P, T)*1000;
Sexp3 = Sexp3.*ro3.*10^(-3);


beta0 = [30 10000 -9000 -5];
B0 = valleP(beta0, ro3, Sexp3, TK);
options = optimset('MaxFunEvals', 3000, 'MaxIter', 1e10);
B3 = fminsearch(@valleP, beta0, options, ro3, Sexp3, TK);
k1 = B3(1);
a1 = B3(2);
a2 = B3(3);
a3 = B3(4);
disp(B3);


Sv3 = ro3.^k1.*exp(a1./TK.^2+a2./TK+a3);
res3 = 100.*sum(abs((Sv3-Sexp3)./Sexp3))./length(Sexp3);
disp('res3');
disp(res3);


Tc = zeros(1, length(Pc));
for i = 1:length(Pc)
    Tc(i) = 65;
end
roc3 = density(Pc, Tc)*1000;
Scalv3 = roc3.^k1.*exp(a1./TK.^2+a2./TK+a3);


% Plot

figure1 = figure;
axes1 = axes('Parent',figure1,'FontSize',18,'FontName','Times New Roman')
    ;
box(axes1,'on');
hold(axes1,'all');


plot(Pc/10, Scalv1, 'b');
hold on
plot(Pc/10, Scalv2, 'r');
plot(Pc/10, Scalv3, 'g');
```

```matlab
plot(P/10, Sexp1, 'ob');
plot(P/10, Sexp2, '^r');
plot(P/10, Sexp3, 'sg');

legend('45°C','55°C','65°C','Location','SouthEast');
xlabel('Pressure (MPa)','FontSize',24,'FontName','Times New Roman');
ylabel('Solubility (g/L)','FontSize',24,'FontName','Times New Roman');

figure1 = figure;
axes1 = axes('Parent',figure1,'FontSize',18,'FontName','Times New Roman')
    ;
box(axes1,'on');
hold(axes1,'all');
plot(roc1, Scalv1, 'b-');
hold on

plot(roc2, Scalv2, 'r-');
plot(roc3, Scalv3, 'g-');

plot(ro1, Sexp1, 'o');
plot(ro2, Sexp2, '^r');
plot(ro3, Sexp3, 'sg');

legend('45°C','55°C','65°C','Location','SouthEast');
xlabel('Density (g/L)','FontSize',24,'FontName','Times New Roman');
ylabel('Solubility (g/L)','FontSize',24,'FontName','Times New Roman');

figure1 = figure;
axes1 = axes('Parent',figure1,'FontSize',18,'FontName','Times New Roman')
    ;
box(axes1,'on');
hold(axes1,'all');
plot(Pc/10, roc1, 'b');
hold on
plot(Pc/10, roc2, 'r');
plot(Pc/10, roc3, 'g');

plot(P/10, ro1, 'ob');
plot(P/10, ro2, '^r');
plot(P/10, ro3, 'sg');
legend('45°C','55°C','65°C','Location','SouthEast');
xlabel('Pressure (MPa)','FontSize',24,'FontName','Times New Roman');
ylabel('Density (g/L)','FontSize',24,'FontName','Times New Roman');
```

The script that fits only the equation of Chrastil to model the solubility as a function of temperature, with parametric pressure, is:

```matlab
% Solubility modeling

clear all; clc;
close all;

% P = 300;

P1 = [300 300 300];
T = [45 55 65];
TK = T+273.15;
Sexp1 = [0.0394 0.0423 0.0453]*10;
ro1 = density(P1, T)*1000;
Sexp1 = Sexp1.*ro1.*10^(-3);

a0 = [0 -1000 0];

A0 = chrastilP(a0, ro1, Sexp1, TK);
options = optimset('MaxIter', 1e20, 'MaxFunEvals', 2000, 'TolFun', 1e-10)
    ;
a = fminsearch(@chrastilP, a0, options, ro1, Sexp1, TK);
disp(a);

S1 = ro1.^(a(1)).*exp(a(2)./TK+a(3));
res1 = 100.*sum(abs((S1-Sexp1)./Sexp1))./length(Sexp1);
disp(res1);

Tc = 40:0.1:70;
tk = Tc+273.15;
Pc = zeros(1,length(T));
for i = 1:length(Tc)
    Pc(i) = 300;
end
roc1 = density(Pc, Tc)*1000;

Scalc1 = roc1.^(a(1)).*exp(a(2)./(tk)+a(3));

% P = 150

P2 = [150 150 150];
Sexp2 = [0.0286 0.0235 0.0166]*10;
ro2 = density(P2, T)*1000;
Sexp2 = Sexp2.*ro2.*10^(-3);
```

```matlab
b0 = [10 -1000 -15];

B0 = chrastilP(b0, ro2, Sexp2, TK);
options = optimset('MaxIter', 1e20, 'MaxFunEvals', 2000, 'TolFun', 1e-10)
    ;
b = fminsearch(@chrastilP, b0, options, ro2, Sexp2, TK);
disp(b);

S2 = ro2.^(b(1)).*exp(b(2)./TK+b(3));
res2 = 100.*sum(abs((S2-Sexp2)./Sexp2))./length(Sexp2);
disp(res2);

Pc = zeros(1,length(T));
for i = 1:length(Tc)
    Pc(i) = 150;
end
roc2 = density(Pc, Tc)*1000;

Scalc2 = roc2.^(b(1)).*exp(b(2)./(tk)+b(3));

% P = 250

P3 = [250 250 250];
Sexp3 = [0.0370 0.0329 0.0296]*10;
ro3 = density(P3, T)*1000;
Sexp3 = Sexp3.*ro3.*10^(-3);

c0 = [10 -1000 -20];


C0 = chrastilP(c0, ro3, Sexp3, TK);
options = optimset('MaxIter', 1e20, 'MaxFunEvals', 2000, 'TolFun', 1e-10)
    ;
c = fminsearch(@chrastilP, c0, options, ro3, Sexp3, TK);
disp(c);

S3 = ro3.^(c(1)).*exp(c(2)./TK+c(3));
res3 = 100.*sum(abs((S3-Sexp3)./Sexp3))./length(Sexp3);
disp(res3);

Pc = zeros(1,length(T));
for i = 1:length(Tc)
    Pc(i) = 250;
end
```

```matlab
roc3 = density(Pc, Tc)*1000;

Scalc3 = roc3.^(c(1)).*exp(c(2)./(tk)+c(3));

% Plot

figure1 = figure;
axes1 = axes('Parent',figure1,'FontSize',18,'FontName','Times New Roman')
    ;
box(axes1,'on');
hold(axes1,'all');

plot(tk-273, Scalc1, 'b');
hold on
plot(tk-273, Scalc3, 'r');
plot(tk-273, Scalc2, 'g');

plot(TK-273, Sexp1, 'o');
plot(TK-273, Sexp3, '^r');
plot(TK-273, Sexp2, 'sg');
xlabel('Temperature (°C)','FontSize',24,'FontName','Times New Roman');
ylabel('Solubility (g/L)','FontSize',24,'FontName','Times New Roman');
legend('30 MPa','25 MPa','15 MPa','Location','SouthWest');

figure1 = figure;
axes1 = axes('Parent',figure1,'FontSize',18,'FontName','Times New Roman')
    ;
box(axes1,'on');
hold(axes1,'all');
%plot(roc1, Scalc1, 'b');
hold on
plot(roc3, Scalc3, 'b');
plot(roc2, Scalc2, 'r');
plot(ro3, Sexp3, 'o');
plot(ro2, Sexp2, '^r');
xlabel('Density (g/L)','FontSize',24,'FontName','Times New Roman');
ylabel('Solubility (g/L)','FontSize',24,'FontName','Times New Roman');
legend('25 MPa','15 MPa','Location','SouthEast');

figure;
plot(Scalc3, roc3, 'b');
hold on
plot(Scalc2, roc2, 'r');
plot(Sexp3, ro3, 'o');
```

```matlab
plot(Sexp2, ro2, '^r');

figure1 = figure;
axes1 = axes('Parent',figure1,'FontSize',18,'FontName','Times New Roman')
    ;
box(axes1,'on');
hold(axes1,'all');

plot(tk-273, roc1, 'b');
hold on
plot(tk-273, roc3, 'r');
plot(tk-273, roc2, 'g');

plot(TK-273, ro1, 'o');
plot(TK-273, ro3, '^r');
plot(TK-273, ro2, 'sg');
xlabel('Temperature (°C)','FontSize',24,'FontName','Times New Roman');
ylabel('Density (g/L)','FontSize',24,'FontName','Times New Roman');
legend('30 MPa','25 MPa','15 MPa','Location','SouthEast');
```

Bibliography

Adachi, Y. and B. C.-Y. Lu

    1983   "Supercritical fluid extraction with carbon dioxide and ethylene", *Fluid Phase Equilibria*, 14, pp. 147-156.

Ahmad, A.L., N. H. Mat Yasin, Derek C. J. C., and Lim J. K.

    2011   "Microalgae as a sustainable energy source for biodiesel production: A review", *Renewable and Sustainable Energy Reviews*, 15, pp. 584-593.

Andrich, G., A. Zinnai, B. Nesti, F. Venturi, and R. Fiorentini

    2006   "Supercritical fluid extraction of oil from microalga *Spirulina (arthrospira) platensis*", *Acta Alimentaria*, 35, pp. 195-203.

Asghari-Kiavi, M., Y. Yamini, and M. A. Farajzadeh

    2004   "Solubilities of two steroid drugs and their mixtures in supercritical carbon dioxide", *Journal of Supercritical Fluids*, 30, pp. 111-117.

Bligh, E. G. and W. J. Dyer

    1959   "A rapid method of total lipid extraction and purification", *Canadian Journal of Biochemistry and Physiology*, 37 (8), pp. 911-917.

Brennan, L. and P. Owende

    2010   "Biofuels from microalgae—A review of technologies for production, processing, and extractions of biofuels and co-products", *Renewable and Sustainable Energy Reviews*, 14, pp. 557-577.

Bruno, T., C. A. N. Castro, J. F. Hammel, and A. M. F. Palavra

    1993   "Supercritical fluid extraction of biological products", in *Recovery Processes for Biological Materials*, J. Wiley & Sons, chap. 11.

Cavallini, A. and L. Mattarolo

    1990   *Termodinamica applicata*, CLEUP.

Chrastil, J.

    1982 "Solubility of solids and liquids in supercritical gases", *Journal of Physical Chemistry*, 86, pp. 3016-3021.

Crampon, C., A. Mouahid, Toudji S.-A.A., O. Lépine, and E. Badens

    2013 "Influence of pretreatment on Supercritical CO_2 Extraction from *Nannochloropsis oculata*", *The Journal of Supercritical Fluids*, 79, pp. 337-344.

Del Valle, J. M. and J. M. Aguilera

    1988 "An improved equation for predicting the solubility of vegetable oils in supercritical CO_2", *Indusrtial & Engineering Chemistry Research*, 27, pp. 1551-1553.

Demirbas, M. F.

    2011 "Biofuels from algae for sustainable development", *Applied Energy*, 88, pp. 3473-3480.

Domingo, J. L., A. Bocio, Falcó G., and J. M. Llobet

    2007 "Benefits and risks of fish consumption Part I. A quantitative analysis of the intake of omega-3 fatty acids and chemical contaminants", *Toxicology*, 230, pp. 219-226.

Ghazouani, J., O. Chouaieb, and A. Bellagi

    2005 "Evaluation of the parameters of the Bender equation of state for low acentric factor fluids and carbon dioxide", *Thermochimica Acta*, 432, pp. 10-19.

Gouveia, L., B. P. Nobre, F. M. Marcelo, S. Mrejen, M. T. Cardoso, A. F. Palavra, and R. L. Mendes

    2007 "Functional food oil coloured by pigments extracted from microalgae with supercritical CO_2", *Food Chemistry*, 101, pp. 717-723.

Halim, R., M. K. Danquah, and P. A. Webley

    2012 "Extraction of oil from microalgae for biodiesel production: A review", *Biotechnology Advances*, 30, pp. 709-732.

Herrero, M., A. Cifuentes, and E. Ibañez

    2006 "Sub- and supercritical fluid extraction of functional ingredients from different natural sources: Plants, food-by-products, algae and microalgae. A review", *Food Chemistry*, 98, pp. 136-148.

Jenkins, T. C.

2010 "Technical note: Common analytical errors yielding inaccurate results during analysis of fatty acids in feed and digesta samples", *Journal of Dairy Science*, 93, pp. 1170-1174.

Lam, M. K. and K. T. Lee

2013 "Catalytic transesterification of high viscosity crude microalgae lipid to biodiesel: Effect of co-solvent", *Fuel Processing Technology*, 110, pp. 242-248.

Lv, J.-M., L.-H. Cheng, X.-H. Xu, L. Zhang, and H.-L. Chen

2010 "Enhanced lipid production of *Chlorella vulgaris* by adjustment of cultivation conditions", *Bioresource Technology*, 101, pp. 6797-6804.

Macías-Sánchez, M. D., C. Mantell Serrano, M. Rodríguez Rodríguez, and E. Martinéz de la Ossa

2009 "Kinetics of the supercritical fluid extraction of carotenoids from microalgae with CO_2 and ethanol as cosolvent", *Chemical Engineering Journal*, 150, pp. 104-113.

Macías-Sánchez, M. D., C. Mantell Serrano, M. Rodríguez Rodríguez, E. Martinéz de la Ossa, L. M. Lubián, and O. Montero

2008 "Extraction of carotenoids and chlorophyll from microalgae with supercritical carbon dioxide and ethanol as cosolvent", *Journal of Separation Science*, 31, pp. 1352-1362.

Mairet, F., O. Bernard, P. Masci, T. Lacour, and A. Sciandra

2011 "Modelling neutral lipid production by the microalga *Isochrysis aff. galbana* under nitrogen limitation", *Bioresource Technology*, 102, pp. 142-149.

Mendes, R. L., A. D. Reis, and A. F. Palavra

2006 "Supercritical CO_2 extraction of γ-linolenic acid and other lipids from *Arthrospira (Spirulina) maxima*: Comparison with organic solvent extraction", *Food Chemistry*, 99, pp. 57-63.

Mercer, P. and R. E. Amenta

2011 "Developments in oil extraction from microalgae", *European Journal of Lipid Science and Technology*, 113, pp. 539-547.

Mohammady, N. G.-E. D., Y.-C. Chen, A.-E.-R. A. El-Mahdy, and R. F. Mohammad

2005 "Temporal alterations of *Nannochloropsis salina* (Eustigmatophyceae) grown under aqueous diesel fuel stress", *Journal of Applied Phycology*, 17, pp. 161-170.

Mouahid, A., C. Crampon, S.-A. A. Toudji, and E. Badens

    2013   "Supercritical CO_2 extraction of neutral lipids from microalgae: Experiments and modelling", *Journal of Supercritical Fluid*, 77, pp. 7-16.

Palavra, A. M. F., J. P. Coelho, J. G. Barroso, A. P. Rauter, J. M. N. A. Fareleira, A. Mainar, J. S. Urieta, B. P. Nobre, L. Gouveia, R. L. Mendes, J. M. S. Cabral, and J. M. Novais

    2011   "Supercritical carbon dioxide extraction of bioactive compounds from microalgae and volatile oils from aromatic plants", *The Journal of Supercritical Fluids*, 60, pp. 21-27.

Poling, B. E., G. H. Thomson, D. G. Friend, R. L. Rowley, and W. V. Wilding

    2008   "Physical and Chemical Data", in *Perry's Chemical Engineers' Handbook*, ed. by R. H. Perry and D. W. Green, McGraw-Hill, chap. 2.

Quadrelli, R. and S. Peterson

    2007   "The energy–climate challenge: Recent trends in CO2 emissions from fuel combustion", *Energy Policy*, 35, pp. 5938-5952.

Rawat, I., R. Ranjith Kumar, T. Mutanda, and F. Bux

    2013   "Biodiesel from microalgae: A critical evaluation from laboratory to large scale production", *Applied Energy*, 103, pp. 444-467.

Rosa, P. T. V. and M. A. A. Meireles

    2005   "Rapid estimation of the manufacturing cost of extracts obtained by supercritical fluid extraction", *Journal of Food Engineering*, 67, pp. 235-240.

Rubio-Rodríguez, N., S. Beltrán, I. Jaime, S. M. De Diego, M. T. Sanz, and J. R. Carballido

    2010   "Production of omega-3 polyunsaturated fatty acid concentrates: A review", *Innovative Food Science and Emerging Technologies*, 11, pp. 1-12.

Santana, A., S. Jesus, M. A. Larrayoz, and Filho R. M.

    2012   "Supercritical carbon dioxide extraction of algal lipids for the biodiesel production", *Procedia Engineering*, 42, pp. 1755-1761.

Setianto, W. B., P. Atmaji, and D. D. Anggoro

    2012   "Solubility examination of palm kernel oil in supercritical CO_2 and its correlation with solvent density based model", *Proceeding of International Conference on Chemical and Material Engineering 2012*.

Setianto, W. B., S. Yoshikawa, R. L. Smith Jr., H. Inomata, L. J. Florusse, and C. J. Peters

    2009   "Pressure profile separation of phenolic liquid compounds from cashew (*Anacardium occidentale*) shell with supercritical carbon dioxide and aspects of its phase equilibria", *Journal of Supercritical Fluid*, 48, pp. 203-210.

Sforza, E., R. Cipriani, T. Morosinotto, A. Bertucco, and G. M. Giacometti

    2012   "Excess CO_2 supply inhibits mixotrophic growth of *Chlorella protothecoides* and *Nannochloropsis salina*", *Bioresource Technology*, 104, pp. 523-529.

Sforza, E., M Enzo, and A. Bertucco

    2013   "Design of microalgal biomass production in a continuous photobioreactor: An integrated experimental and modeling approach", *Chemical Engineering Research and Design*.

Sievers, U.

    1984   *Die thermodynamischen Eigenschaften von Kohlendioxid*.

Simopoulos, A. P.

    2002   "The importance of the ratio of omega-6/omega-3 essential fatty acids", *Biomed Pharmacother*, 56, pp. 365-379.

Sovová, H.

    2005   "Mathematical model for supercritical fluid extraction of natural products and extraction curve evaluation", *Journal of Supercritical Fluids*, 33, pp. 35-52.

    2012   "Steps of supercritical fluid extraction of natural products and their characteristic times", *Journal of Supercritical Fluids*, 66, pp. 73-79.

Sovová, H. and R. P. Stateva

    2011   "Supercritical fluid extraction from vegetable materials", *Reviews in Chemical Engineering*, 27, pp. 79-56.

Sukhija, P. S. and D. L. Palmquist

    1988   "Rapid method for determination of total fatty acid content and composition of feedstuffs and feces", *Journal of Agricultural and Food Chemistry*, 36, pp. 1202-1206.

Tomaselli, Luisa

    2004   "The Microalgal cell", in *Handbook of Microalgal Culture: Biotechnology and Applied Phycology*, ed. by Amos Richmond, Blackwell Science Ltd, chap. 1.

Vatanara, A, A. R. Najafabadi, M. Khajeh, and Y. Yamini

    2005 "Solubility of some inhaled glucocorticoids in supercritical carbon dioxide", *Journal of Supercritical Fluids*, 33, pp. 21-25.

Vonshak, Avigad

    1997 *Spirulina Platensis (Arthrospira): Physiology, Cell-Biology And Biotechnology*, Taylor & Francis Ltd.

Web Sites

Urieli, Israel [2013], *Ohio University - Mechanical Engineering Department*, `http://www.ohio.edu/mechanical/thermo/property_tables/CO2/ph_CO2.html`.